High energy muons in large extensive air showers

K. J. Orford

High Energy Muons in Large Extensive Air Showers

by

K.J. Orford, B.Sc.

A Thesis submitted to the University of Durham in accordance with the Regulations for admittance to the Degree of Doctor of Philosophy.

Department of Physics
University of Durham

August, 1968.

Abstract.

A magnet spectrograph in the centre of a large array of diffused-light water Čerenkev detectors has been used to measure the momentum spectrum and lateral distribution of muons in large extensive air showers. The data cover the ranges: 1–100 GeV/c in muon momentum, 10–700 metres in core distance, and 10^5–10^8 particles in shower size. The spectra are presented in the form of integral and differential densities as functions of muon momentum and EAS core distance.

Details are given of the construction of the spectrograph and EAS arrays, the collection and treatment of the data, and the derivation of the momentum spectra and the analysis of the results. Experimental results are also presented on the charge ratio of EAS muons, and an interpretation is offered for the bursts, observed in the visual detectors, which are produced in the spectrograph iron. Wherever possible, comparison is made between the results of the experiment and the observations of other workers.

Previous theoretical models of EAS muon production have been critically examined and it is shown that the assumptions on which they are based are not valid for all EAS muons. In particular, the density of muons possessing large momenta far from the shower core is sensitive to the assumptions made about the first interaction of the primary cosmic ray. A careful analysis of the problem shows that such muons provide a means of estimating the mass of primary cosmic rays in the EAS energy region.

Preface.

The results presented in this thesis were obtained during the period October, 1965 to July, 1968, while the author was under the supervision of Professor G.D. Rochester, F.R.S., in the Department of Physics of the University of Durham and at the Cosmic Ray station operated by the Universities of Durham and Leeds, and Imperial College, at Haverah Park, in Yorkshire.

The author has shared with his colleagues the collection of data, and has been responsible for the derivation of the momentum spectra, and for the development of EAS model calculations.

Preliminary reports on some aspects of the experimental results have been published: Earnshaw et al. (1967, 1968a, 1968b), Orford and Turver (1968), and Orford et al. (1968).

CONTENTS.

Chapter 1

Introduction.

1.1 General.

Primary cosmic rays consist of atomic nuclei (about 90% protons, 10% α-particles and a small fraction of heavier nuclei), possessing energies from less than a GeV to about 10^{10} GeV, low energy electrons, and X-rays. Particulate cosmic rays interact with the interplanetary and terrestrial magnetic fields, and with the solar wind, and the study of their time, energy and spacial distributions, using satellites and high-altitude balloons, has provided much information on the distribution of matter and fields in the solar system. The close correlation in time between the bursts of cosmic ray activity and the occurrence of solar flares demonstrates that the sun is a source of cosmic rays. All cosmic rays do not, however, originate from the sun, as no known solar process can be responsible for their acceleration to energies exceeding about 10 GeV. The origin of the most energetic cosmic rays is, as yet, unknown, but the majority are supposed to be produced and accelerated in our galaxy.

At energies less than about 5×10^4 GeV, the nature of primary cosmic rays and the properties of their interactions have been studied directly using nuclear emulsions flown in high-altitude balloons. The flux of high energy cosmic rays is extremely low (about one particle of energy greater than 10^9 GeV per 3000 years per square metre) so that their direct observation is virtually impossible. These

particles, however, interact in the earth's atmosphere with air nuclei and a chain of interactions ensues, which is termed an extensive air shower (EAS). The particles in this shower, which are mostly electrons, are distributed symmetrically about the central region, the 'core' of the shower, and move through the atmosphere with practically the same direction as the primary cosmic ray, until at sea level up to about 10^{10} particles may be observed over an area of many square kilometres. This magnifying effect of the atmosphere, and the retention of the direction of the primary by the majority of the shower particles, enables ultra-high energy cosmic rays to be observed, and affords the possibility of locating their sources through a search for an anisotropy of EAS arrival direction.

The secondary particles created in EAS provide a rich source of knowledge about fundamental particles and their interactions, and for the forseeable future they will be the only source of particles of energies greater than about 10^3 GeV.

1.2 Muon Studies.

The secondaries produced in high energy nuclear interactions are thought to be mainly pions, with a small proportion of heavy mesons and strange particles. The study of cosmic ray muons may then make possible a knowledge of the parameters of the interactions in which pions are produced, as a muon, unlike other secondary particles, is relatively unaffected by its passage through matter, sensibly retaining the initial spacial direction and energy of the

parent pion.

Solitary muons observed at sea level originate in showers of low energy which have been absorbed in the atmosphere. The many measurements which have been made on these muons have shown that the secondaries of interactions of energies about 10^3 GeV are mainly pions, about 20% being kaons. At much higher energies, the muons observed at sea level are a component of EAS. A knowledge of the properties of the parent EAS makes it possible to investigate in greater detail the mechanism of ultra-high energy interactions. The possible answers to a number of questions, the nature of the muon parents, the parameters of an interaction, such as the multiplicity of created particles, and the nature of the primary cosmic ray are contained in the muons of an EAS, and it is the purpose of this and other muon studies to seek these answers.

1.3 Previous EAS Muon Work.

For many years it has been known that about 5% of all charged particles in an EAS are muons, and early experiments such as these of Barrett et al.(1952) and Devzhenko et al.(1957) established the approximate muon momentum and spacial distributions. Contemporary theoretical EAS models, e.g. Oda (1957), had some success in explaining these results, but showed the necessity for much more detailed and extensive measurements.

The magnetic deflection technique was used by Bennett and Greisen (1961) to measure the integral momentum spectrum of muons of momenta less than 20 GeV/c for EAS core distances up to 450 m.

A small (acceptance volume 25 cm^2 ster.) air-gap magnetic spectrograph using G-M counters to delineate muon tracks was employed in conjunction with a number of independently operated, well-spaced scintillators. Coincidences were recorded between a single scintillator and the spectrograph, and hence the core distance and size of each EAS was not determined. The large statistical errors on the spectra, and the lack of precise EAS measurements limited the usefulness of the results for comparison with theoretical predictions.

The lateral distributions of muons for threshold energies of 5 GeV and 10 GeV were obtained by Khrenov(1962) and for a 40 GeV threshold by Barnaveli (1964), with a knowledge of the core distance and size of each shower. The measurements were performed using the absorption technique, the former using G-M counters under a large (500m. diameter) G-M array, and the latter using scintillators under a 40m. scintillator array. The absorption technique has the disadvantages that an individual muon's energy is not known, and that for higher threshold energies, and consequently great thicknesses of absorber, the EAS core arrival direction must be determined in order that large systematic errors are not introduced; in neither case was this determined.

The results of previous EAS muon work do not overlap to any great extent, but where they do there is agreement, except for the results of de Beer et al.(1962). In this work measurements of the angular scattering of muons in an absorber were used to produce

momentum spectra for muon momenta up to 10 GeV/c and core distances of 100m. and 300m. These spectra are much steeper than those of Bennett and Greisen, and the muon densities given do not agree with those given by Khrenov. No explanation was offered by the authors for this discrepancy.

No consistent picture of EAS muons emerges from the results of previous experiments, and such a picture is necessary for the acquisition of new knowledge on the mechanism of ultra-high energy nuclear interactions and the nature of primary cosmic rays.

1.4 The Present Work.

The present study was initiated in 1964 because of the need for accurate measurements of the EAS muon momentum spectrum over a wide range of muon momenta, together with precise measurements of the characteristics of each EAS recorded. The large magnet spectrograph and EAS array to be described in chapter 2 have provided measurements of the momentum spectrum of muons in the ranges $1 <$ muon momentum < 100 GeV/c, $10 <$ core distance < 700 metres, and $10^5 <$ shower size $< 10^8$ particles. The first results of the experiment were published by Earnshaw et al.(1967).

Chapter 2

The Haverah Park 'Solid' Iron Magnet Spectrograph.

2.1 Introduction.

The Haverah Park spectrograph was constructed in 1964 by Professor G.D.Rochester and Dr. K.E.Turver in the centre of the Leeds University EAS array at Haverah Park, in Yorkshire. In 1965 the small arrays to be described later were added. The details of the construction of the magnet and visual detectors have been published (J.C.Earnshaw et.al.,1967), but the more important details are given here. The EAS arrays at Haverah Park are briefly described and the characteristics of EAS which they measure are given, together with the accuracy of measurement attainable.

2.2 The Spectrograph.

2.2.1 The Magnet.

The magnet, which is of the 'picture-frame' type developed by the Durham and Nottingham groups (O'Connor and Wolfendale,1960; Bennett and Nash,1960), consists of 46 iron plates of total thickness 60 cm., each of area 4.9 m^2. and with a central hole of area 0.22 m^2. About two sides of the toroid so formed are wound coils of 14-guage copper wire through which is passed a current of 13.9 A, giving 9,100 Ampère-turns. Over a horizontal area of 1.8 m^2. and a cross-section of 0.48 m^2. the applied field produces an induction of 14.6 $\pm$0.3 Kgauss with a saturation of 0.015 gauss/Ampère-turn. The acceptance volume of the spectrograph for undeflected particles is 1.1x 10^4 cm^2.ster. Side and front sections of the spectrograph are shown in figure 2.1. The composition of the iron is identical to that

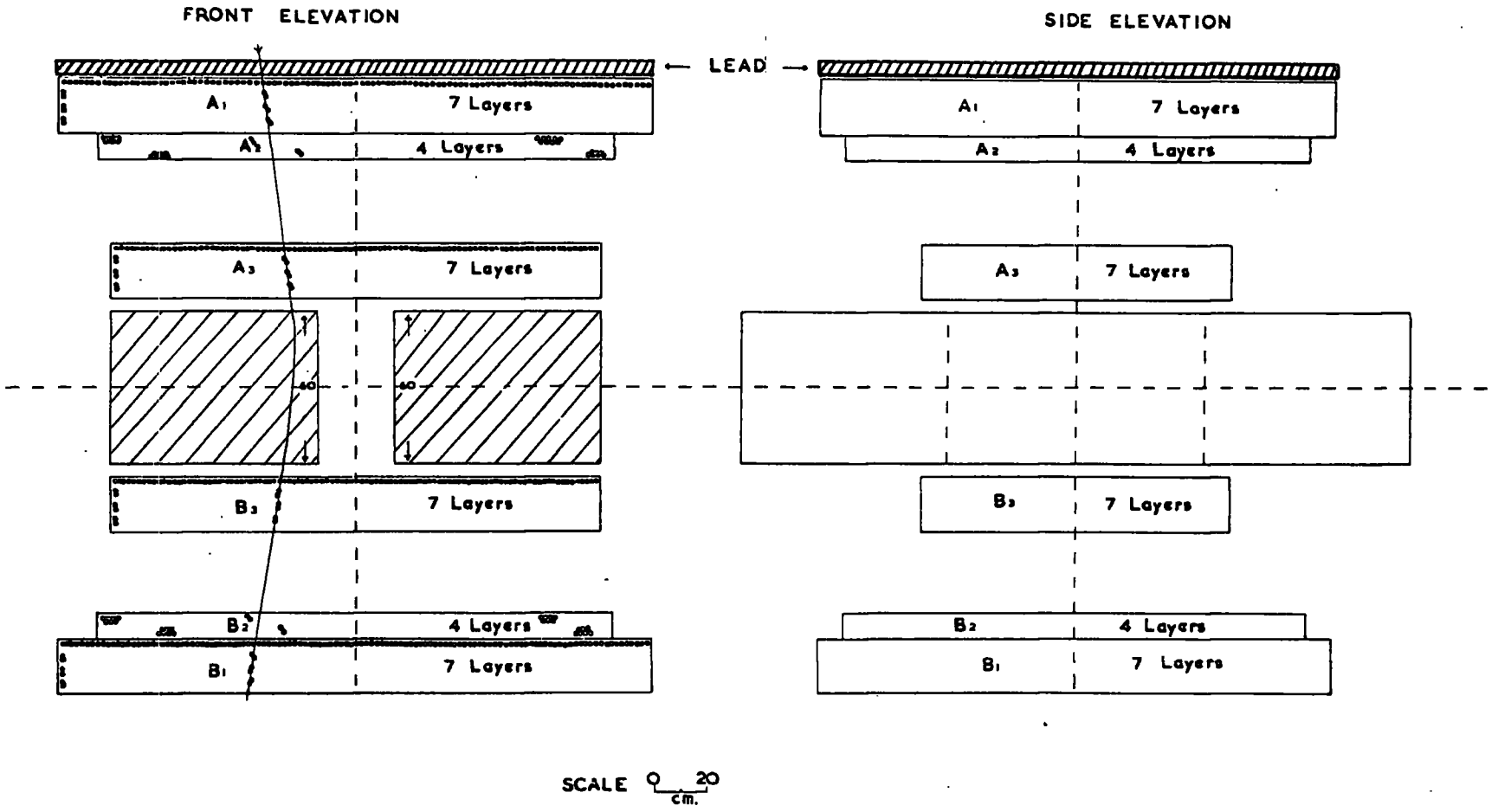
FRONT ELEVATION
SIDE ELEVATION
LEAD
A1
7 Layers
A2
4 Layers
A3
7 Layers
B3
7 Layers
B2
4 Layers
B1
7 Layers
40
40
SCALE 0 20 cm.

FIGURE 2.1

given by Bennett and Nash (1960). The variation of the magnetic induction over the homogeneous field volume has been investigated by Walton (1966) using a calibrated flux-meter coupled to search coils inserted between the iron plates, and has been found to be less than 3%. The effect of time-dependent biases has been minimised during the operation of the spectrograph by reversing the direction of the magnetising field at regular intervals.

2.2.2 The Visual Detectors.

The tracks of charged particles are delineated in the spectrograph by trays of neon flash-tubes, labelled A1,A3,B3,and B1, the 'momentum trays', and A2,B2, the 'direction trays' in figure 2.1. Each of the four momentum trays contains seven layers of tubes of length 200 cm., in trays A1 and B1, and 120 cm. in trays A3 and B3. The direction trays contain two double layers of tubes of length 200 cm., crossed at an angle of 3.5°. The former have been used to measure the angular deflections of muons in the magnet, projected into the plane parallel to the front section of the spectrograph, i.e. the measuring plane, and the latter to measure the incident angle distribution of muons projected into the vertical plane perpendicular to the measuring plane, and to ensure that only these muons which cross the region of uniform field in the magnet are considered.

The flash-tubes have a mean internal diameter of 1.6 cm., a mean external diameter of 1.8 cm., and are filled with ' 98%

industrial' neon to a pressure of 600 mm. Hg. About 60% of the tubes are located in accurately machined duralumin mountings and have been made parallel to within 0.006°, and their positions measured to an accuracy of 0.2 mm. relative to an arbitrary vertical plane defined by plumb-lines, using an optical bench and a travelling microscope. The remaining 40% of the tubes form the upper of the double layers and rest on the accurately positioned tubes.

On the arrival of an EAS, a field of 4.6 KV/cm. is applied to the tubes for a period of 10 μsec., after a delay of 15 μsec. in order to avoid 'pick-up' by the electronics of the EAS arrays. The internal flashing efficiency of the tubes under these conditions is very close to 100% (Walton, 1966), and the layer efficiency, a measure of the number of tubes expected to flash on the track of a charged particle, is 80%. Random triggering of the spectrograph shows that the probability of spurious flashing, due to natural radio-activity, is less than 0.1%. The images of the flash-tube trays are brought together by a mirror system and are photographed on a single frame of Ilford HPS film using a Shackman 35 mm. automatic recording camera.

2.3 The EAS Trigger.

2.3.1 General.

The Haverah Park EAS complex is situated at a mean altitude of 220 m. above sea level, corresponding to a vertical atmospheric depth of 1016 gm.cm.$^{-2}$, and at a latitude 53°58.2' North, longitude 1°38.1' West. The detectors consist of large tanks of water of depth 120 cm.

and area 2.25 m^2., acting as diffused-light Čerenkov counters. These are viewed by single photomultipliers, and their performance as particle detectors has been described by Turver(1963). A plan of the arrays is shown in figure 2.2. The arrays at spacings of 50 m. and 150 m. from the central detector were constructed and have been operated by members of the Physics Department of the University of Durham, and the other arrays by members of the Physics Department of the University of Leeds.

2.3.2 The 500 m. Array.

This array selects showers of size greater than 10^7 particles at a rate of about 40 per day. It comprises four stations situated at the centroid and corners of an equilateral triangle of side 870 m., each containing sixteen Čerenkov detectors of total area 34 m^2.(Wilson et al., 1964). The distribution in zenith angle of arrival of detected EAS is much wider than for a G-M or scintillator array, due to the depth of the detectors. The mean zenith angle of the showers detected is 40^0, at which angle the mean detected shower size is $2x10^7$ particles.

2.3.3 The Small Arrays.

The small arrays at spacings of 50 m. and 150 m. are of similar geometry to the 500 m. array, and each station contains two Čerenkov detectors giving an area of 4.5 m^2. The arrays select showers in the size range 10^5 to 10^7 particles and are operated independently, the trigger rates being 400 and 100 showers per day respectively.

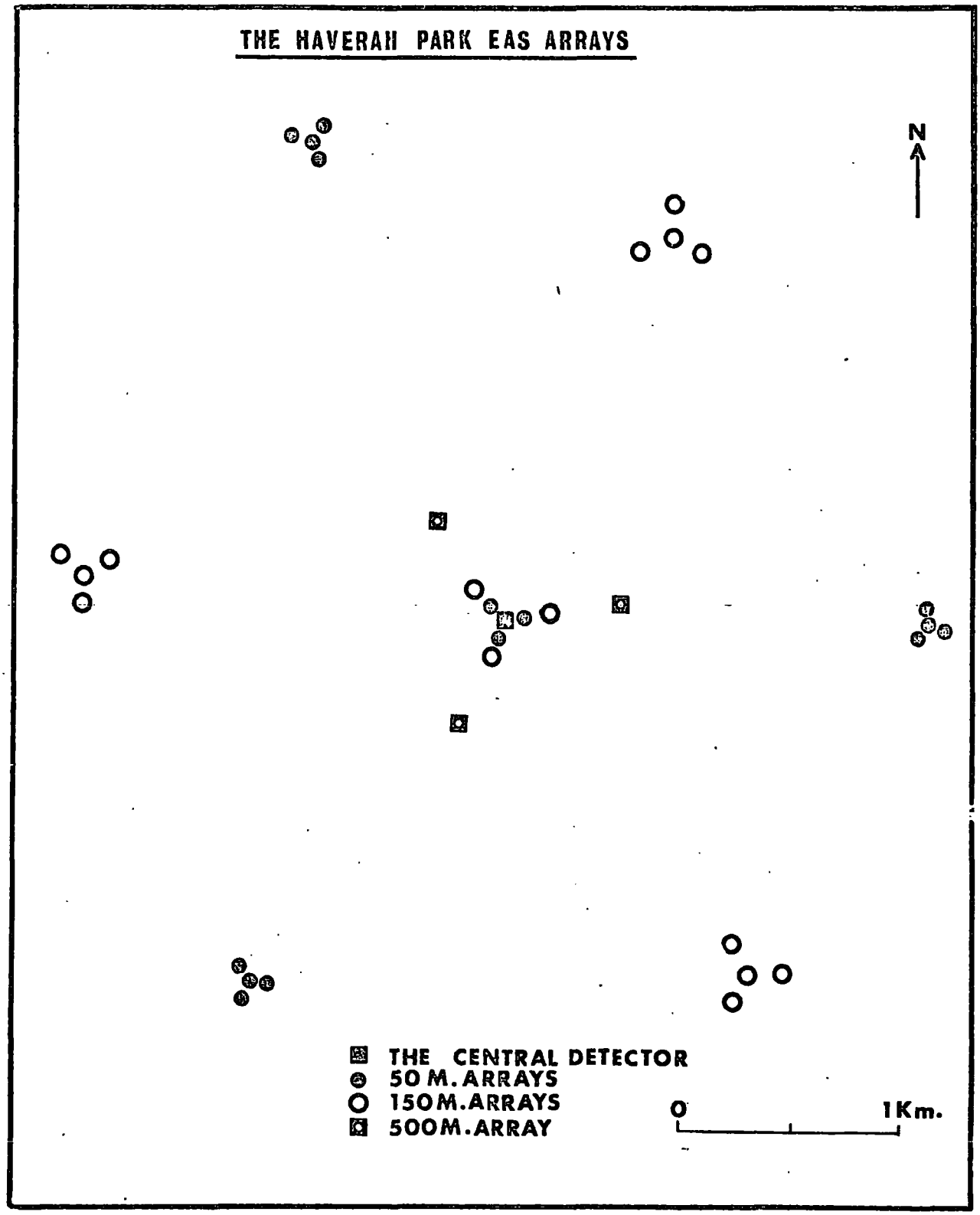
THE HAVERAH PARK EAS ARRAYS
N
THE CENTRAL DETECTOR
50 M. ARRAYS
150M. ARRAYS
500M. ARRAY
1Km.

FIGURE 2.2

2.3.4 The 2 Kilometre Array.

The purpose of this array is to record extremely large showers of sizes up to about 10^{10} particles. The array consists of six Čerenkov detectors, each comprising a 50 or 150 m. array, of area 54 m^2 situated nearly symmetrically around the central detector. Preliminary results on showers detected by this array have been given by R.A.Earnshaw et al. (1968) which indicate that the collecting area of the array may be as large as 40 km^2. The expected rate of detection of showers of primary energy greater than 10^{10}GeV is therefore about one per week.

2.3.5 EAS Characteristics Measured.

The data on showers triggering the 500 m. array are analysed by members of the University of Leeds, and the quantities obtained for each shower are made available to the universities collaborating in the Haverah Park experiment. The following quantities are determined for each shower:

r: the distance of the core of the shower from the central detector, measured in the plane of the shower front, obtained by the method of intersecting loci (Allan et al. 1960 and 1962),

N: the conventional electronic size of the shower,

X,Y: the cartesian co-ordinates, in the plane of the ground, of the impact point of the shower core, with the central detector as origin and grid north as the X-axis,

n: the exponent of the shower lateral structure function which gives the 'best' fit to the observed densities,

θ: the angle of arrival in zenith of the shower core,

ϕ: the angle of arrival in azimuth of the shower core,

1/R: the curvature of the shower front at the central detector,

t: the siderial and solar times of arrival of the shower.

All the quantities obtained for showers triggering the 500 m. array are also obtained for the smaller showers selected by the 50 and 150 m. arrays, with the exception of 1/R, which cannot be measured because of the short base-lines. The quantities θ,ϕ,and 1/R are obtained from the relative times of arrival of the shower front at the detectors.

2.3.6 The Accuracy of EAS Measurements.

Tennent (1967) has given the accuracy attainable for the quantities listed above. From a study of artificial showers generated by a computer program, it is concluded that the overall uncertainty in the location of a shower core is 30 metres, for nearly vertical showers falling within the 500 m. array. The uncertainty in core location for all showers is less than 50 m.

The size of a shower is obtained by integrating over the shower front the energy lost by the shower particles in traversing 120 cm. of water, the depth of the detectors, (Suri,1966). The limits of integration are 100 m. to 1000 m. and this quantity, which is termed E_{100}, is related via V_{100}, the energy which the same shower would have deposited had it arrived vertically, to the primary energy, by a comparison

of the rate of arrival of showers with a given V_{100} with showers with a given primary energy. The accuracy of determination of E_{100} is typically, for near-vertical showers, 20%.

The quantities θ,ϕ,and 1/R are determined from the relative times of arrival of the shower front at each detector station and so the errors in these reflect the errors in time estimation. The r.m.s. errors in θ and ϕ, when θ lies between 20° and 70° are given by Tennent as 4° for each angle. The r.m.s. error in 1/R is about 30%.

The characteristics of showers selected by the small arrays are obtained by methods similar to those employed on the larger showers. The uncertainties in core distance and θ for the 50 and 150 m. arrays are 10 m. and 20 m., and 30° and 10° respectively.

Chapter 3

The Momentum Spectrum of Muons in EAS

3.1 Selection of Data and Treatment.

3.1.1 General.

The spectrograph has been operating continuously since April 1965, during which time 19,500 hours of effective exposure have been obtained. The 500 metre array was operational during the whole of this time, and the 150 metre and 50 metre arrays were operational for 1,700 and 2,400 hours respectively. The numbers of showers recorded in each shower size range are:

Array	Size Range	Showers Recorded
50m.	$10^5 - 10^6$	14,100
150m.	$10^6 - 10^7$	6,000
500m.	$> 10^7$	25,100

3.1.2 Reconstruction of Muon Trajectories.

The film records are scanned in Durham to select the frames containing possible muon tracks. The criterion for this choice is the existence of a charged particle track in tray B3 of figure 2.1, the tray immediately below the magnet. The frames thus chosen are projected onto scale drawings of the spectrograph, and the discharged tubes are indicated. The reconstructed drawing of a

typical frame containing an accepted muon trajectory is shown in figure 3.1. The reconstructed spectrograph pictures are then scrutinised to confirm the existence of a muon track. An eight-tenths scale model of the flash-tube trays is used to obtain the best fit muon trajectory to the discharged tubes, defined as that line which traverses the maximum amount of path length in the gas of discharged tubes and the minimum in the gas of tubes which have not discharged. The spacial co-ordinates of the trajectory so fitted are recorded and a computer programme is employed to calculate the co-ordinates of the intersection point of the two halves of the track, and other track parameters needed to determine the acceptability of the track.

A typical picture containing a trajectory of an EAS muon is confused by the presence of electron tracks, single discharged tubes due to materialising photons, and cascades produced in the shielding lead layer above the spectrograph by electrons, photons and hadrons. The average frame contains about five electron and muon tracks in the flash-tube trays above the magnet and about three in the trays below. Thus, precautions must be taken to ensure that uncorrelated half-tracks are not connected. For acceptance as a muon track, the following conditions must be satisfied:

(a) The half-tracks must intersect within the constant-field volume of the magnet.

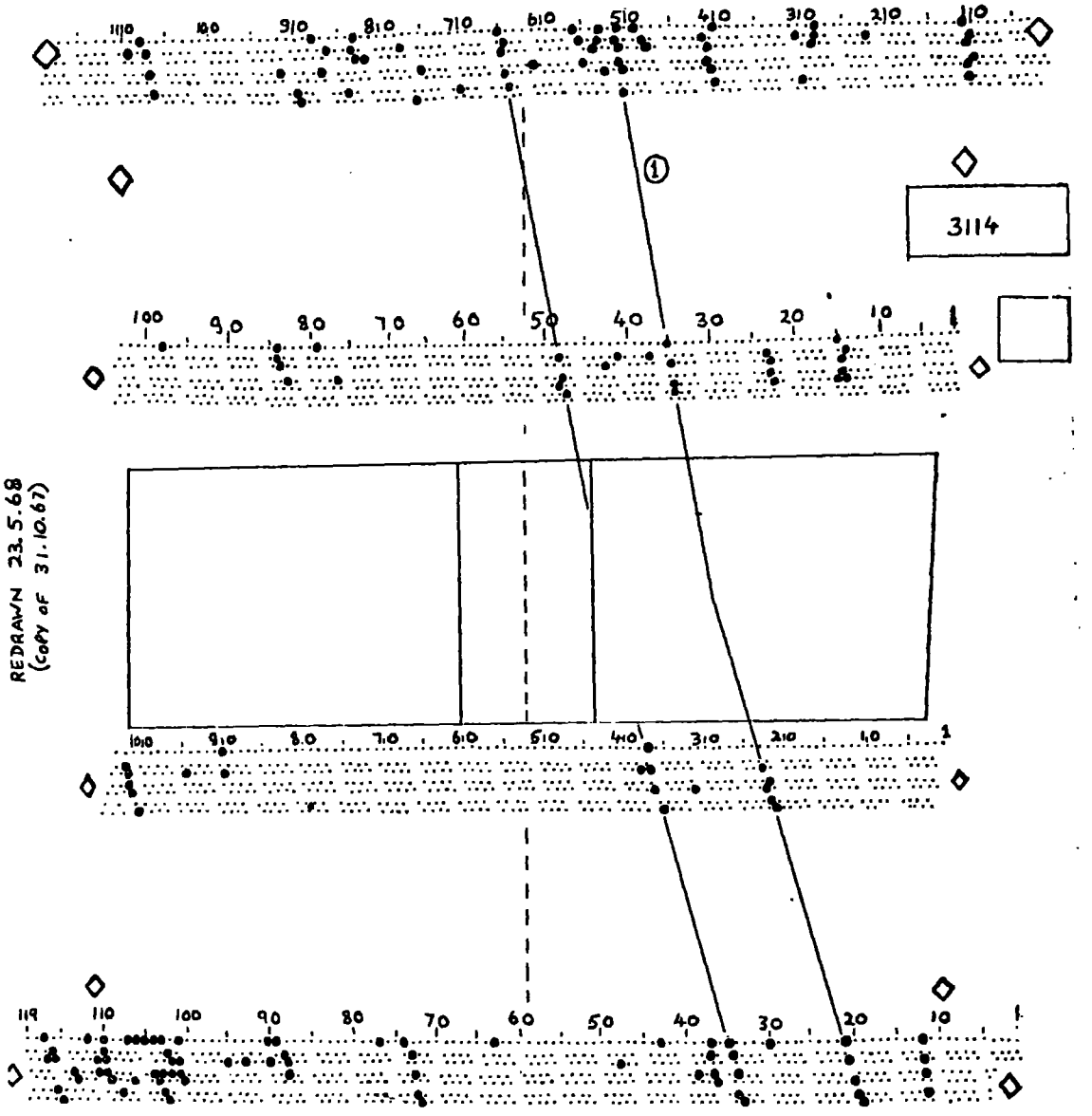

				1	
				A	B
F243	TRIG	500	p_1	10.70	15.65
	N	$2.4_{10}7$	p_2	3.20	7.30
H –	r_1	225m	N	22	23
	Θ	25°			
	Φ	295°	Ψ_0	-15.05°	
3351051	λ	-227m	$\Delta\Psi$	-1.62°	
	Y	+105m			
	V/R	——			

FIGURE 3.1

(b) The upper half-track must be within 20^{o} of the projected direction of the normal to the shower front in the spectrograph measuring plane, because of the possibility of unassociated cosmic ray muons arriving during the sensitive time of the flash-tubes, and contaminating the EAS muon spectrum.

(c) The number of tubes which have not discharged, but through which a trajectory passes, must be less than two.

(d) The whole track must be completely within the acceptance volume of the spectrograph.

(e) There must be no equally probable alternative half-tracks.

The biases possibly introduced by the application of these conditions are discussed in section 3.4.

A computer method of track analysis, similar to that used in unassociated cosmic ray muon studies by Bull et al.(1962a) has been investigated by G.C. Maslin, (private communication), but it is found to be unsatisfactory for two reasons:

(1) The accuracy of the fit obtained for a muon track is critically dependent on the flash-tube efficiency, in particular to the exact form of the variation of flashing probability with the track length of a particle in the gas of a tube. No satisfactory provision is possible for the occasional apparent non-flashing of a tube due to scanning errors or photographic faults. (2) The occurrence of other tracks, and single tubes due to materialising photons and low energy electrons, in a flash-tube tray occasionally causes the best fit track to deviate markedly from the actual trajectory.

These disadvantages do not, however, prevent the method being used on low momentum muons.

3.1.3 Detailed Treatment of the Data

For each muon which satisfies all the criteria for acceptance, the following parameters are recorded, together with the properties of the accompanying EAS:

t: The G.M.T. time of arrival.

ψ_0: The projected muon arrival direction in the spectrograph measuring plane.

$\Delta\psi$: The projected angular deflection of the muon.

H: The direction of the field in the magnet.

C: The charge of the muon.

Deflection spectra, or histograms in $\Delta\psi$, can be constructed from this information, and these are the starting points for the procedure described later. The choice of $\Delta\psi$ intervals is governed by the need to obtain the maximum information from the data. The intervals chosen contain approximately equal numbers of particles, with the exception of the lowest deflection interval, which includes those particles with deflections less than the r.m.s. measurement noise. For the spectrum at a core distance of 225 metres, the intervals are those of figure 3.2.

In order to construct lateral distributions, deflection spectra are obtained for a number of arbitrary intervals of EAS core distance.

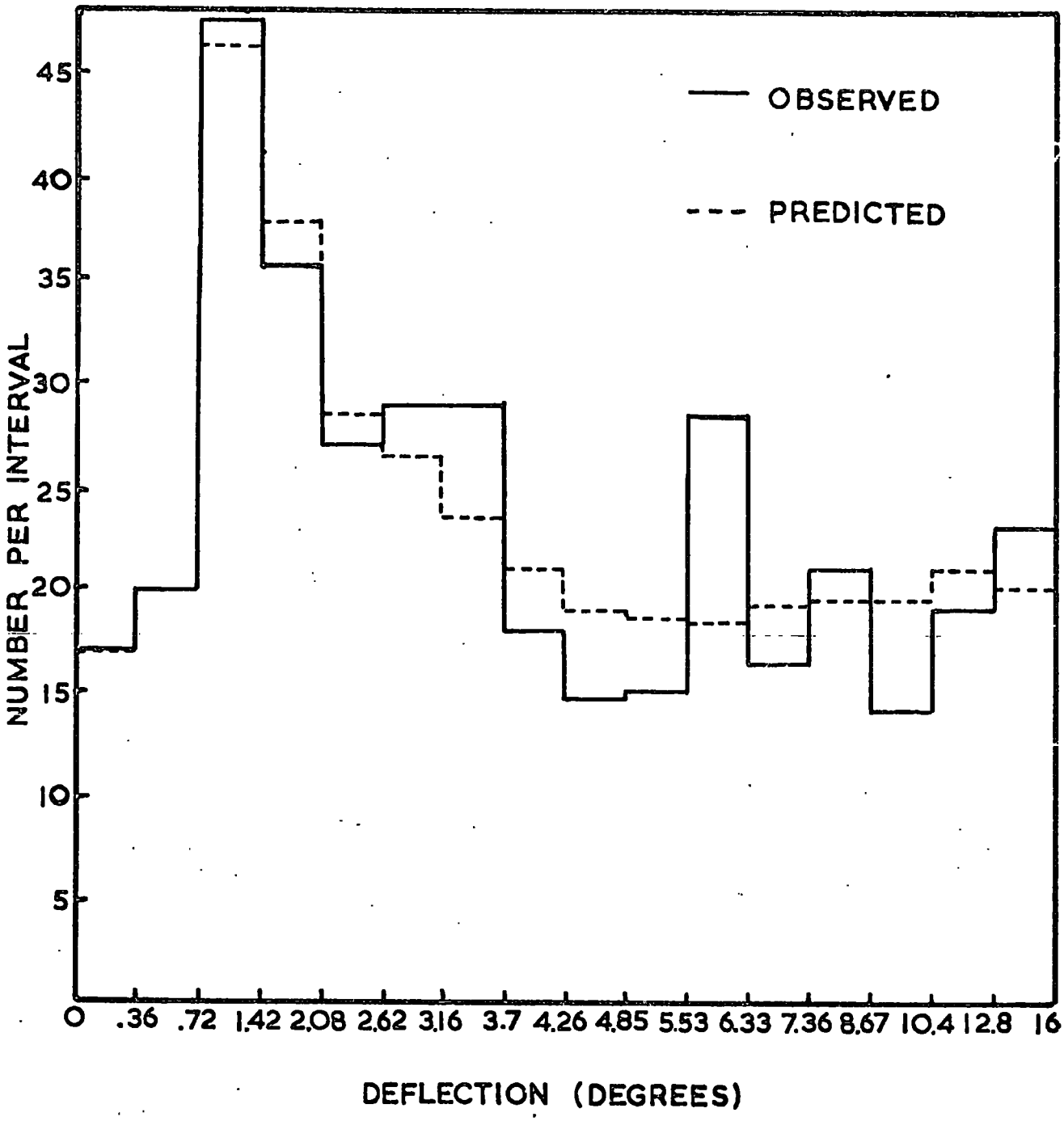
OBSERVED
PREDICTED
NUMBER PER INTERVAL
45
40
35
30
25
20
15
10
5
0
.36
.72
1.42
2.08
2.62
3.16
3.7
4.26
4.85
5.53
6.33
7.36
8.67
10.4
12.8
16
DEFLECTION (DEGREES)

FIGURE 3.2

From the distribution of core distance, r, within an interval N(r), the mean core distance $\bar{r}$ can be obtained. However, since the density of muons varies within an interval, a weighted mean distance must be used as follows:

$$\bar{r}_{eff} = \frac{\int S(r).N(r).r\,dr}{\int S(r).N(r)\,dr} \qquad \ldots 3.1.1$$

where S(r) is the lateral distribution of all muons. The values of $\bar{r}_{eff}$ so obtained are very close to $\bar{r}$, indicating that the intervals in r are not too wide and that the variation of muon density within an interval is not important.

3.2 Derivation of the Momentum Spectra

3.2.1 General

Both inductive and deductive methods of analysis have been employed previously to transform deflection distributions into momentum spectra. Walton (1966) describes a deductive method which enables a momentum spectrum to be obtained from a limited sample of data. The first results from the Haverah Park Spectrograph (J.C. Earnshaw et al., 1967) were obtained by this method. However, most work has been carried out using an inductive method, e.g. Hayman et al.,(1962), and since the mathematics of this method are simpler, the application less laborious, and the size of the samples of muons are now sufficiently large, it is used here.

3.2. 2 Derivation of a Momentum Spectrum from a Deflection Distribution.

The procedure consists of converting an assumed momentum spectrum into an expected deflection distribution in the spectrograph, taking into account magnetic deflection, coulomb scattering, track location errors, energy loss of muons, the distribution in muon arrival direction, and the acceptance of the spectrograph. The steps taken are:

1) The deflections in the magnet corresponding to a range of muon momenta and arrival directions are calculated, neglecting coulomb scattering, but including energy loss.

2) The acceptance probability of muons, averaged over all momenta, from a given arrival direction is used to correct the number of events observed from this direction to obtain the true arrival direction distribution of muons incident on the spectrograph.

3) For each (momentum) x (arrival direction) interval calculated in 1), the deflection distribution is calculated, including the effects of coulomb scattering and track location errors.

4) Each interval in the deflection distribution is weighted according to the probability of its acceptance with the given values of arrival direction and angular deflection.

5) The contributions to each deflection interval from each (momentum) x (arrival direction) cell are weighted by the assumed

momentum spectrum, then summed to produce an expected deflection distribution. The details of the derivation are now given.

A function of $\Delta\psi$ is defined:

$$N^1(\Delta\psi)\, d(\Delta\psi) = \int_0^\infty S(p)\, W(\Delta\psi, p)\, dp\, d(\Delta\psi) \quad \ldots 3.2.1$$

where N^1 is the expected intensity of the deflection distribution at $\Delta\psi$, $S(p)\,dp$ is a trial momentum spectrum, and $W(\Delta\psi, p)$ is the probability that a muon of momentum p is deflected by an angle $\Delta\psi$ and accepted. The observed deflection distributions are histograms, so for comparison the expected histograms of deflection are calculated.

$$N(\Delta\psi_i) = \int_{\Delta\psi_i}^{\Delta\psi_{i+1}} \int_0^\infty S(p)\, W(\Delta\psi, p)\, dp\, d(\Delta\psi) \quad \ldots 3.2.2$$

The weighting function, W, is given by:

$$W(\Delta\psi_i, p) = \int_{-40^\circ}^{40^\circ} \int_{-30^\circ}^{30^\circ} A(\Delta\psi_i, \psi_0)\, B(\phi_0)\, C(\phi_0, \psi_0, \Delta\psi_i, p)\, d(\psi_0)\, d(\phi_0) \quad \ldots 3.2.3$$

where A is the probability that a muon deflected by an angle $\Delta\psi_i$ will be accepted at an arrival angle ψ_0, B is the distribution in ϕ_0 for all muons, C is the distribution in ψ_0 for all muons, and Q is the probability that a muon of momentum p, incident at an angle (ψ_0, ϕ_0) will be deflected by an angle $\Delta\psi$ and will be accepted by the spectrograph. ϕ_0 is the projected angle of arrival of a muon in the vertical plane perpendicular to the measuring plane. The details of the spectrograph acceptance, coulomb scattering, magnetic deflection and measurement noise are given in the next section, 3.2. 3.

Equation 3.2. 3 is evaluated numerically to provide a large matrix of values of W. Obviously the applicability of these weightings to any particular momentum spectrum depends on the spectrum having functions A,B and C closely similar to those used in deriving W. In the spectra reported in this thesis, the functions A,B and C are in fact very similar, and so the same weightings are used for all spectra.

In order to obtain the momentum spectrum which gives the deflection distribution which best fits the observations, an arbitrary momentum spectrum is taken as a starting point, and using the comparison between the observed and predicted distributions, the trial spectrum is modified thus:

$$S_{j+1}(p)dp = \sum_i \frac{S_j(p).W(\Delta\psi_i,p).M(\Delta\psi_i)/N_j(\Delta\psi_i)dp}{\Sigma_i W(\Delta\psi_i,p)} \qquad \ldots 3.2.4$$

where $M(\Delta\psi_i)$ is the observed deflection distribution and $N_j(\Delta\psi_i)$ is the distribution predicted from the j^{th} attempted momentum spectrum $S_j(p)$. The reiteration is computed until $(S_{j+1} - S_j)/S_j$ is less than 1%. A typical deflection distribution, that at a core distance of 225m, is shown compared with the best fit predicted distribution in figure 3.2.

This method is similar to that described by Ward (1967), in that the solution obtained is inherently smooth, and the statistical errors must be treated carefully. The statistical errors are obtained by finding the percentile points of the edge of each deflection interval in the observed distribution and interpolating points

from one standard deviation movements of the extremities. This procedure gives an approximation to the steepest and flattest deflection distributions which could have produced the observed distribution. Momentum spectra are fitted to these in the same way as to the observed distribution.

The above procedure is repeated twice with different values of the function $W(\Delta\psi_i, p)$, corresponding to the statistical limits on the measurement noise distribution standard deviation. This extra error is interpreted as an error in the momentum of a spectrum point, but it has been transformed into an error in the density in figures 3.6, 3.7 and 3.8.

3.2.3 Corrections for Instrumental Effects

The simple theory of the motion of a charged particle in a magnetic field gives a unique relation between the momentum of the particle, p, and its angular deflection $\Delta\psi$, namely:

$$p = \frac{300 \times \int H(l)\,dl}{c \cdot \Delta\psi} \qquad \ldots 3.2.5$$

where H is the magnetic field strength, l is the distance traversed in the field and C is the velocity of light. However, muons lose energy in the material of the spectrograph, and to construct a momentum spectrum, account must be taken of the effects of coulomb scattering, instrumental acceptance, track location errors, and the muon arrival direction, in that this affects the path length of a muon in the magnetic field.

3.2. 3-1 Magnetic Deflection

A muon incident at an angle ψ_0 on the magnet and emerging at an angle ψ_1, has a most probable momentum, neglecting the effects of coulomb scattering and track location errors of:

$$p = \frac{l.k.(1+q^2/k^2)}{\exp\left\{\frac{q}{k}.(\psi_0-\psi_1).(\cos\psi_1+\frac{q}{k}.\sin\psi_1)-(\cos\psi_0+\frac{q}{k}.\sin\psi_0)\right\}} \quad \ldots 3.2.6$$

where K is the magnetic field strength, in(gauss x 300), q is the energy loss of the muon in GeV per cm., and l is the thickness of the magnet in cm. (Rastin, 1964). As the energy loss, q, is a function of the muon momentum, equation 3.2.6 is reiterated to determine p.

3.2. 3-2 The Acceptance Function

The effective area of the spectrograph presented to a muon is a function of the projected arrival angle ψ_0 in the measuring plane, the angle of arrival ϕ_0 projected into the vertical plane perpendicular to the measuring plane, and the angular deflection, $\Delta\psi$. This area has been evaluated using an one quarter scale drawing of the side and front spectrograph sections for a range of angles $-16^\circ \leqslant \Delta\psi \leqslant 16^\circ$, $-30^\circ \leqslant \psi_0 \leqslant 30^\circ$, and $-40^\circ \leqslant \phi_0 \leqslant 40^\circ$, for intervals of 1° in each. The acceptance function is considered as two separate, independent functions, $A(\psi_0, \Delta\psi)$ and $B(\phi_0)$, the latter being a simple trigonometric function, independent of $\Delta\psi$, of the form:

$$B(\phi_0) = 1 - a \times \tan(\phi_0) \quad \ldots 3.2.7$$

where $a = 0.77$ for $|\phi_0| \leqslant 31^\circ$ and $a = 0.89$ for $|\phi_0| > 31^\circ$.

The analogue method of evaluating $A(\psi_0, \Delta\psi)$ does not take into

account the variation in apparent flash-tube brightness across a tray, which appears as a variation in flash-tube efficiency, and because of condition (C) in the list of acceptance conditions in section 3.1. 2 can cause a muon to be rejected. This apparent brightness variation is caused by the decrease in light intensity with increasing angle of viewing, a well-known characteristic of flash-tubes. To evaluate this effect, a large number of frames have been drawn in the normal way and the dependence of the average number of tubes flashed on a track on the lateral track position obtained. It is found that there is no effect for muons with small deflections, and that the number of muons with deflections of 16° is underestimated by less than 0.5%.

The total function $A(\psi_0, \Delta\psi) \times B(\phi_0)$ is shown in figure 3.3 for $\Delta\psi = 0^{\circ}$ and figure 3.4. for $\Delta\psi = 16^{\circ}$, displayed in polar co-ordinates ($A \times B$, ϕ) for various values of the zenith angle of arrival θ, where $\phi_0 = \tan^{-1}(\tan\theta \sin\phi)$ and $\psi_0 = \tan^{-1}(\tan\theta \cos\phi)$. Small residual acceptance effects are minimised by the use of two similar magnet volumes, magnetised in opposite directions, and by reversing the direction of magnetisation of each periodically.

3.2. 3-3 Coulomb Scattering

Muons are multiply scattered in the iron, so that the angular deflection of an emerging muon is distributed about the most probable deflection according to the distribution given by Eyges (1948), which is approximately gaussian with a standard deviation σ given by:

$$\sigma = \left[\frac{E_s^2 \times S}{2 \times P \times (P - q \times S)} \right]^{\frac{1}{2}} \quad \ldots 3.2.8$$

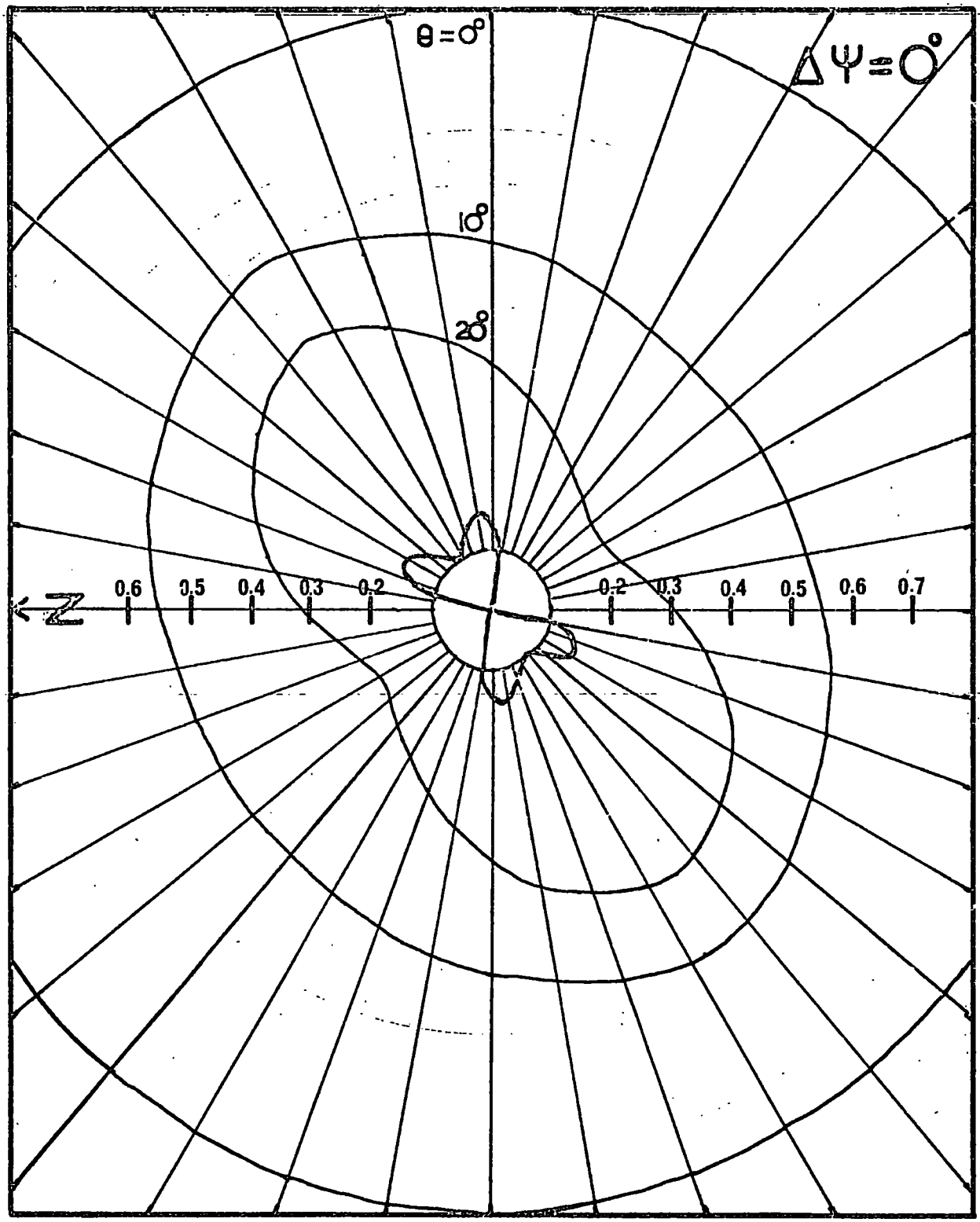

FIGURE 3.3

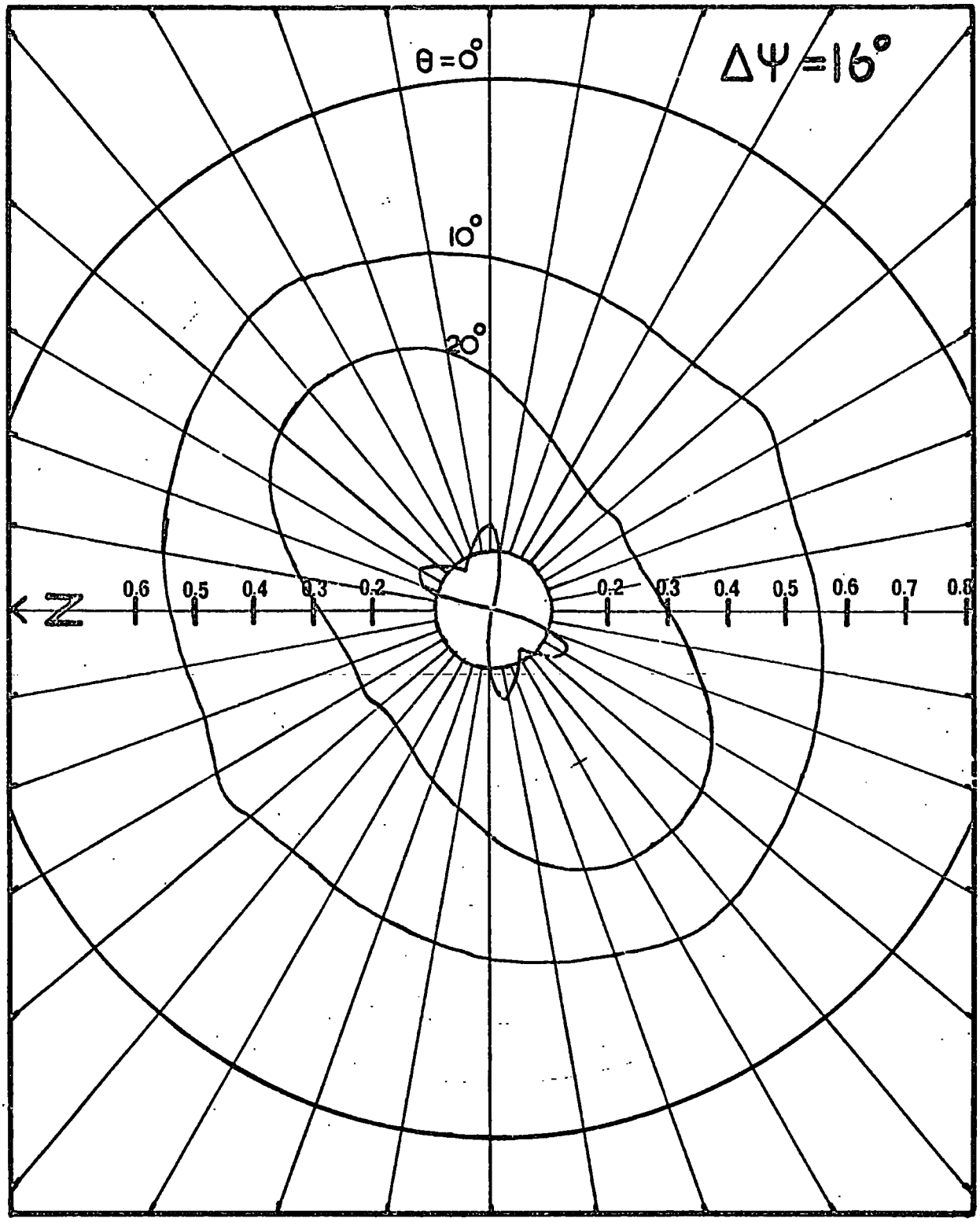

FIGURE 3.4

where p is the momentum of the muon in eV/C , E_s is a constant with the dimension of energy and has a value 21 x 10^6eV, q is the energy loss in eV per radiation length and S is the thickness of the scattering material in radiation lengths. It is assumed that muons are not angularly scattered in the flash-tube trays, which is valid since the standard deviations of the scattering distributions in the trays and the iron are in the ratio 1: 30.

3.2. 3-4 Track Location Errors

When a muon track, delineated by flash-tubes, is fitted, a random error is made in the angle of the fit, which is distributed randomly about the true track. This error is inherent in the use of flash-tubes and has been examined by many authors, notably by Bull et al. (1962b).

The trajectories can be estimated using a track simulator, or by using a computer analysis to obtain the best fit with a precise knowledge of the tube flashing probability function. The latter method has been examined and found to be unsuitable for use on EAS muons. The track simulator method has therefore been used, although it is relatively slow and laborious. Four quantities have been measured to investigate the form of the error function:

1. The lateral separation of the intersection points of the two halves of a track with the mid plane of the magnet, Δy_m.

2. The deflections of the muons which have traversed to the central hole of the magnet.

3. The deflections of the muons observed during a preliminary zero-field run.

4. The deflection distribution from a repeated simulation over a period of time of a number of tracks.

Method 1 has been used by Walton (1966) to estimate the r.m.s measurement noise which is found to be 0.49^0 for muons with deflections less than 1^0. The quantity Δy_m is related to the measurement noise because at the highest momenta, muon trajectories should be practically straight lines through the spectrograph. The measuring errors on each half-track distort these to produce a separation of the half-tracks. The figure obtained for the r.m.s. noise, 0.49^0, contains the effects of the coulomb scattering of the lower momentum muons. If a momentum spectrum of the form $S(p)\,dp \propto p^{-2}\,dp$ is assumed, and the r.m.s. coulomb scattering angle, evaluated from equation 3.2.8, is taken as $\sigma(p) = 6/p$, then the average r.m.s. scattering angle, coulomb plus measuring noise, is given by:

$$\bar{\sigma} = \frac{\int_{17}^{\infty} p^{-2} \cdot \left((6/p)^2 + \sigma_n^{\,2}\right)^{\frac{1}{2}}\,dp}{\int_{17}^{\infty} p^{-2}\,dp} \qquad \ldots 3.2.9$$

This can be solved for the r.m.s. measurement noise σ_n which for $\bar{\sigma} = 0.49^0$ is found to be $\sigma_n = 0.33^0$.

The distribution in Δy_m indicates that the distribution of measurement noise approximates to a gaussian.

In method 2, muons which have traversed the central hole of the magnet are used to estimate σ_n. Such muons are expected to be undeflected, so that the deflection distribution obtained should be

the measurement noise distribution. The distribution is found to be closely gaussian with a standard deviation $\sigma_n = 0.32 \pm 0.03^{\circ}$.

Before the magnetic field was switched on at the commencement of the experiment a run was made to measure the scattering angle distribution, using the unassociated cosmic ray muon beam. The measured deflection distribution includes the coulomb scattering of the muons, and after unfolding this, in a similar manner to that of method 1, it is found that $\sigma_n = 0.35 \pm 0.08^{\circ}$.

These three methods do not give an estimate of the standard deviation of the measurement noise distribution under the same conditions that apply during the routine measurement of muon trajectories. Repeated simulation of a number of muon tracks of all deflections inserted into the measurement routine should provide this estimation. Since, however, the simulation may be subjective, the tracks are inserted into the routine over a period of time, without the knowledge of the operator. The noise distribution obtained for half-tracks in this way is found to be closely gaussian, with an equivalent overall track location error of $\sigma_n = 0.25^{\circ} \pm 0.03^{\circ}$

In conclusion, consideration of all the results on the noise distribution indicates that this distribution is normal with a standard deviation of $0.3 \pm 0.03^{\circ}$.

3.3 The Momentum Spectrum of EAS Muons.

3.3.1 Normalisation Measurements.

Deflection spectra are obtained for intervals of EAS core distance from 10m. to 800m., and are fitted by differential, unnormalised momentum spectra. These are then normalised so that the density of muons of momenta not less than 1 GeV/c for a given distance interval is that given by the 1 GeV/c lateral distribution. This distribution has been measured by Earnshaw (1968c), using the iron of the Haverah Park Spectrograph as an absorber, and is reproduced in figure 3.5. Since the range of distances covered by the distribution involves measurement of muon densities in showers of size 10^5 to 10^8 particles, the dependence of the number of muons in a shower on shower size must be known. Although this dependence has been investigated by many workers, e.g. Bennett and Greisen (1961), Allan et al. (1968), the measurement of Earnshaw (1968c) has been used, because the same equipment was used as in the spectrum measurements, that is at a distance of 300 metres, $\Delta\mu(\geq 1\text{GeV/c}, 300\text{m.}) \propto N_e^{0.75}$. The assumption is made that the shape of the muon lateral distribution does not depend strongly on shower size. Since it is difficult to obtain measurements over all lateral distances in a shower of a given size, the assumption may be unjustifiable if, for example, the composition of primary cosmic rays varies with energy. Such a variation would be expected to produce a variation in the shape and the absolute normalisation of the muon lateral distribution. This point

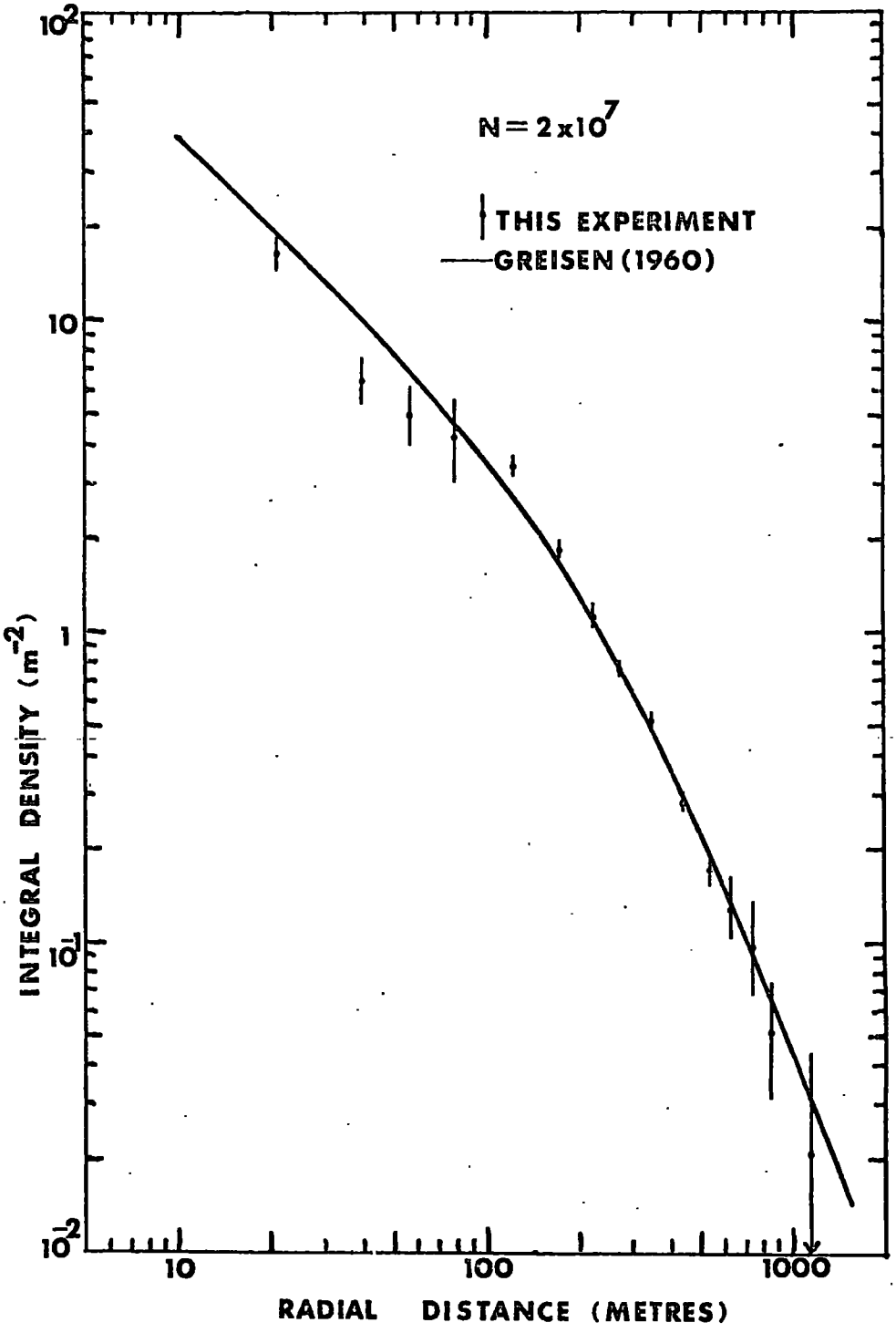
10^2
10
1
10^{-1}
10^{-2}
$N = 2 \times 10^7$
THIS EXPERIMENT
GREISEN (1960)
INTEGRAL DENSITY (m^{-2})
10
100
1000
RADIAL DISTANCE (METRES)

FIGURE 3.5

will be discussed further, in connection with the theoretical predictions of the lateral distribution of EAS muons, in section 6.2. 2.

3.3. 2 The Variation of Momentum Spectrum with Core Distance

The differential momentum spectra of muons in a number of intervals of core distance are shown, normalised for a shower size of 2×10^7 particles and a zenith angle of 22°, in figure 3.6. Corresponding integral spectra with an upper momentum limit of 500 GeV/c are shown in figure 3.7. These spectra refer to showers triggering the 500metre array, for which the shower size distribution is very narrow, i.e. 1.0 to 3.0×10^7 particles. Spectra at core distances of 50m. and 100m. from the smaller arrays are shown separately in figure 3.8. To obtain lateral distributions for muons of various threshold momenta, these two spectra have been normalised using the relation $N\mu \propto N_e^{0.75}$ and the resultant distributions are shown in figure 3.9, the broken lines indicating the points obtained by scaling. To obtain the form of the lateral distributions for core distances smaller than 50m., the 50m. spectrum has been resolved into spectra for core distances down to 10m. The superimposition of these spectra to give one spectrum at 50 metres is possible because of the slow change of shape of the spectrum with core distance for less than 100m.

3.3. 3 Variation of Spectrum with other EAS Parameters.

Only two EAS parameters, other than core distance, would be expected to cause a variation in the shape of the muon momentum spectrum, namely the shower size N_e, and the zenith angle of shower

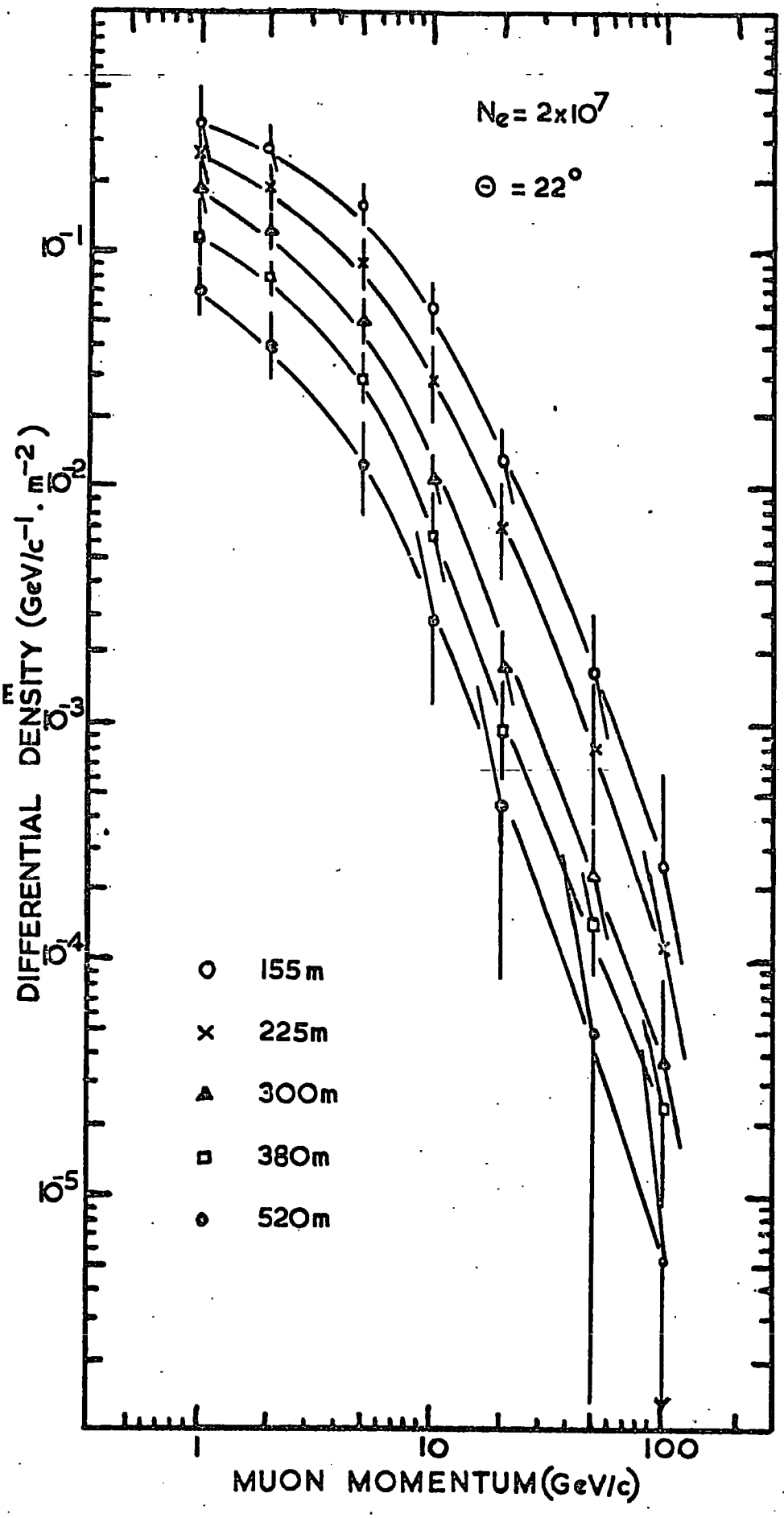
$N_e = 2 \times 10^7$
$\Theta = 22°$
$\overline{\sigma}_1$
$\overline{\sigma}_2$
$\overline{\sigma}_3$
$\overline{\sigma}_4$
$\overline{\sigma}_5$
DIFFERENTIAL DENSITY (GeV/c^{-1}. m^{-2})
155m
225m
300m
380m
520m
1
10
100
MUON MOMENTUM(GeV/c)

FIGURE 3.6

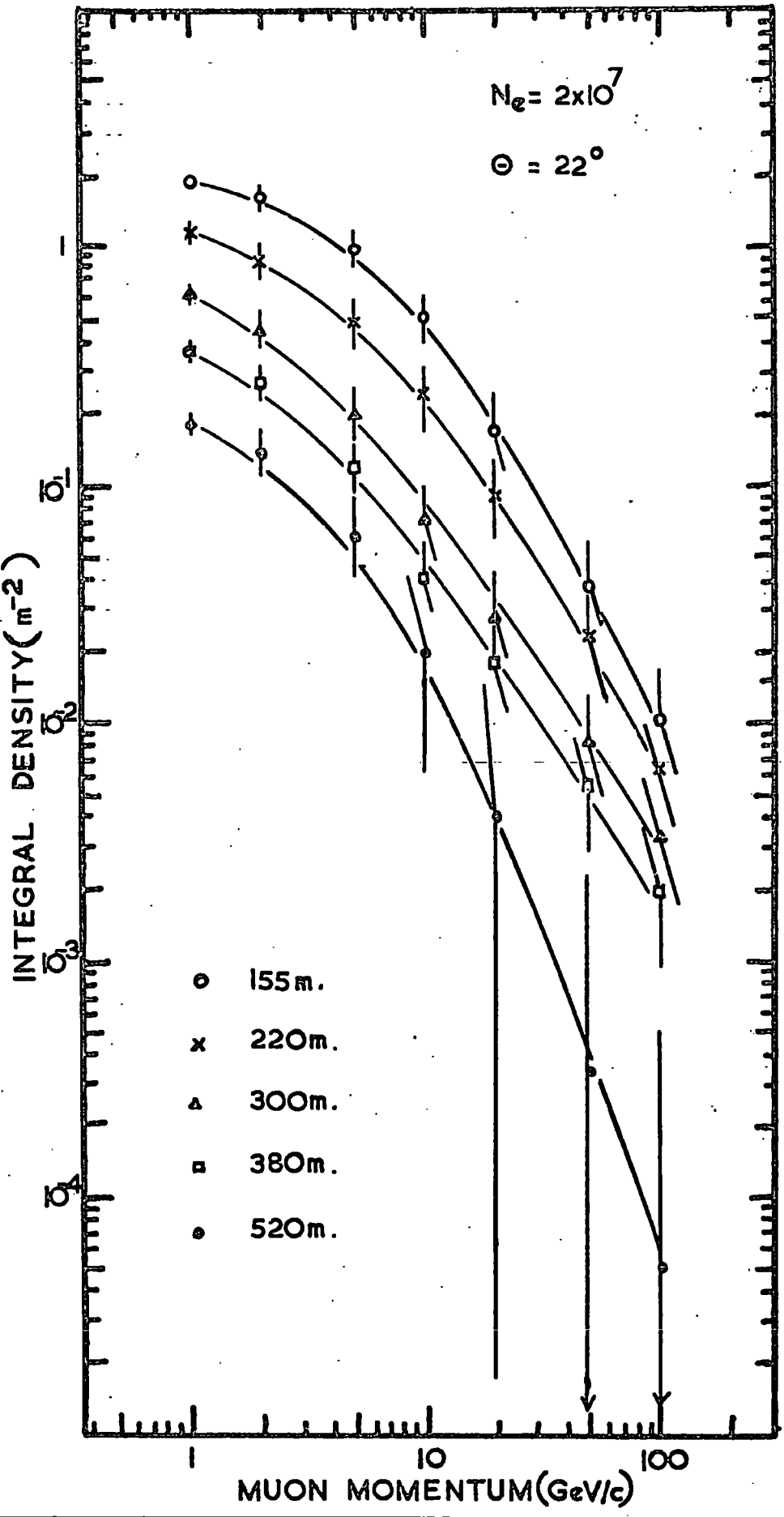
$N_e = 2 \times 10^7$
$\Theta = 22°$
INTEGRAL DENSITY (m^{-2})
$\bar{\sigma}_1$
$\bar{\sigma}_2$
$\bar{\sigma}_3$
$\bar{\sigma}_4$
155m.
220m.
300m.
380m.
520m.
1
10
100
MUON MOMENTUM (GeV/c)

FIGURE 3.7

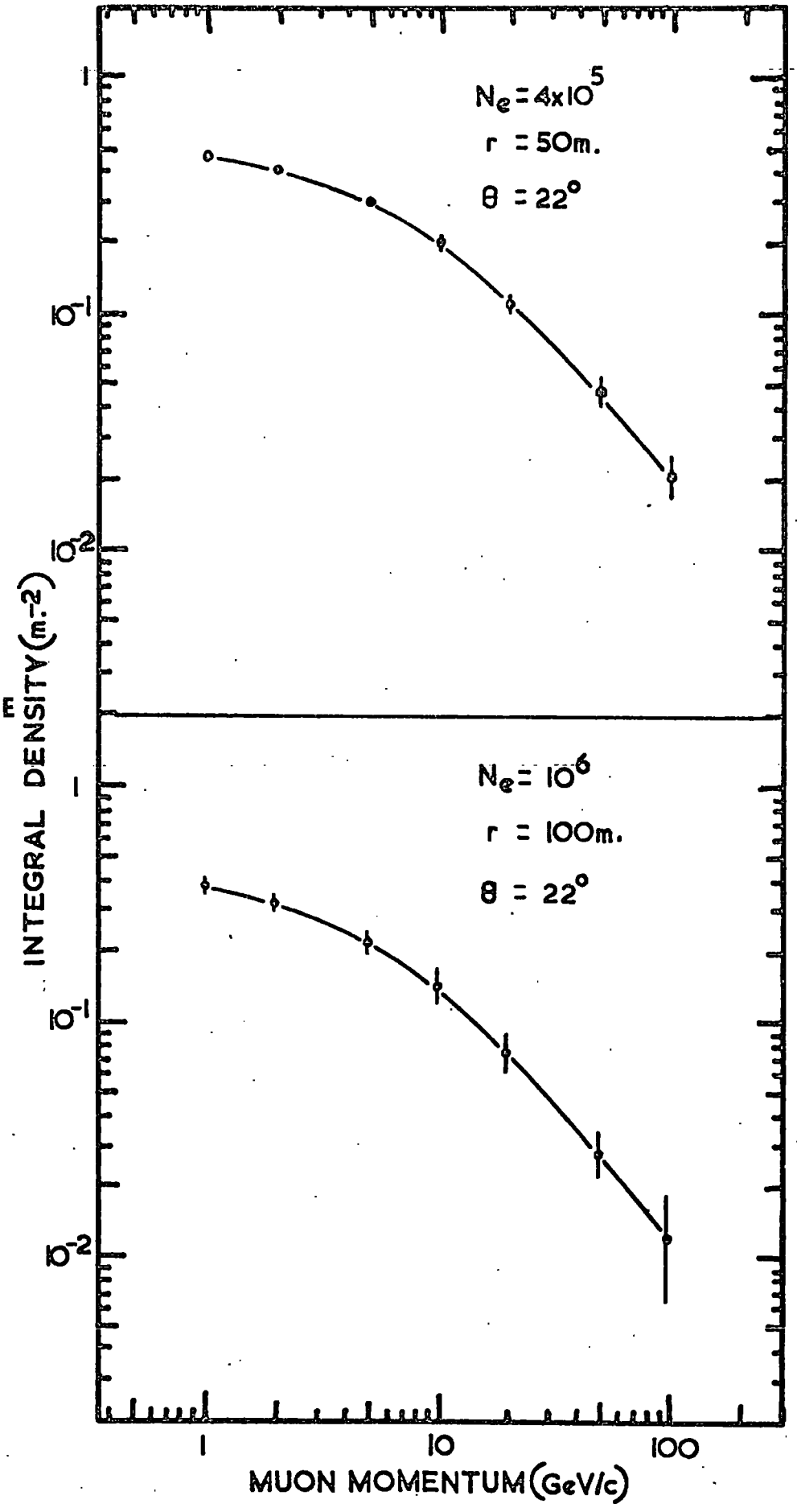
$N_e = 4 \times 10^5$
r = 50m.
θ = 22°
$N_e = 10^6$
r = 100m.
θ = 22°
INTEGRAL DENSITY (m^{-2})
1
10^{-1}
10^{-2}
1
10
100
MUON MOMENTUM (GeV/c)

FIGURE 3.8

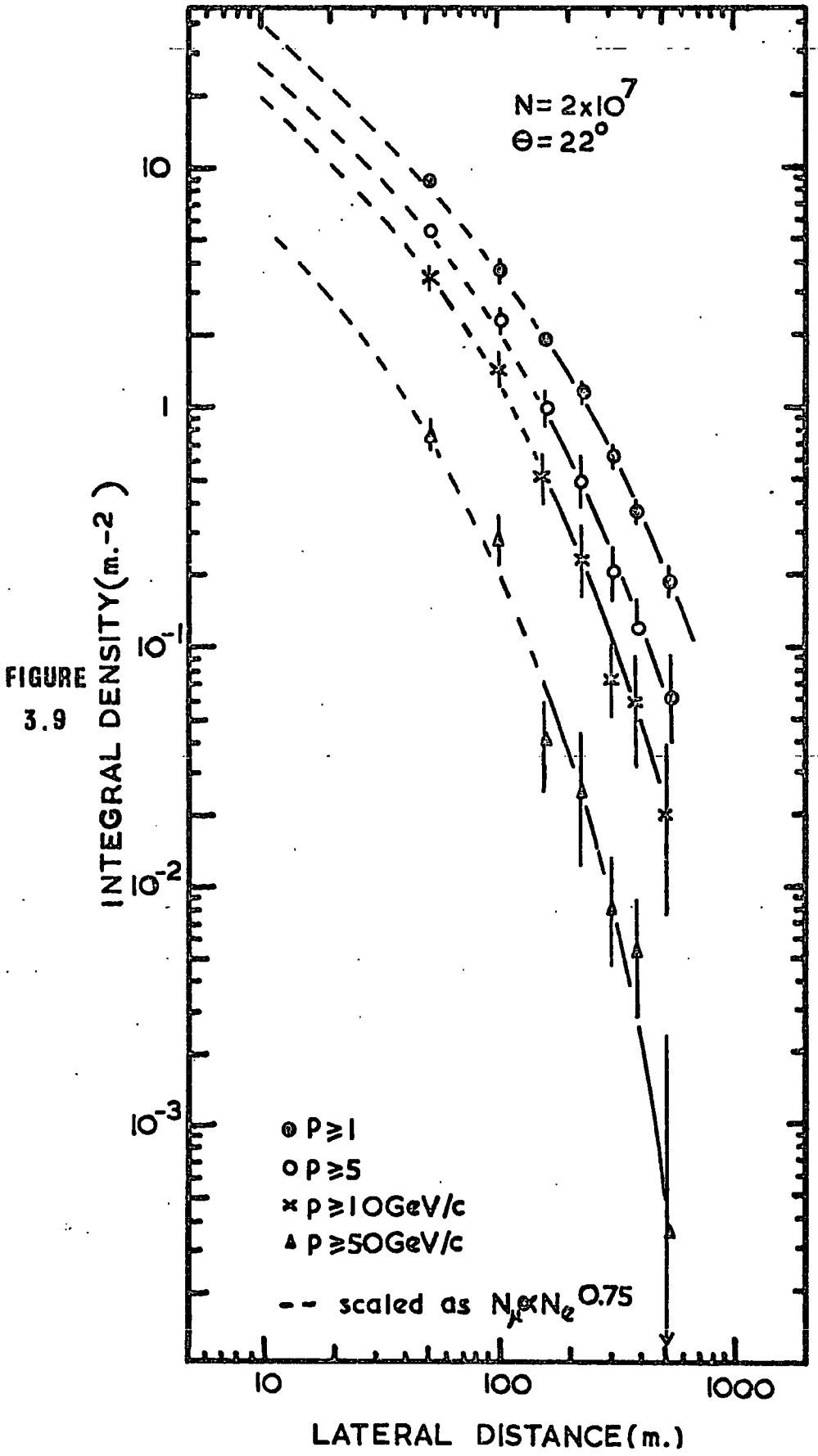
N= 2x10^7
Θ= 22°
10
1
10^-1
10^-2
10^-3
INTEGRAL DENSITY(m.-2)
⊙ p≥1
o p≥5
× p≥10GeV/c
▲ p≥50GeV/c
-- scaled as N_μ∝N_e^0.75
10
100
1000
LATERAL DISTANCE(m.)

FIGURE 3.9

arrival θ. The other quantities, ϕ the azimuth shower arrival angle, and X and Y the cartesian co-ordinates of the impact point of the shower core with the plane of the ground have been examined to discover any systematic effect on the momentum spectrum, but no effect has been found.

The shower size, N_e, through its connection with the composition of primary cosmic rays, and zenith angle θ, through its variation of the atmospheric depth might be expected to cause observable variations in the shape of the momentum spectrum. To investigate the variation, however, the muons must be sorted into intervals of these parameters, adjusted to compensate for the correlated variation in core distance. No significant variation is found. A variation cannot be excluded, but it could only be detected by a very much larger sample of data.

One further EAS characteristic which is measured by the Haverah Park 500 metre array is R, the radius of curvature of the shower front. No variation in the shape of momentum spectrum is found with this parameter, which may be related to the average height of production of muons, suggesting that the majority of the showers observed posses similar true shower front curvatures, the apparent differences in curvature being caused by errors in the timing of the arrival of the shower front at the detectors.

3.3.4 The Average Properties of EAS Muons.

The average properties of EAS muons are those which, because of the relative simplicity of the apparatus required, have been

measured most often, and so can provide a rough check of the accuracy of the present measurements.

3.3. 4 - 1 The Total Number of Muons in a Shower.

The total number of muons in a shower is obtained by evaluation of the integral:

$$N\mu\ (\geqslant \rho) \quad = \int_0^{\infty} f\mu\ (r, \geqslant \rho)\ 2\pi r\ dr \qquad \ldots 3.3.1$$

where $f\mu$ is the lateral distribution of muons of momenta not less than P. In this experiment, the limits of integration are taken to be 1 metre to 1000 metres, the form of the lateral distributions for distances outside the regions of measurement being obtained by extrapolation. The errors incurred by this extrapolation are expected to be small because of the lowweight of the product $f\mu(r, \geqslant \rho) \times 2\pi r$ in these regions. The value of $N\mu\ (\geqslant \rho)$ has been found using equation 3.3. 1 for a number of threshold momenta, and the data is well fitted by the Bennett and Greisen (1961) relation:

$$N\mu\ (\geqslant \rho) \quad = \quad 1.9 \times 10^5 \times (N_e/10^6)^{\frac{3}{4}} \times \left(\frac{2}{p+2}\right)^{1.3} \qquad \ldots 3.3.2$$

3.3. 4-2 The Total Momentum Carried by the Muon Component.

The total momentum carried by muons in an EAS is obtained by evaluating:

$$Q_T = \int_0^{500} S_T(p)\ dp \qquad \ldots 3.3.3$$

where $S_T(p)$ is the total differential momentum spectrum of EAS muons, which is easily obtained from equation 3.3. 2:

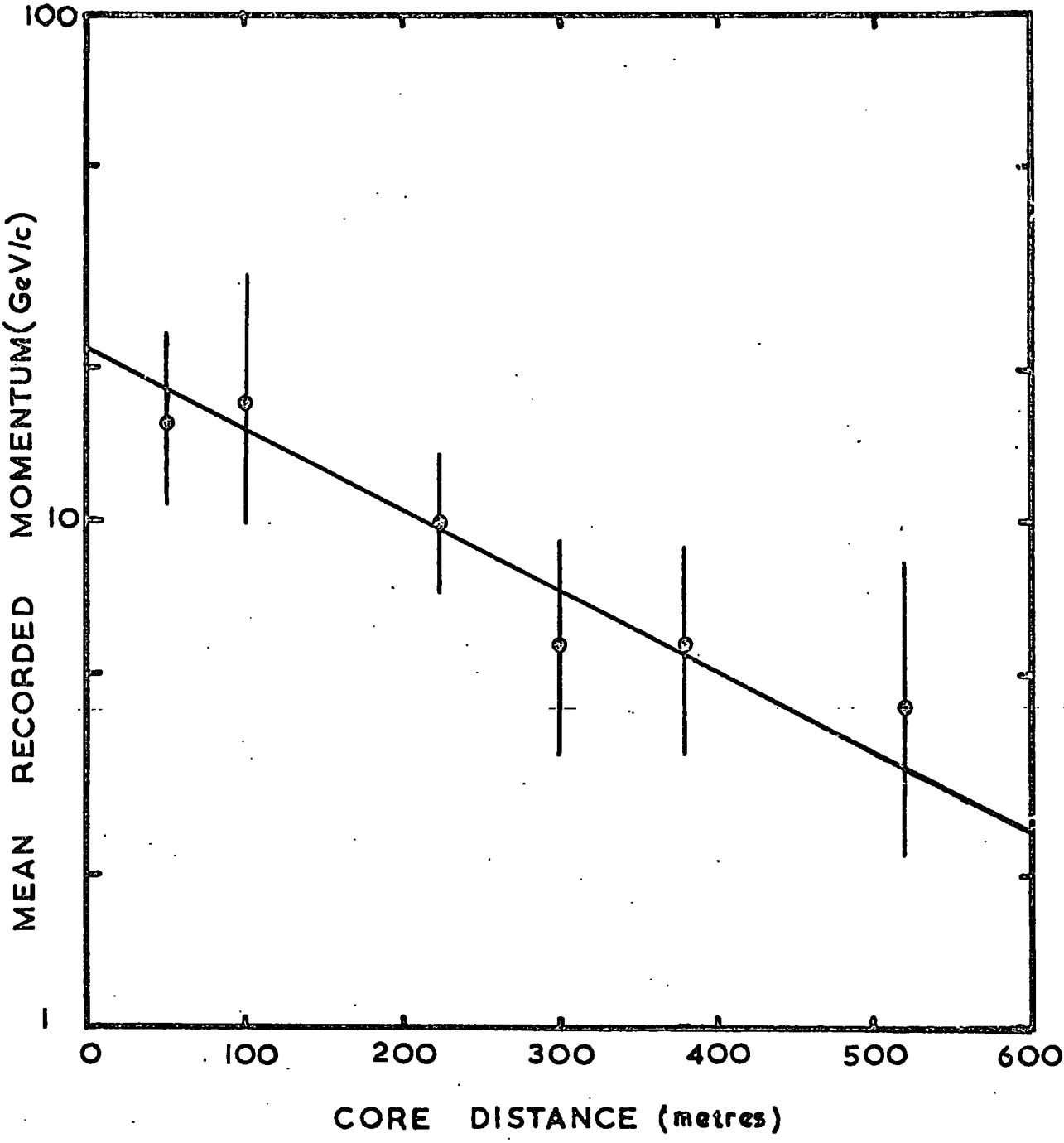
100
10
1
MEAN RECORDED MOMENTUM (GeV/c)
0
100
200
300
400
500
600
CORE DISTANCE (metres)

FIGURE 3.10

$$S_T(p)\,dp = 1.23 \times 10^5 \left[\frac{N_e}{10^6}\right]^{0.75} \left[\frac{2}{p+2}\right]^{2.3} dp \qquad \ldots 3.3.4$$

Evaluation of equation 3.3. 3 within the momentum limits 0 to 500 GeV/c gives:

$$Q_T = 1.2^{+0.6}_{-0.5} \times 10^7 \text{ GeV/c}$$

Since this value is not sensitive to the shape of the momentum spectrum for momenta greater than 100 GeV/c, this region has been allowed for by extrapolation.

3.3. 4-3 The Mean Momentum of EAS Muons

Since the shape of the momentum spectrum of EAS muons varies with core distance there will be a corresponding variation of mean momentum. The variation of this mean momentum $\bar{q}(r)$ may be obtained from:

$$\bar{q}(r) = \frac{\int_0^{500} S(p,r).p\,dp}{\int_0^{500} S(p,r)\,dp} \qquad \ldots 3.3.5$$

where $S(p, r)$ is the differential muon momentum spectrum at a core distance r. This equation cannot be evaluated exactly without a knowledge of the form of the momentum spectrum for momenta less than 1 GeV/c. The shape of the spectrum in this region is not known, so the evaluation of equation 3.3. 5 has been made with a lower momentum limit of 1 GeV/c. The variation of mean momentum with core distance is shown in figure 3.10 and is fitted well by a relation:

$$\bar{q}(r) = 22 \times \exp(-0.0037 \times r) \qquad \ldots 3.3.6$$

with $\bar{q}$ in GeV/c when r is measured in metres.

The mean momentum of all muons at a given distance may be obtained approximately by assuming that a constant fraction of muons, independent of core distance, possess momenta less than 1 GeV/c and a mean momentum of 0.5 GeV/c. The result is not sensitive to this last figure as the momentum carried by these particles is negligible. The fraction may be obtained from equation 3.3. 2 and is found to be 41%. An approximate form of $\bar{q}$ (r) may then be given as,

$$\bar{q}\ (r, p \geq 0\ \text{GeV/c}) = 15.6 \times \exp\ (-0.0037 \times r) \qquad \ldots 3.3.7$$

The mean momentum of all muons in an EAS is found to be

$$\bar{p} = 6.7^{+3.2}_{-2.0}\ \text{GeV/c}$$

3.4 Investigation of Possible Sources of Bias

In order to derive the momentum spectra, approximations and assumptions have been occasionally made and in the following sections the extent of any such biases is examined.

3.4.1 Muon Interactions

In the analysis of the spectra, it is assumed that muons lose energy in their passage through iron, at a rate of 1.8 MeV $gm.^{-1}$ $cm.^{-2}$ for a muon momentum of 0.5 GeV/c, rising smoothly to 2.8MeV $gm.^{-1}$ $cm.^{-2}$ for 100 GeV/c. However, there is a finite probability that a muon will lose a considerable fraction of its energy in one interaction. At the momenta within the range of measurement of the spectrograph, the major energy loss mechanism is collision loss; other, fluctuating, contributions being on average $\sim 10^{-3}$ of the collision loss at 1 GeV/c to $\sim$ 0.3 at 100 GeV/c muon momenta. Low energy muons

are therefore correctly allowed for, and the effect on the observed density of 100 GeV/c muons, calculated from results obtained during the interpretation of muon-induced bursts in chapter 5, is an underestimate of the density by $\sim 5\%$.

3.4.2 The Loss of Low Energy Muons.

The loss of low energy muons can, by normalisation, affect the density of muons of momentum 100 GeV/c. Low energy muons can be scattered laterally in such a way that the half-tracks intersect outside the magnet, and be rejected (see section 3.1.2).

It can be shown that the probability, P, that a muon, after traversing x gm.cm.$^{-2}$ of scattering material and possessing an r.m.s. scattered angular deflection $\overline{\theta^2}y$, will appear at y gm.cm^{-2}. lateral displacement with a projected angular deflection θy is given by:

$$P(x,y,\theta y)dy\,d\theta y = \frac{\sqrt{3}}{\pi} \times \frac{1}{\overline{\theta^2}_y . x} \times \exp\left\{ \frac{-2}{\overline{\theta y_o^2}\, x} \times \left\{ \frac{\theta y^2}{x} - \frac{3y.\theta y}{x^2} + \frac{3y^2}{x^3} \right\} \right\} d\theta y dy \qquad \ldots 3.4.1$$

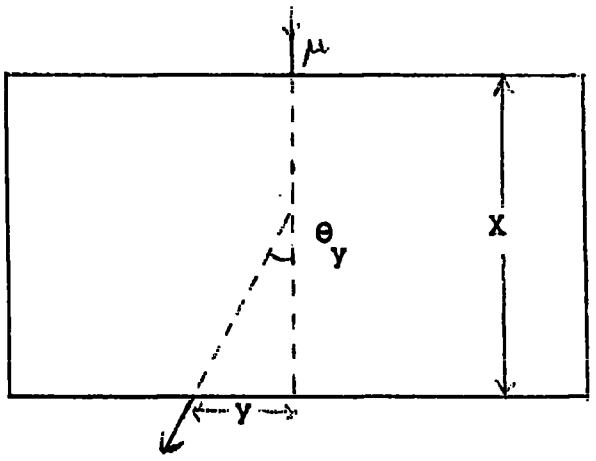

In the presence of a magnetic field, the muon trajectory follows the arc of a circle, and a full analysis reveals that the probability that a low energy muon will be wrongly rejected is:

$$P^1 = \int_{-\Delta}^{\Delta}\int_{A}^{\infty} P(x,y,\theta y)dy\ d\ \theta y + \int_{0}^{\Delta}\int_{-\infty}^{B} P(x,y,\theta y)dy\ d\ \theta y + \int_{-\Delta}^{0}\int_{B}^{\infty} P(x,y,\theta y)\ dy\ d\ \theta y \qquad \ldots 3.4.2$$

where $A = x.[\tan \theta y - \tan (\Delta\psi m/2)]$, and

$B = -x \,.\, \tan (\Delta\psi m/2)$

$\Delta\psi m$ = angular deflection of a muon in the absence of coulomb scattering.

Δ = maximum deflection allowed by acceptance function.

The evaluation of equation 3.4. 2 shows that the density of 1 GeV/c muons is underestimated by 1%.

3.4. 3 "Event" Selection.

The selection of muons is made at three stages; before drawing a frame from a film record, before track simulation, and before final acceptance of a muon. Each stage has been examined for sources of bias. A typical film, chosen at random, containing 450 spectrograph exposures has been scanned during the routine collection of data. The film has subsequently been carefully drawn, frame by frame, to ascertain the scanning efficiency. It is found that about 1% of muons are lost during the initial scanning. There is no evidence, however, for a momentum bias in those so lost. In carrying out stage 2 of the selection, care is taken to select any event which could

contain an acceptable muon. Those drawings rejected have been filed and have subsequently been rescanned, but no appreciable number of muons have been missed. The final selection stage has been closely scrutinised for bias. All accepted muons have been checked by three experimenters for strict adherence to the selection conditions of section 3.1.2. About 5% of all muons passing the original routine selection tests have been found later to be unacceptable, due largely to marginal acceptance and obscuration. No momentum bias has therefore been found.

3.4.4 EAS Selection.

It has been suggested (de Beer et al.,1966) that EAS arrays with few, well-spaced detectors will have a bias towards selecting showers with lateral particle distributions flatter than average, because the muon lateral distribution reported by Khrenov (1962), measured on a well-filled Geiger counter array, is steeper than the corresponding distribution from the present experiment. The possibility of this type of bias affecting the measurements of the muon energy spectra has been investigated by J.C. Earnshaw (private communication), and he has shown that the average exponent of the shower particle lateral distribution is 3.13 for all showers and 3.04 for showers in which a high energy muon is observed in the spectrograph. The normal range of exponent from shower to shower, for showers with zenith angles less than 40^{0}, is 2.0 to 4.0, hence the difference is insignificant. It is concluded that the showers containing high

energy muons are typical of all showers triggering the array, but it is difficult to relate the average exponent to that observed in Geiger-counter arrays because of the different characteristics of the detectors. The relative steepness of Khrenov's lateral distribution will be discussed in section 3.5.

3.4.5 Track Reconstruction.

Measurements of the random error inherent in the analysis of tracks delineated by neon flash-tubes have already been described. However, a source of bias not included in the analysis could arise from the mechanics of track reconstruction. The co-ordinates of the best-fit trajectory on the flash-tube simulator are obtained from the intersection points of the track with two arbitrary measuring planes. These co-ordinates are read to an accuracy corresponding to an angular interval of approximately 0.08^{0}, the size of which depends on the inclination of the track. This may cause a bias in the deflection spectrum for very small deflections.

To check this effect, a computer programme produced 5000 artificial tracks distributed with flat ψ_0 and $\Delta\psi$ distributions. The expected number of tracks in the lowest deflection interval if the deflections are not quantised is 848. The number of tracks expected for quantised deflections is 840. For larger deflections the effect is smaller. It is concluded that there is no appreciable momentum bias introduced by quantising angles.

3.4.6 Obscuration and Contamination.

Two further possible sources of error may arise from a) muons being obscured by electrons and other muons at small core distances and b) the contamination of a spectrum by unassociated cosmic ray muons.

The number of cosmic ray muons incident on and accepted by the spectrograph per exposure is:

$$N\mu(P)dp = \dot{N}\mu^{1}(P) \times 2\times10^{4} \times \tau \times \int_{0}^{40^{\circ}} B(\theta)\cos^{2}\theta d\theta \int_{0}^{30^{\circ}} A(\theta,P)\cos^{2}\theta \, d\theta \, dp \quad \ldots 3.4.3$$

where τ is the sensitive lifetime of the flash-tubes, B is the momentum independent acceptance function and A the momentum dependent acceptance of the spectrograph. Evaluation of equation 3.4.3 gives the probability of a single muon's acceptance as 0.4% per exposure. Approximately 3000 random triggers have been applied to the spectrograph and a frequency of 0.5% observed. The probability of contamination is reduced considerably by the selection condition (b) in section 3.1.2, which demands that a muon be within 20° of the projected direction of the normal to the shower plane at the spectrograph. The effect on a spectrum of the inclusion of less than 0.5% of unnassociated muons will be negligible. As the cosmic ray muon spectrum is steeper than the majority of the EAS muon spectra the only effect could be a marginal steepening.

The effect on the muon momentum spectra at large core distances of obscuration of muon tracks is also negligible. Total obscuration of all tracks is not observed for core distances greater than 10m.

At intermediate distances the acceptance condition (e) of section 3.1. 2, i.e. that there must not be two (or more) equally probable alternative half-tracks,can cause a muon to be rejected. Low energy muons will be affected most because the higher angle between incident and emergent half-tracks increases the probability of a spurious intersection of uncorrelated half-tracks. The effect on the spectrum of this bias is small, the fraction of muon tracks which cannot be estimated because of obscuration being less than 1%.

3.4. 7 Systematic Instrumental Effects.

A search has been made for systematic biases due to:

(a) Misalignment of flash-tube trays relative to the magnet.

(b) Misalignment of flash-tube trays relative to each other.

(c) Non-correspondence of flash-tube simulator and flash-tube trays.

(d) Internal inconsistencies in the flash-tube simulator.

(e) Measurements of the flash-tubes used in the computer programme processing the co-ordinates obtained from the track simulator.

All but (e) were initially measured at length and have since been checked by examining the symmetry of distributions in projected muon arrival direction and of the distributions in deflection.

With the distributions obtained, an asymmetry of less than 0.03^{o} in angle could be detected. No such asymmetry is found. The computer programme has been checked by comparing a sample deflection distribution with that obtained by inserting the co-ordinates of the mirror images of the same tracks in the vertical plane. No errors which would produce systematic biases have been found.

3.4. 8 The Unassociated Cosmic Ray Muon Spectrum.

A final check of the whole procedure is the measurement of the momentum spectrum of unassociated cosmic ray muons, which is well known for momenta less than 100 GeV/c. The Haverah Park Spectrograph has been triggered by a Geiger counter telescope, placed above the spectrograph, for a sufficient time to collect a sample of muons of a similar size to the typical sample for an EAS muon spectrum. The momentum spectrum has been derived using the same procedure as described in section 3.2., and is shown, compared with that of Osborne et al. (1964a) in figure 3.11. There is good agreement between the spectra and it is concluded therefore that the analysis provides an accurate assessment of a muon momentum spectrum, at least for momenta up to 50 GeV/c.

3.4. 9 Conclusion.

Since the overall effect on the observed momentum spectra of the biases discussed in the previous sections is small compared with the statistical errors, no corrections have been made to the observed spectra.

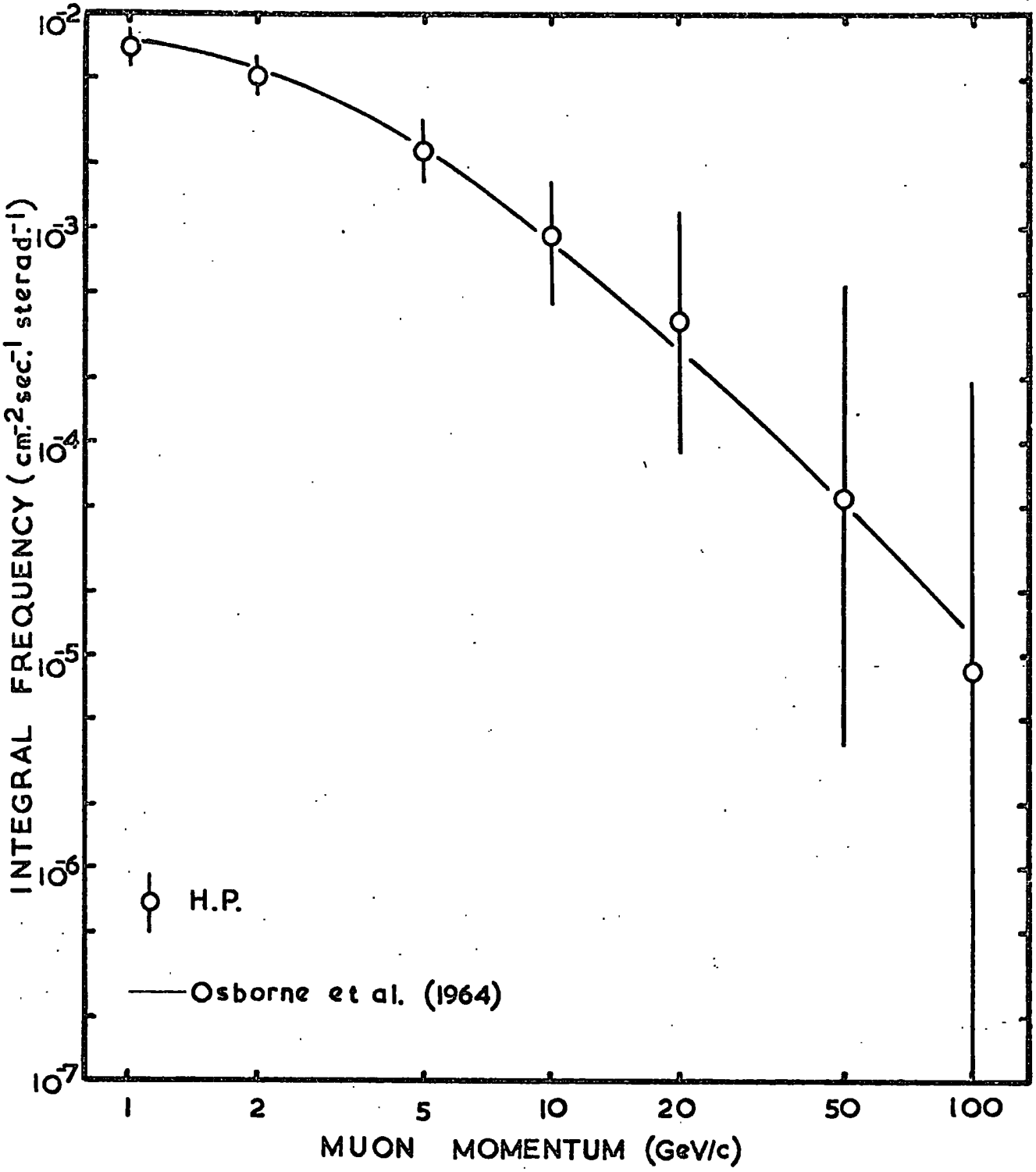
INTEGRAL FREQUENCY (cm.$^{-2}$sec.$^{-1}$ sterad.$^{-1}$)
10^{-2}
10^{-3}
10^{-4}
10^{-5}
10^{-6}
10^{-7}
H.P.
Osborne et al. (1964)
1
2
5
10
20
50
100
MUON MOMENTUM (GeV/c)

FIGURE 3.11

3.5. Previous Measurements.

3.5.1 Detailed EAS Muon Spectra.

Comprehensive, directly comparable, energy spectra or lateral distributions have been measured by only two groups, those at Moscow State University and Cornell University. The results of the Moscow group are shown in figure 3.12, compared with the relevant lateral distributions from 3.8.(Khrenov, 1962, 1963).

The results fit the formula:

$$\rho_\mu(N,r) = k.N^{\alpha}.r^{-n}. \exp(-r^2/r_0^2) \qquad \ldots 3.5.1$$

where $k = 5.8 \times 10^{-5}$, $n = 0.7 \pm 0.1$, $\alpha = 0.85 \pm 0.1$,

$r_0 = 195 \pm 15$ for $E\mu \geqslant 5$ GeV.

and $k = 4.1 \times 10^{-5}$, $n = 0.7 \pm 0.1$, $\alpha = 0.85 \pm 0.1$,

$r_0 = 155 \pm 15$ for $E\mu \geqslant 10$ GeV.

These results were obtained from an array with hodoscoped G - M detectors under 20 and 40 metres water equivalent of earth, in the centre of a G - M EAS array. For core distances greater than 10 metres, the zenith angle of arrival of each shower was not known, and so the average core distances and muon threshold energies were calculated on an assumed shower zenith angle variation and a lateral distribution which did not vary markedly with shower zenith angle. Data on the lateral distributions were obtained directly for core distances less than 100m. The point given at 250m. was obtained by triggering the muon detecters by a six-fold G - M array with a 250m spacing. The mean distance of showers triggering this array was found by calculation to be 250m. In view of the uncertainties introduced by

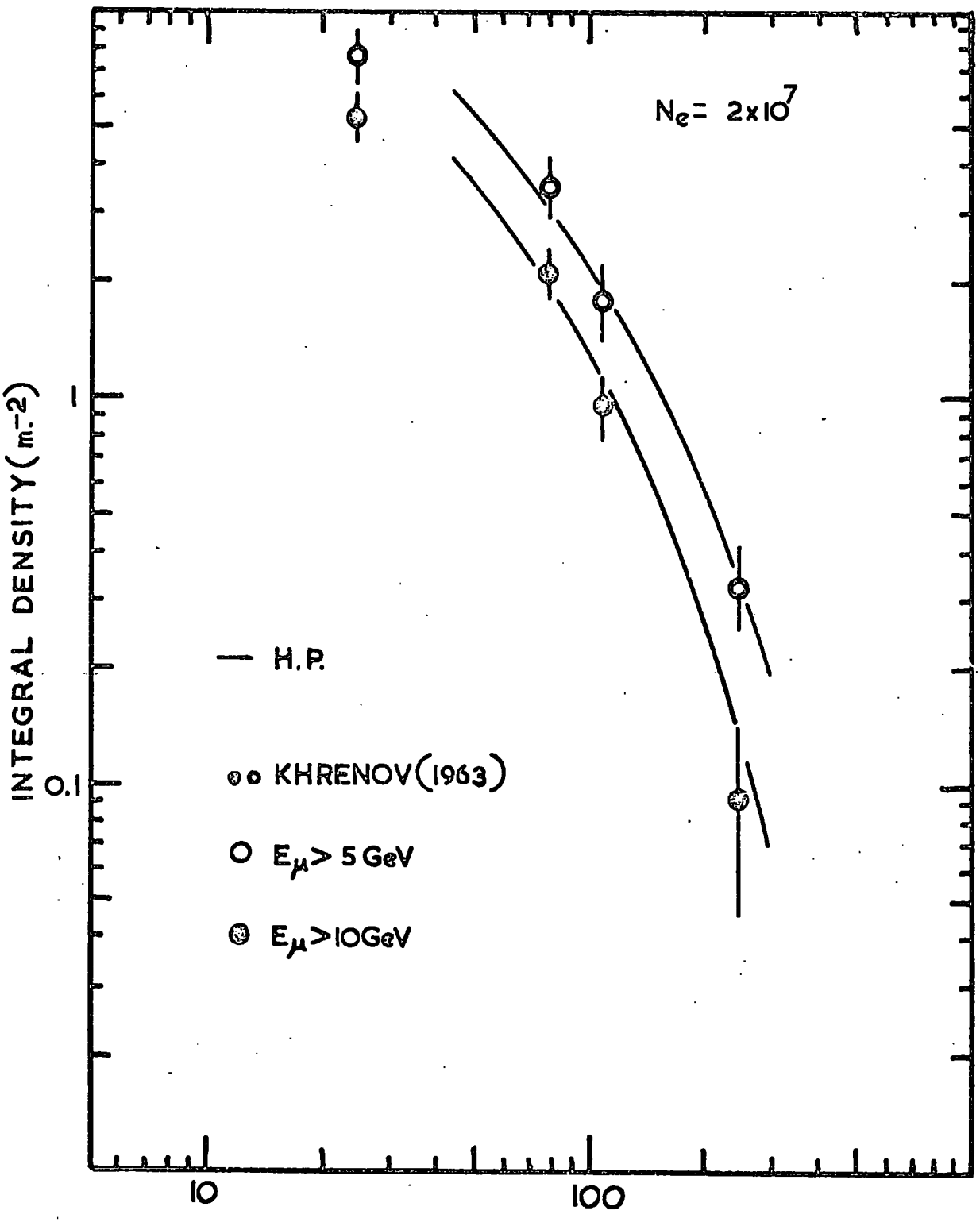
$N_e = 2 \times 10^7$
INTEGRAL DENSITY (m^{-2})
1
0.1
— H.P.
oo KHRENOV (1963)
O $E_\mu > 5$ GeV
⊗ $E_\mu > 10$ GeV
10
100
LATERAL DISTANCE (m.)

FIGURE 3.12

these assumptions, the agreement between the lateral distributions measured at Moscow and those at Haverah Park is good.

The most comprehensive measurement of muon momentum spectra in EAS is that of Bennett and Greisen (1961), which is based on measurements of the 1 GeV/c lateral distribution measured at Cornell University and by Clark et al. (1958), and the measurements of the integral momentum spectra of muons in the range 1 to 20 GeV/c using an air-gap magnetic spectrograph. The integral points of Bennett and Greisen are shown in figure 3.13, compared with the lines best fitting the data of the present experiment. Bennett and Greisen express their results in the form of a relation giving the density of muons $\Delta\mu$ in a shower of size N_e at a core distance r and a momentum threshold p:

$$\Delta\mu\,(N,r,\geq p) = \frac{14.4 x r^{-0.75}}{(1+r/320)^{2.5}}\left(\frac{N}{10^6}\right)^{0.75}\left(\frac{51}{p+50}\right)\left(\frac{3}{p+2}\right)^{\gamma} \qquad \ldots 3.5.2$$

$$\text{where } \gamma = 0.14 \times r^{0.37}$$

At large core distances and muon momenta, this distribution is appreciably flatter than that given by Khrenov, equation 3.5.1. Equation 3.5.2 fits the present data well in shape but the absolute intensity is somewhat lower, a coefficient of 23.6 instead of 14.4 being needed to obtain the fit shown in figure 3.13. This difference in normalisation is difficult to explain except in terms of differences in the mean shower sizes of the measurements.

The core distances given by Bennett and Greisen for their spectra were obtained in a similar way to that used by Khrenov for

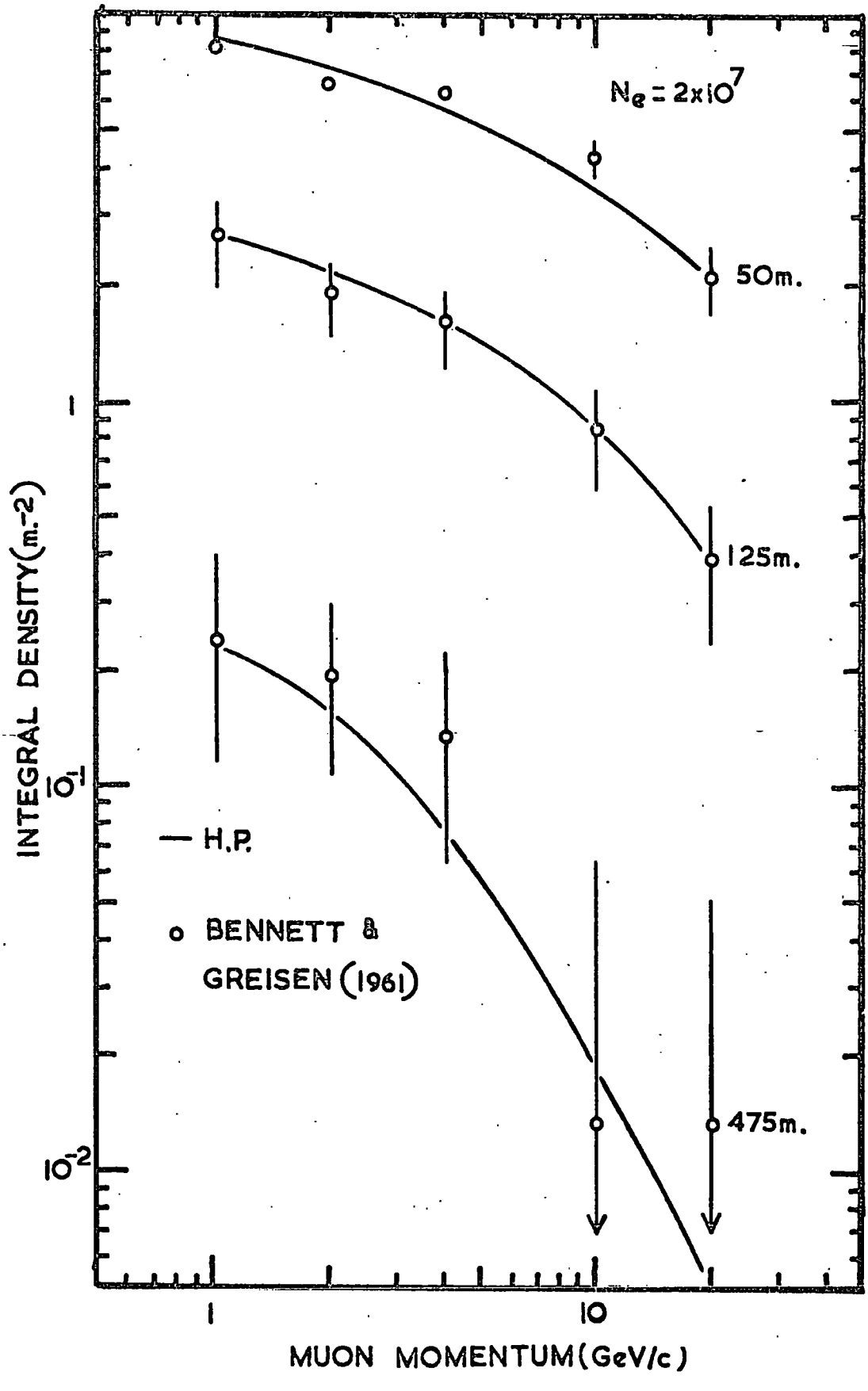
$N_e = 2 \times 10^7$
50m.
125m.
475m.
— H.P.
o BENNETT & GREISEN (1961)
INTEGRAL DENSITY ($m.^{-2}$)
1
10^{-1}
10^{-2}
1
10
MUON MOMENTUM (GeV/c)

FIGURE 3.13

his largest array. The location of the core was not determined for each shower, but the mean core distances were calculated for showers which triggered given configurations of detectors. The width of the probability distribution in core distance for a set of detector coincidences is very large in this case as a coincidence between only one scintillator and the spectrograph was demanded. A careful analysis can still, however, produce accurate lateral distributions, given the precise form of the muon and electron lateral distribution function. The shapes of the distributions used by these workers are now well established.

A measurement of the muon lateral distribution for a threshold energy of 40 GeV has been reported by Barnaveli (1964 and 1965) for a unique shower size and a small range of core distances. As can be seen in figure 3.14 , the agreement between the points given by Barnaveli and the corresponding lateral distribution from the present experiment is good, except for the point at 80 metres. The EAS array used by Barnaveli had a diameter of 40 metres, so that the observed slight discrepancy could indicate a systematic error in the positions of distant cores of about 30m.

3.5.2 Average Properties of EAS Muons.

The average properties measured in this experiment are Q_T , the total momentum carried by muons in a shower, $N_\mu (> p)$ the total integral momentum spectrum of EAS muons, and $\bar{p}$, the mean EAS muon momentum. The results of other workers are shown, compared

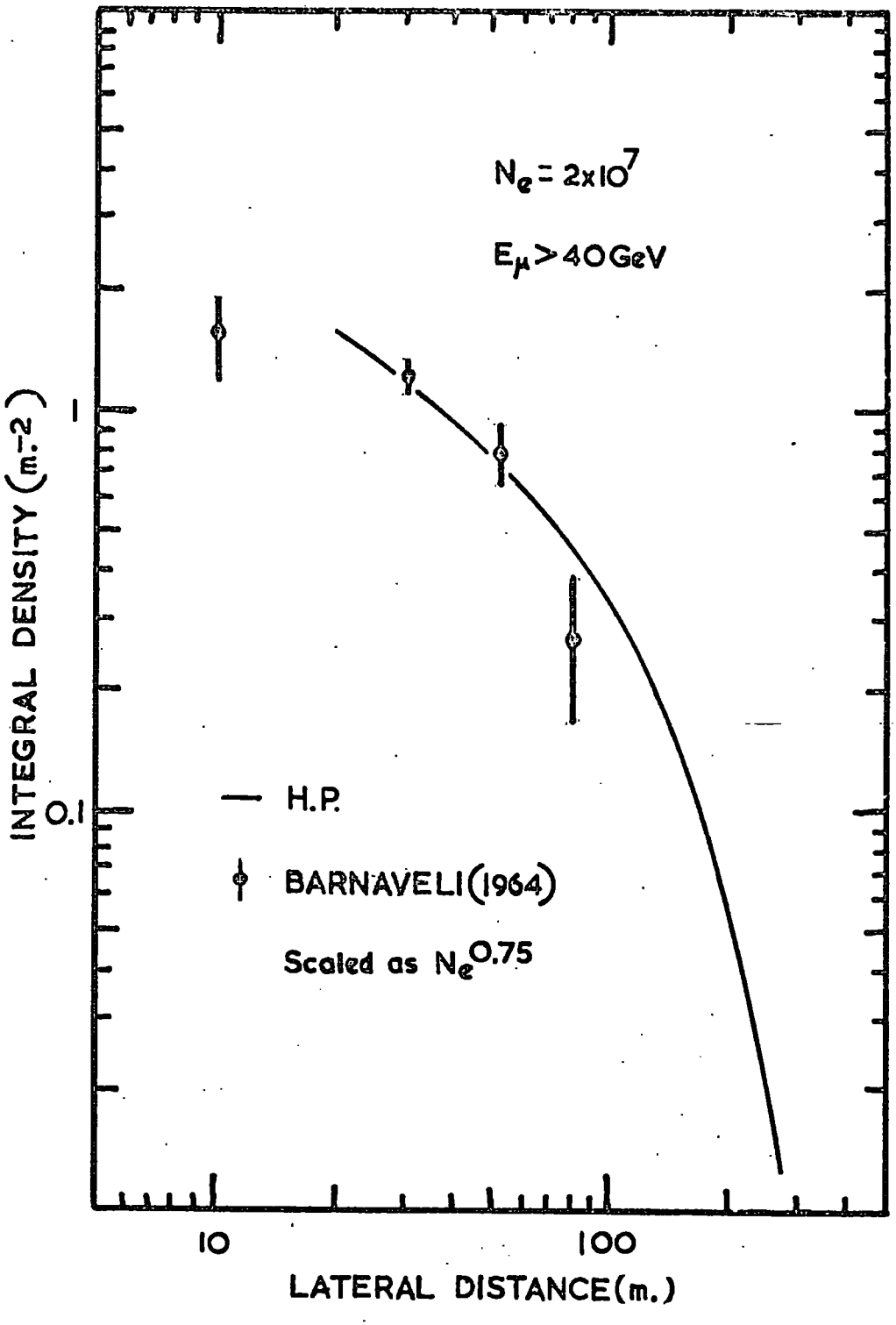
$N_e = 2 \times 10^7$
$E_\mu > 40$ GeV
INTEGRAL DENSITY (m^{-2})
1
0.1
H.P.
BARNAVELI (1964)
Scaled as $N_e^{0.75}$
10
100
LATERAL DISTANCE (m.)

FIGURE 3.14

Table 3.1

Author	Ne	QT	$\overline{P}$	Nμ(> 0)	γ
This experiment	2×10^7	$1.2^{+0.6}_{-0.5}\times10^7$	$6.7^{+3.2}_{-2.0}$	$1.9\pm0.2\times10^6$	1.3 ± 0.1
Bennett and Greisen (1961)	—	9.0×10^6	7.0	1.3×10^6	1.29
Greisen (1960)	—	9.0×10^6	5.4	1.7×10^6	1.37
Khrenov (1962)	10^6	7.2×10^6	5.0	1.45×10^6	1.40
Chatterjee (1966)	5×10^5	$8.8^{+2.2}_{-1.5}\times10^6$	$4.0^{+1.0}_{-0.7}$	2.2×10^6	1.5 ± 0.1
Barnaveli (1965)	6×10^5	—	—	—	1.1 ± 0.1

Ne is the meon shower size at which the measurements were performed. N.B. the data of Chatterjee et al.(1966) have been scaled as $N\mu \propto N_e^{0.75}$.

with the results of the present experiment, in table 3.1. They are normalised to a shower size 2×10^7, using the scaling law of the author, or if none is given, $N_\mu \propto N^{0.75}$. The exponent γ is the exponent of the total integral momentum spectrum:

$$N_\mu (\geq p) = \text{Const.} \times \left(\frac{2}{P+2}\right)^{\gamma}$$

It can be seen that there is a good agreement between all the experimental results. The points from which they are derived are shown, compared with the points obtained in the present experiment, in figure 3.15. For future analysis it will be assumed that the total integral momentum spectrum of EAS muons is well represented by equation 3.3. 2:

$$N_\mu (\geq p) = 1.9 \times 10^5 \times \left(\frac{N}{10^6}\right)^{0.75} \left(\frac{2}{p+2}\right)^{1.3}$$

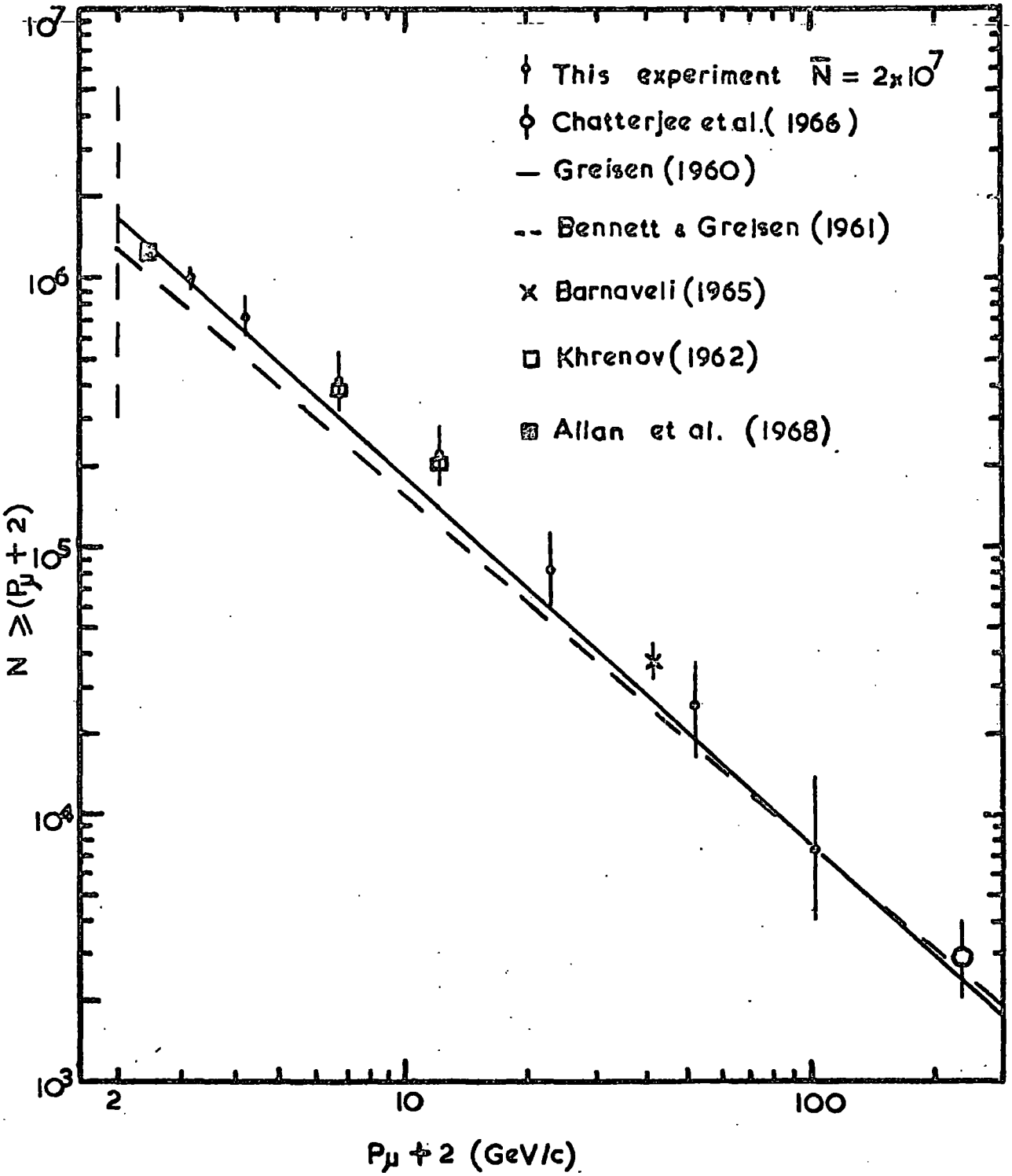
This experiment $\bar{N} = 2 \times 10^7$
Chatterjee et al. (1966)
Greisen (1960)
Bennett & Greisen (1961)
Barnaveli (1965)
Khrenov (1962)
Allan et al. (1968)
$N \geq (P_\mu + 2)$
10^7
10^6
10^5
10^4
10^3
2
10
100
$P_\mu + 2$ (GeV/c)

FIGURE 3.15

Chapter 4

The Charge Ratio of EAS Muons.

4.1 Introduction

A knowledge of the charge ratio of EAS muons is important if the properties of the muons observed are to be used to obtain information on the nature of the unstable secondaries from ultra-high energy nuclear interactions. The existing experimental data on the nature of such secondaries has been obtained mainly from studies on jets, observed in emulsions, and from cosmic ray muon measurements. A ratio of muon charges significantly different from unity has been established for the majority of unassociated cosmic ray muons. This has been interpreted by MacKeown (1965) as evidence for a proportion of kaons to pions of 1:5, which is similar to the results from accelerator and jet studies, e.g. Aly et al.(1960). Bennett and Greisen (1961) report that the charge ratio of all muons in an air shower is $\mu^+ / \mu^- = 0.97 \pm 0.07$. This led the authors to suggest that pion production exceeds kaon production in the developing nuclear cascade by at least an order of magnitude. It may be expected, however, that the muons which have decayed from kaons produced in the early interactions of the primary cosmic ray may exhibit a charge asymmetry at large core distances in EAS. This follows from measurements such as those of Lock (1964) which shows that heavy mesons created in nucleon-nucleon collisions may possess, on average transverse momenta exceeding those of pions. This, combined with a

kaon's greater instability, would increase the proportion of muons originating from kaons at large core distances.

The charge ratio will be enhanced further by the effect of the positive charge on the primary cosmic ray. This enhancement will be very small, except for those muons which originate from the particles created in the cosmic ray's first interaction. If the primary energy, hence the multiplicity, is low, the effect will be even more marked, but will be somewhat offset by the smaller mean atomic weight of the primaries.

4.2 The Analysis of the Data.

Each muon observed in the spectrograph is ascribed a charge, and for muons with observed deflections greater than the r.m.s. track location error, the true charge is, to a high probability, that observed. Muons with deflections smaller than or near to the r.m.s. error can, however, appear with an apparently reversed charge. For the purposes of this study, this effect is initially ignored, as an observed charge asymmetry can, within the statistical errors, only be a lower limit of the true value. Thus, muons with momenta such that the most probable deflections equal the r.m.s. measuring error have a probability of 0.16 of appearing with reversed charges. If the true charge ratio is R ($\neq$ 1), then the charge ratio which would be observed for a large sample of data is:

$$R^1 = \frac{0.84R + 0.16}{0.16R + 0.84} \qquad \ldots 4.2.1$$

which gives $R^1 > 1$ for $R > 1$.

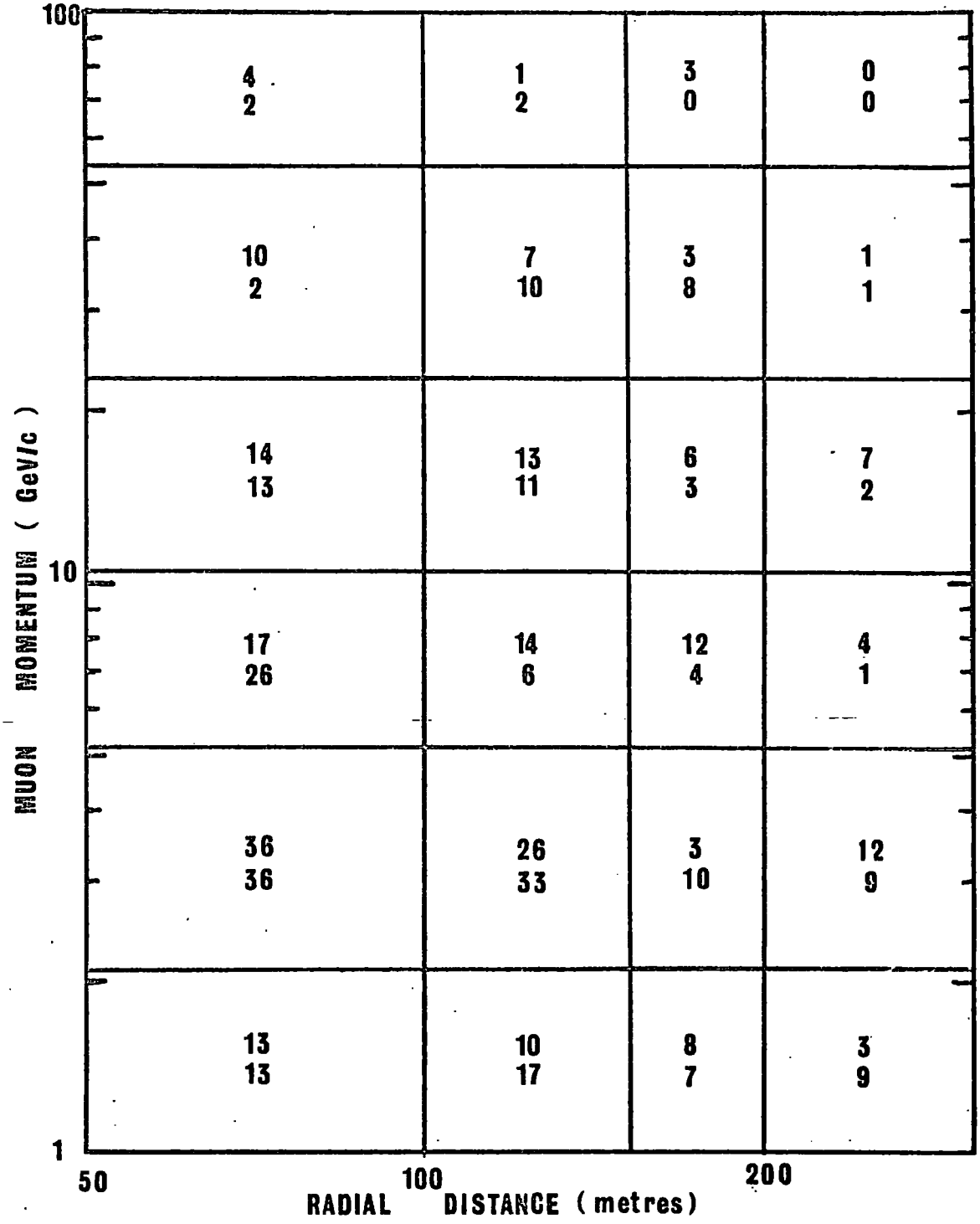
100
10
1
MUON MOMENTUM (GeV/c)
4
2
1
2
3
0
0
0
10
2
7
10
3
8
1
1
14
13
13
11
6
3
7
2
17
26
14
6
12
4
4
1
36
36
26
33
3
10
12
9
13
13
10
17
8
7
3
9
50
100
200
RADIAL DISTANCE (metres)

FIGURE 4.1

The observed muons have been allocated to arbitrary regions of deflection and core distance, and the data from the three EAS arrays, and hence three ranges of shower primary energy, have been treated separately. For the muons observed in showers recorded by the 50m. array, i.e. primary energy $\sim 5\times10^{6}$GeV, no charge ratio significantly differing from unity is observed in any region of deflection or core distance. The charge ratio of all observed muons in this range of shower primary energy is 0.98 ± 0.07. The observed numbers of positive and negative muons in showers recorded by the 150m. and 500m. arrays are shown in figures 4.1 and 4.2 respectively. The mean true momentum of the muons in each deflection interval has been determined using the deductive spectrum analysis method for small samples due to Walton (1966).

4.3 Interpretation of the Data.

From the data given in figures 4.1 and 4.2 it can be shown that the overall charge ratio (μ^{+}/μ^{-}) is close to unity for showers of primary energies $\sim 10^{7}$GeV and 2×10^{8}GeV, being 1.04 ± 0.1 and 0.995 ± 0.04 respectively. However, regions of momentum x distance exist where there appears to be a significant asymmetry. Because the numbers of muons in the regions of asymmetry is small, a check has been made to ensure that the observed muons do not possess arrival angles with respect to the spectrograph, or with respect to the geomagnetic field, such that the acceptance probabilities of positive and negative muons are different.

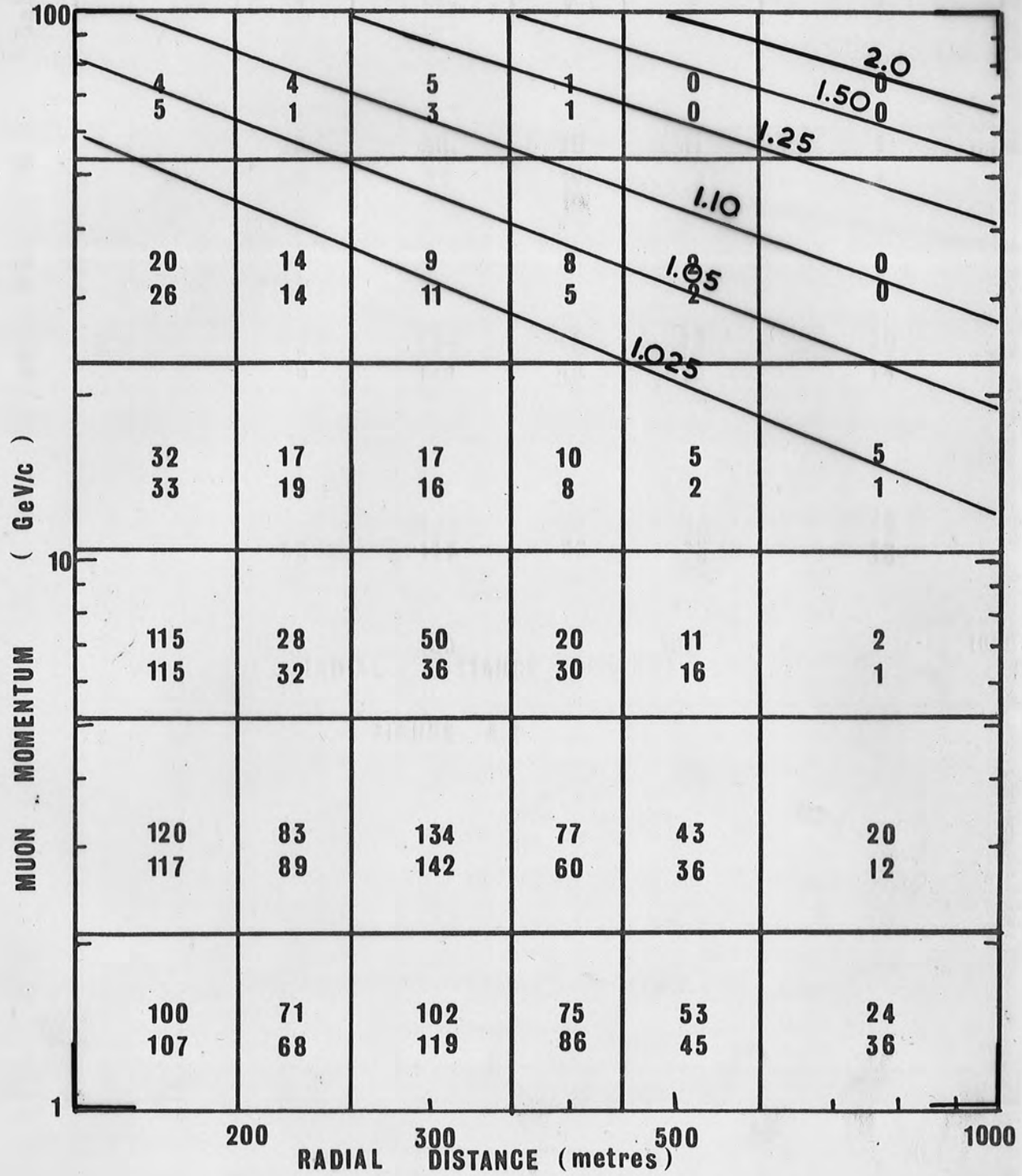
100
10
1
MUON MOMENTUM (GeV/c)
200
300
500
1000
RADIAL DISTANCE (metres)
2.0
1.50
1.25
1.10
1.05
1.025
4
5
4
1
5
3
1
1
0
0
0
0
20
26
14
14
9
11
8
5
8
2
0
0
32
33
17
19
17
16
10
8
5
2
5
1
115
115
28
32
50
36
20
30
11
16
2
1
120
117
83
89
134
142
77
60
43
36
20
12
100
107
71
68
102
119
75
86
53
45
24
36

FIGURE 4.2

Figure 4.2 The charge ratio of EAS muons in a shower of mean size 2×10^7, for intervals of core distance and muon momentum, μ^+/μ^-.

Overlay: Theoretical contours of constant charge ratio for varying core distance and muon momentum, based on the calculations described in chapter 6.

Assuming that the observed asymmetry is due to some muons decaying from charge asymmetric kaons, a calculation has been performed, using the model described in chapter 6, to predict the charge ratio of muons at large distance x momentum products. The proportion of muons in each cell of the distance - momentum matrix of figure 4.2 which are the decay products of secondaries produced in the first interaction of the primary cosmic ray has been calculated, assuming that 25% of these secondaries are kaons, all of which are positive. The results are presented in figure 4.3 as contours of constant proportion of the density of muons with a given momentum and core distance whose parents were produced in the first interaction. These have been interpreted as charge ratio contours which are shown on the overlay to figure 4.2.

There are no direct observations of the charge ratio of kaons created in collisions of total energy about 10^8GeV, but indirect evidence from the charge ratio of unassociated cosmic ray muons reported by MacKeown (1965) suggests that about 50% of the interaction secondaries may be kaons, which possess a charge ratio of $K^+/K^- = 4$. A kaon proportion nearer 25% is more consistent with the evidence supplied in the reviews of Osborne et al.(1964b and 1964c), and that to obtain the maximum expected muon charge asymmetry with the given model assumptions, all kaons should be considered positive. Though the model is limited in that charge asymmetric kaon production is allowed only in the first interaction of the primary cosmic ray,

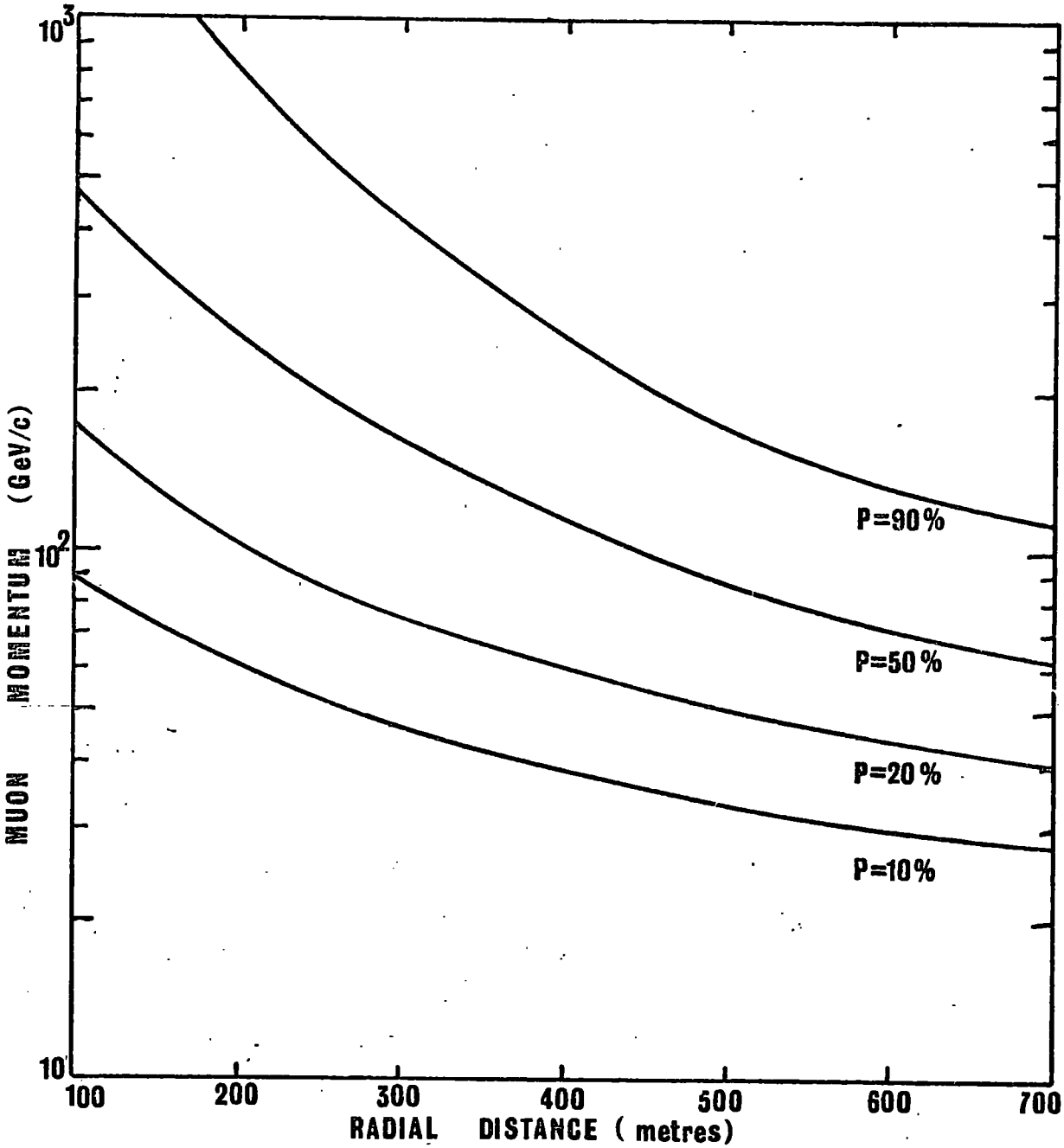
10^3
10^2
10
MUON MOMENTUM (GeV/c)
P=90%
P=50%
P=20%
P=10%
100
200
300
400
500
600
700
RADIAL DISTANCE (metres)

FIGURE 4.3

this calculation should provide a guide to the most sensitive regions of muon momentum and core distance.

A comparison of figure 4.2 with the charge ratio loci on the overlay shows that in those regions where a charge asymmetry is expected, one is observed. The charge ratio of muons in the distance x momentum products enclosed by the locus of $\mu^+/\mu^- = 1.025$ is found to be $\mu^+/\mu^- = 1.31 \pm 0.30$.

In conclusion, the charge ratio observed for the majority of muons in EAS differs insignificantly from unity, indicating that the great majority of muon parents are pions. There is some evidence for the production of secondaries, probably kaons, with a large charge asymmetry in interactions of extremely high primary energies, but it is thought that until a much larger sample of muons has been accumulated, an accurate total assessment of the nature of the secondaries will not be feasible.

Chapter 5

An Interpretation of the Bursts Observed in the Iron of the Spectrograph.

5.1 Introduction.

The Haverah Park spectrograph has been designed and run as a device for measuring the momenta of EAS muons using their deflections in a magnetic field. The iron of the magnet is, however, of sufficient thickness to enable a small, but significant, proportion of the muons traversing the spectrograph to interact, producing bursts. Since bursts are produced preferentially by high energy muons, an attempt has been made to use the results from the bursts to check the muon momentum spectrum.

5.2 The Observation of Bursts.

The iron of the Haverah Park spectrograph has a thickness of 480 $gm.cm.^{-2}$, corresponding to approximately 40 electromagnetic cascade lengths or approximately 5 nuclear interaction lengths. It is therefore to be expected that muons and high energy hadrons will produce bursts which will be observed in the flash-tube trays under the magnet. An example of such a burst is shown in figure 5.1

The information for the majority of bursts includes:

a) the characteristics of the parent EAS,

b) the number of electrons in the burst above a threshold energy of 25 MeV,

c) the presence or absence of a charged primary.

The size of a burst is calculated in two ways. For small bursts,

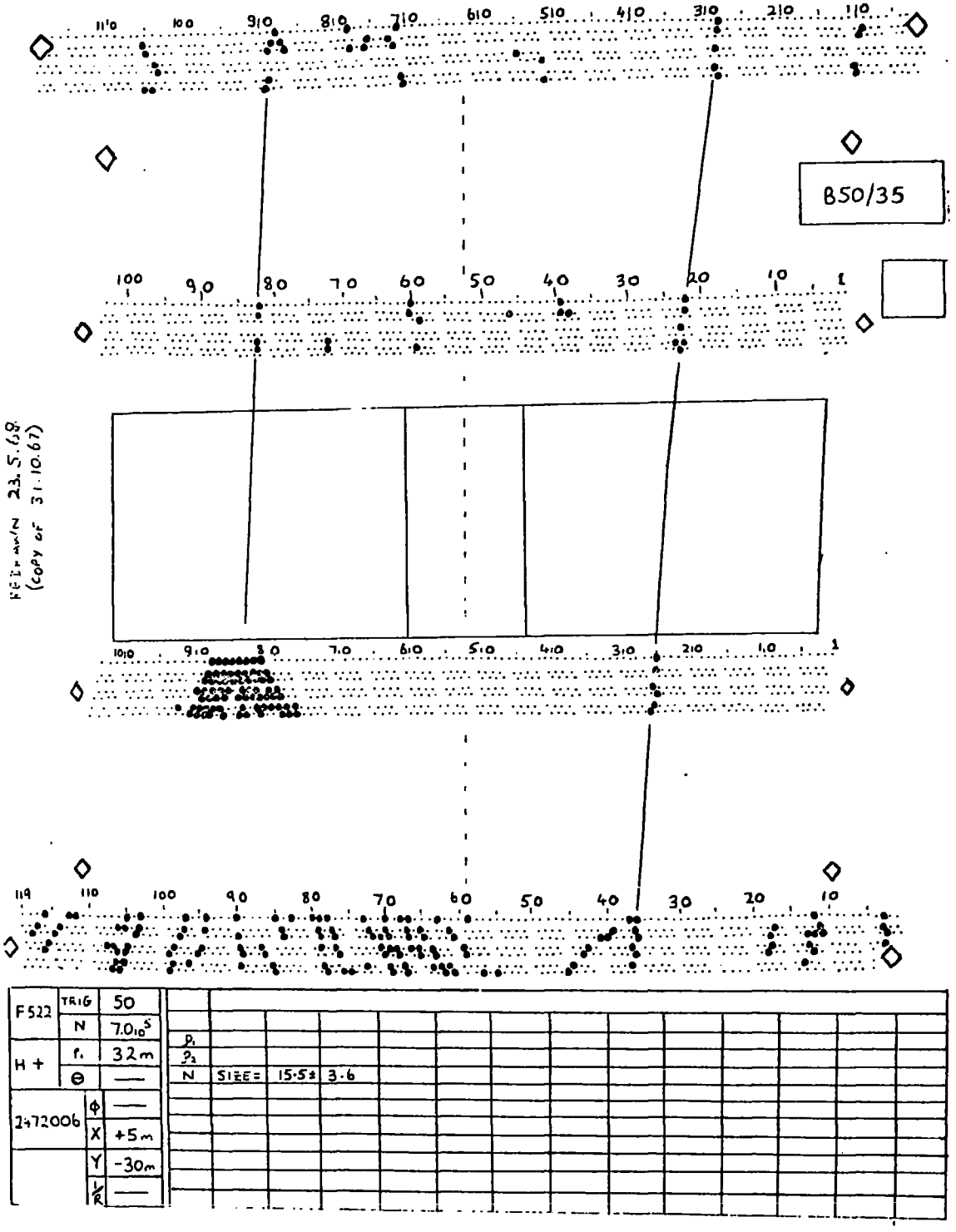
B50/35
F522
TRIG
50
N
7.0 10^5
H +
r.
32m
θ
—
2472006
φ
—
X
+5m
Y
-30m
R
—
N
SIZE=
15·5±
3·6

FIGURE 5.1

a direct count in the tray B1, the tray further from the magnet, is possible. Such a count is usually not possible in the tray immediately below the magnet, and in any tray for large bursts. In this case the burst size is estimated by calculating the particle density required to discharge the observed proportion of flash-tubes. It is assumed that the particle density is distributed evenly over the lateral extent of the burst, and that the burst is radially symmetric. The effect of the first assumption will be to cause a slight underestimate of the burst size. No assumption can be made, however, about the radial distribution of density within the burst without a knowledge of the age parameter of the burst. Burst spectra are measured in the burst size range 5 to 20, the lower limit arising from an arbitrary cut-off to avoid obscuration loss, and the upper to the saturation of the flash-tube trays.

5.3 The Calculation of Burst Spectra Due to Muons.

Burst spectra have been often measured to obtain muon momentum spectra, for example by Bereg et al.(1967), Dmitriev and Khristiansen (1963), and Ashton and Coats (1966). In most cases, the burst size at maximum has been obtained, usually by employing several measuring layers. In this study only one measuring layer is possible, so that bursts at all stages of development are observed.

The expected size spectrum of bursts produced by a muon of momentum p is obtained by evaluating the following expression:

$$S(N,p)\,dN\,dp = \left\{ \int_0^T \int_e^{pc} P_e(E_e,t,p)\,C_e(E_e,t,N)\,dE_e\,dt + \int_0^T \int_e^{pc} P_g(E_g,t,p)\,C_g(E_g,t,N)\,dE_g\,dt \right\} dN\,dp \qquad \ldots 5.3.1$$

where P is the probability of a muon of momentum p producing at a depth t a photon or electron of energy E_g or E_e respectively, which then initiates a cascade, and C is the probability that a photon or electron, originating from a depth t, possessing an energy of E_g or E_e, will produce a burst, observable at a depth T, of size N. The limits e and pc are the minimum and maximum permissible energies of photons or electrons produced by a muon of momentum p. No allowance is made for the effect on the burst size of the magnetic field in the iron, since similar calculations performed by Said(1966) and compared with observations using the near-horizontal cosmic ray muon beam, show that the effect is small. Where comparable, the results of the analysis of Said and the present analysis are in agreement.

The cross-sections used for electron and photon production by the processes of collision, bremsstrahlung, and direct electron pair production are taken from Rossi (1952). The validity of these cross-sections has been checked by several authors, for example Barton (1966), Barton et al. (1966), and Chaudhuri and Sinha (1964) for muon interactions of less than 600 GeV/c muon momentum. The term P is

obtained from the following expressions:

$$P_e(E_e,t,p) = P_1(E_e,p) + 2. \int_e^{E_e} \int_0^{0.5} P_2(E,p,q)\, dq\, dE \qquad \ldots 5.3.2$$

and

$$P_g(E_g,t,p) = P_3(E_g,p) \qquad \ldots 5.3.3$$

where P_1,P_2 are the cross-sections for the production of electrons by collision and direct electron pair production, and P_3 is the cross-section for photon production by bremsstrahlung. The parameter q represents the proportion of energy carried by the electron of the electron-positron pair:

$$q = \frac{E(e^-)}{E(e^+) + E(e^-)} \qquad \ldots 5.3.4$$

It is assumed that positrons and electrons produce identical bursts. As can be seen from equations 5.3.2 and 5.3.3, it is also assumed that the production probabilities are independent of depth. This is valid since the probability of a high energy muon stopping or losing a large fraction of its energy in the magnet is extremely small, so that the flux of muons is independent of depth in the magnet. The effects of the nuclear interaction of muons have been omitted, as these are not important for muon energies less than about 1000 GeV.

The term C in equation 5.3.1 is derived from the theoretical cascade data of Ivanenko and Samusedev (1959). These have been compared, together with those of Buja (1964), against experimental results by Babaev et

al. (1967), and it has been found that the theoretical data of Ivanenko and Samusedev are in good agreement with the observations. These data, calculated for a copper target, have been redrawn for an iron target, allowance being made for the loss of low energy electrons in the flash-tube trays used for estimating the burst size. Since the completion of this work, which has been published (Orford and Turver, 1968), new data have been calculated for a variety of materials , including iron, and electron threshold energies, amongst which is given data for a threshold energy of 25 MeV, the threshold of the flash-tube trays (Ivanenko and Samusedev, 1967). These agree closely with those used in the present analysis.

The effect of poissonian fluctuations in burst size has been included, as it has been shown by Babaev et al.(1967) that these fluctuations are valid for all but very young cascades, for which the fluctuation distribution of Furry (1937) is more appropriate. Since young cascades give only a small contribution to the observed burst spectra, poissonian fluctuations have been used throughout.

The calculation of the burst spectra proceeds as follows. The probability that a burst of size not less than N is produced by a muon of momentum p is evaluated from equation 5.3.1, which is integrated numerically, and this probability is shown for several values of p in figure 5.2. Because of the small probability of a muon of high momentum stopping in the iron, the burst production probabilities change only slowly with depth, after a thickness of about 15 cascade lengths.

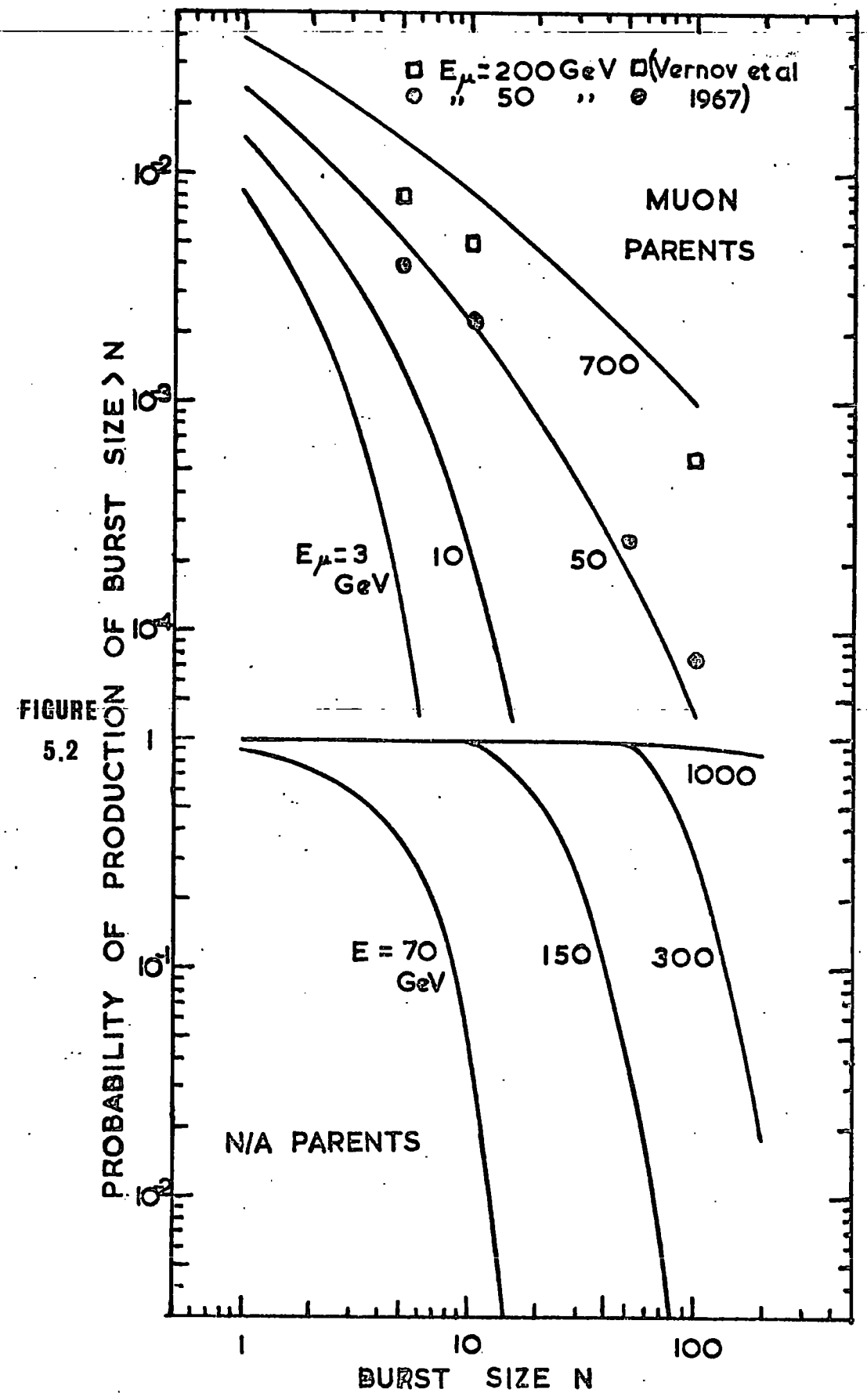
□ E_μ=200GeV □(Vernov et al
○ " 50 " ● 1967)
MUON
PARENTS
700
E_μ=3 GeV
10
50
1000
E = 70 GeV
150
300
N/A PARENTS
PROBABILITY OF PRODUCTION OF BURST SIZE > N
10^{-2}
10^{-3}
10^{-4}
1
10^{-1}
10^{-2}
1
10
100
BURST SIZE N

FIGURE 5.2

This means that bursts with energies less than about 1000 GeV, produced with more than 15 cascade lengths of absorber to penetrate before observation, are not observed. The results shown in figure 5.2 are then comparable with the calculations of Vernov et.al. (1967) and Vernov and Khristiansen (1968) for burst production by muons under great thicknesses of absorber.

The integral frequency of bursts, of size greater than N, is given by:

$$Q(>N) = \int_{0}^{\infty} \int_{N}^{\infty} S'(p).S(p,N)\, dN\, dp \qquad \ldots 5.3.5$$

where $S'(p)\,dp$ is the momentum spectrum of muons responsible for producing the burst spectrum Q. Equation 5.3.5 has been evaluated for the three muon momentum spectra, measured at core distances of 30, 100, and 300 m., which are near the average distances of the showers recorded by the three EAS arrays. The resulant theoretical spectra are compared with the observed spectra in figure 5.3.

5.4 The Comparison of Predicted and Observed Burst Spectra.

The burst spectra observed in showers recorded by the 150 and 500 m. arrays are consistent with the predicted spectra for core distances of 100 and 300 m. respectively. The mean distances of the observed bursts in the two groups are 103 and 270 m. Also shown in figure 5.3 is the burst size spectrum expected from the theoretical 300 m. muon momentum spectrum based on the calculations of de Beer et.al.(1966) (A.W.Wolfendale: private communication).

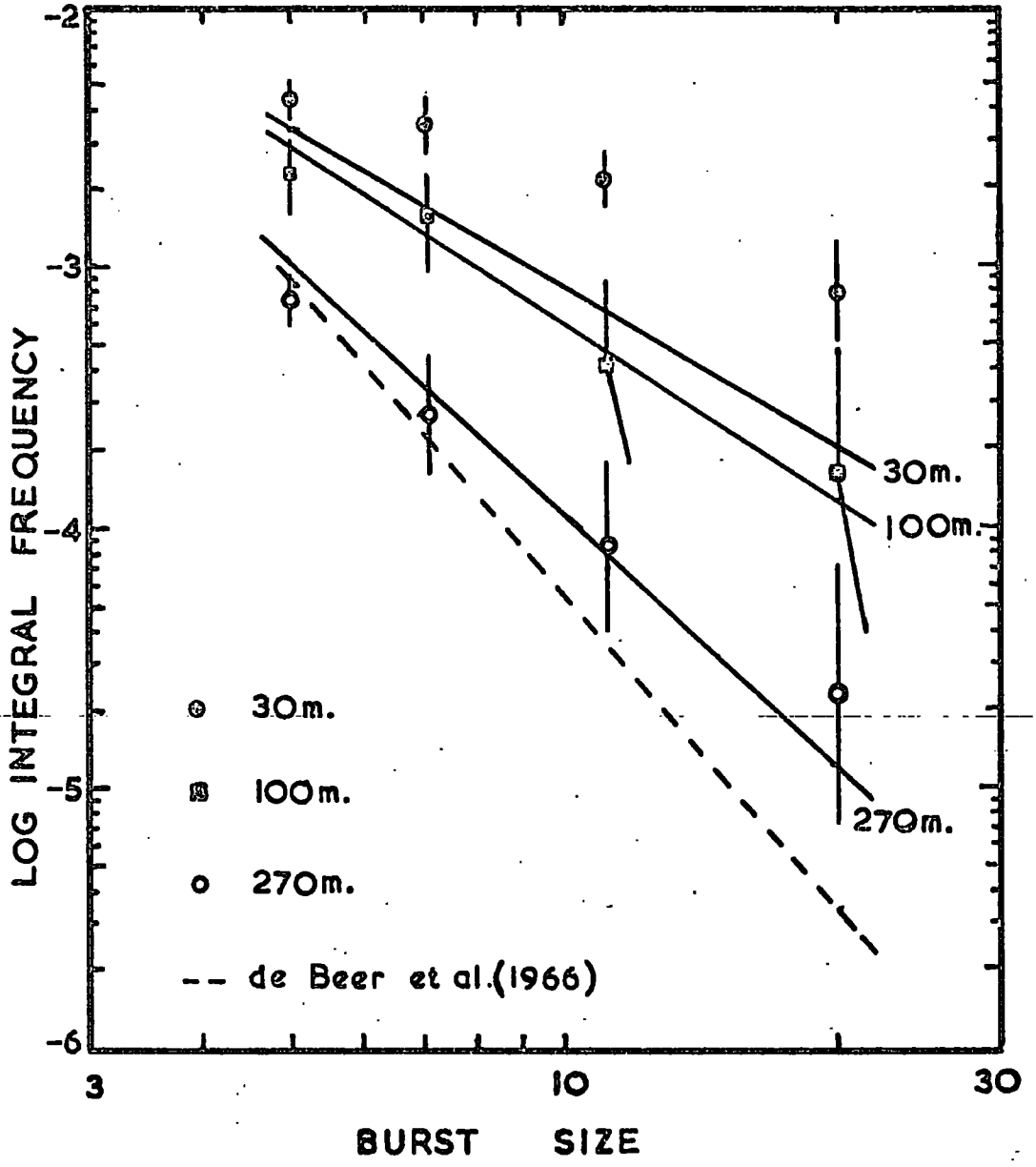
-2
-3
-4
-5
-6
LOG INTEGRAL FREQUENCY
3
10
30
BURST SIZE
30m.
100m.
270m.
30m.
100m.
270m.
-- de Beer et al.(1966)

FIGURE 5.3

The observed burst size spectrum at a core distance of 30 m. is seen to exceed considerably that expected from the 30 m. muon momentum spectrum. The average distance of the observed bursts is less than 30 m., indeed it is approximately 23 m., but since a proportion of the shower cores fell closer than the minimum accurately measurable distance, this figure is uncertain. In this region of the shower, it is expected that high energy hadrons will be present, and may contribute to the observed burst spectrum. An attempt was made to differentiate between the two types of burst, hadron and muon produced, but none other than random differences was found. About 5% of the bursts were observed to have no visible charged primary, but the particle density near to the shower core is too high to enable this burst characteristic to be used to differentiate bursts. The form of the energy spectrum and lateral distribution of hadrons is not well known for distances greater than a few metres, so that a direct comparison of rates is not possible.

In a preliminary analysis of the results (Orford and Turver, 1968a), it was found that, using a very simple EAS model, the observed discrepancy could be explained by hadrons, if the transverse momentum distribution of created particles was as assumed by Earnshaw et.al. (1968b), and not Cocconi, Koester and Perkins (1961). The model on which the calculations were based was not, however, sufficiently realistic to enable a firm conclusion to be drawn; the differences between the two transverse momentum distributions have now been explained by Earnshaw (1968c) in terms of

non-gaussian errors in EAS measurements.

To check that the bursts constituting the discrepancy are produced by hadrons, the excess burst size spectrum has been transformed to a hadron energy spectrum, using the Monte Carlo calculations of Ranft (1964), and compared with the only available data on EAS hadrons in the same energy interval. The calculations of Ranft give the number of charged pions in a nuclear cascade initiated by protons of energies between 10 and 1000 GeV under various thicknesses of steel. From these data has been inferred the neutral pion energy spectrum as a function of production depth; this has been transformed to an electron burst size using the data of Ivanenko and Samusedev (1959), assuming that a neutral pion decays immediately into two photons of equal energy. The total size of a burst, pionic plus electronic, has been used to produce a hadron energy spectrum. It has been assumed also that pions and protons of energies near 100 GeV produce identical bursts under 480 gm.cm.$^{-2}$ of steel.

The resultant energy spectrum is shown, compared with the data given by Greisen (1960), in figure 5.4. The observed spectrum agrees with the spectrum obtained by extrapolating Greisen's data to a core distance of 12 m. This figure is consistent with the expected mean distance of the EAS containing the excess bursts. It is most probable, therefore, that the observed discrepancy is due to the observation of bursts initiated by high energy hadrons near the shower core.

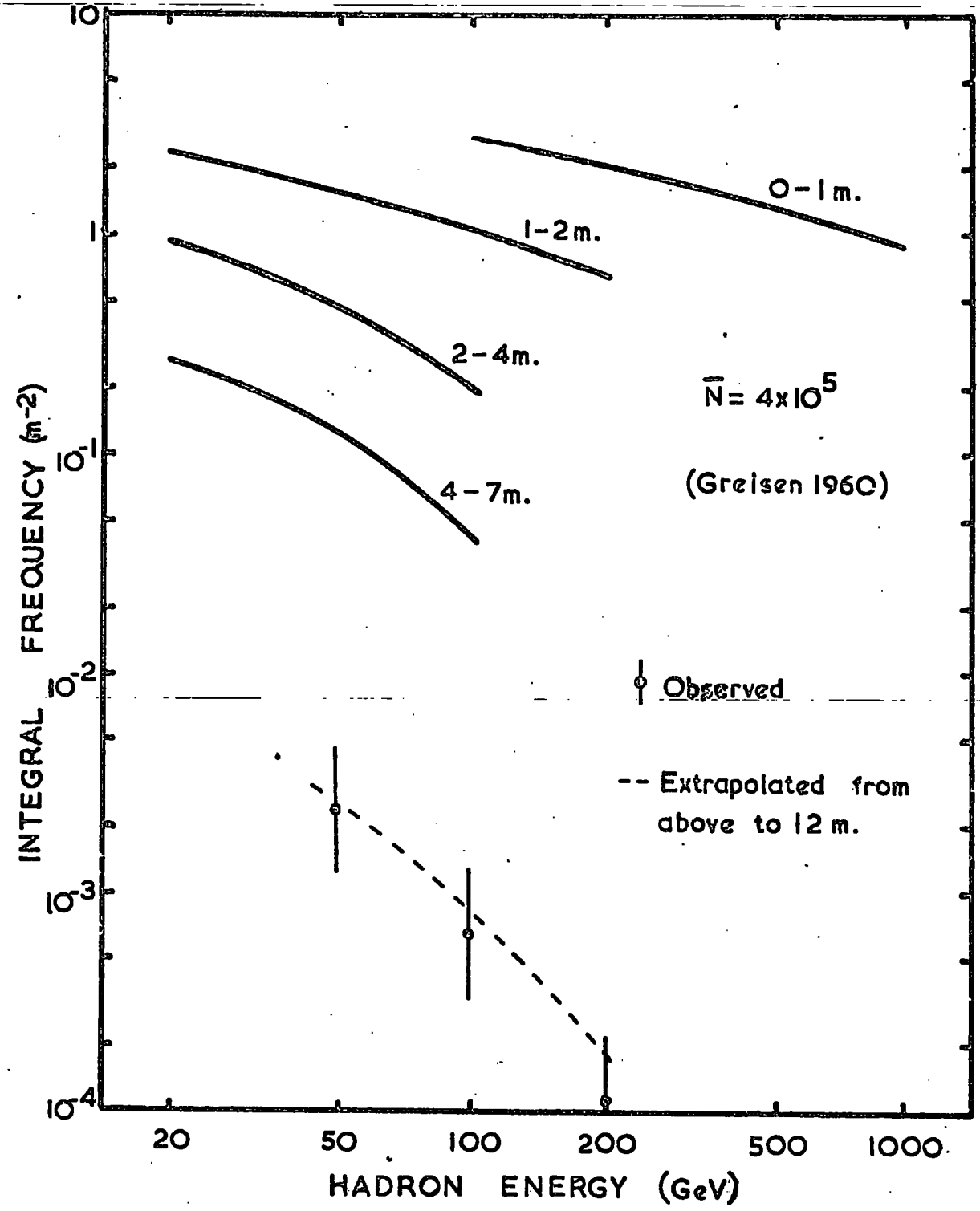
10
1
10^{-1}
10^{-2}
10^{-3}
10^{-4}
INTEGRAL FREQUENCY (m^{-2})
0-1 m.
1-2 m.
2-4m.
4-7m.
$\bar{N} = 4 \times 10^5$
(Greisen 1960)
Observed
-- Extrapolated from above to 12 m.
20
50
100
200
500
1000
HADRON ENERGY (GeV)

FIGURE 5.4

5.5 Conclusions.

It is shown that the measurements of bursts observed in the iron of the Haverah Park spectrograph substantiate the direct measurements on the EAS muon spectra; in particular, there is good agreement between the directly measured and inferred spectra at core distances of 100 m. and 300 m. The discrepancy between the observed and predicted burst spectrum near to the shower core is explained as bursts initiated by high energy hadrons.

Chapter 6.

Interpretation of Experimental Results and Conclusions.

6.1 Introduction.

The purpose of this thesis is twofold: to measure the lateral and momentum distributions of muons in EAS and to infer, from a comparison of the results with model predictions, values for the parameters specifying the high energy interactions producing the muons' parents; and secondly to establish the connection, if any, between the form of the lateral and momentum distributions and the nature of primary cosmic rays. To achieve these aims a model, or models, of EAS development must be employed, incorporating the best available knowledge on the mechanism of particle interactions, and which can make use of all the evidence provided by the experiment. A brief review is therefore given in this section of the present state of knowledge of those parameters of high energy interactions and of primary cosmic rays which will be seen later to influence the interpretation of the EAS muon data.

6.1.1 High Energy Interactions.

Since the discovery of multiple production of mesons in energetic collisions, many phenomenological models have been proposed to account for the observations, for example those of Landau (1953), Heisenberg (1952), Kraushaar and Marks (1954) and Pal and Peters(1964). All have success in explaining at least some of the collision parameters. Five of these parameters are of importance in this analysis: the mean multiplicity of secondary mesons (N_s), the energy

spectrum (f_s), the fraction of the primary energy of the collision appearing as mesons (K_s), the distribution in transverse momentum ($g[p_t]$) and the inelastic interaction cross-sections for $\pi - p$ and $p - p$ collisions.

6.1. 1-1 The Multiplicity Law.

Figure 6.1(a) summarises the results of experiments, mainly on jets, which give information on the variation of the mean pion multiplicity with collision energy. Various multiplicity laws have been previously quoted which are objective fits to such observed points, but they depend strongly on the actual contents of a survey, for example the logarithmic law of Malhotra (1966).

There are three forms of the function $N_s(E)$ which have been proposed on semi-empirical grounds:

1) Yash Pal and Peters(1964), for nucleon-nucleon collisions (charged secondaries only).

$$N_s = 4.64 + \frac{E^{0.5}}{4} \qquad \ldots 6.1.1$$

the two terms corresponding to the contributions from isobar and fireball production.

2) Fermi (1950),

$$N_s = 3kE^{0.25} \qquad \ldots 6.1.2$$

obtained by applying thermodynamical methods to a closed system of pions.

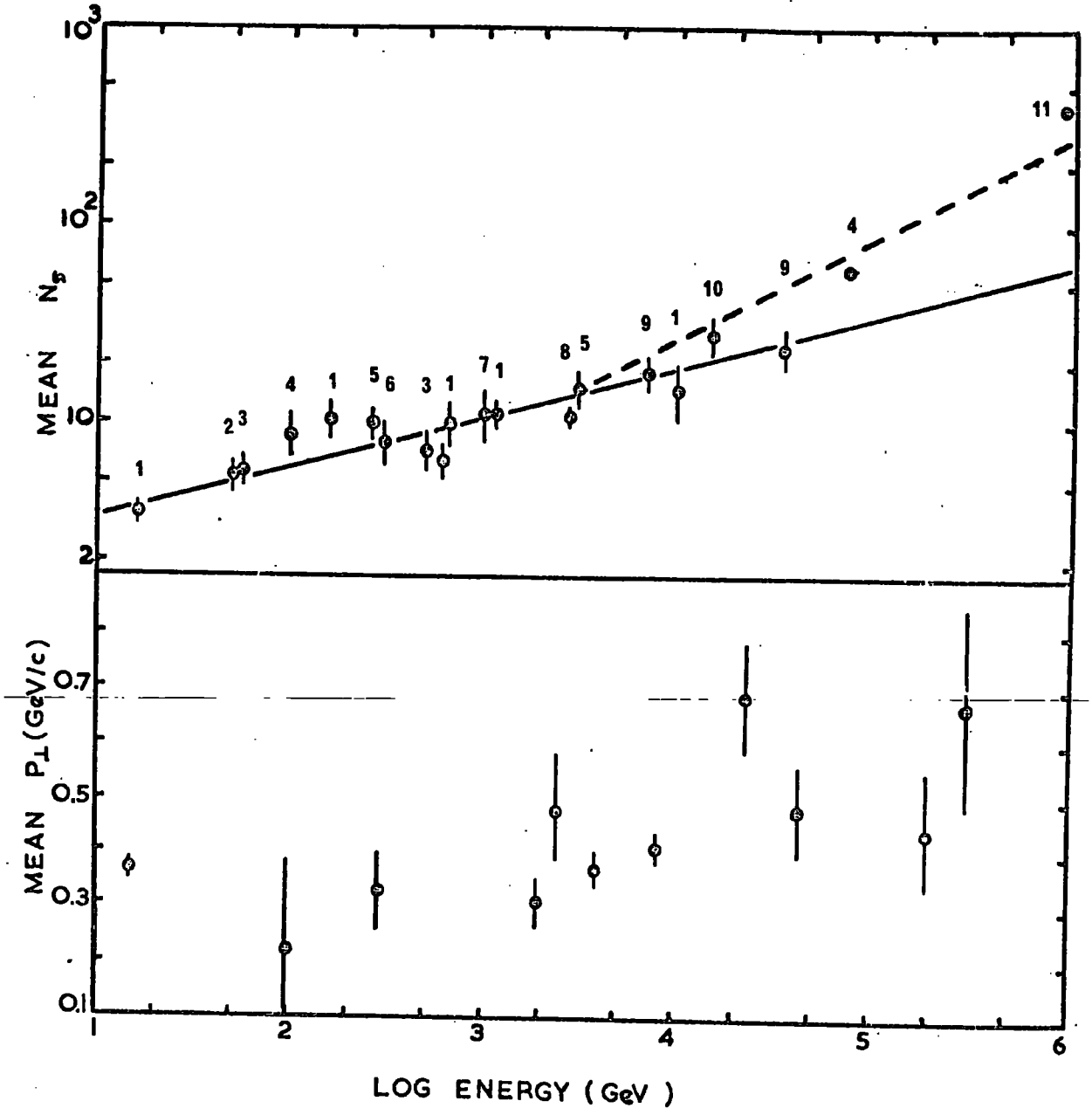
MEAN N_s
10^3
10^2
10
2
1
2 3
4
1
5 6
3 1
7 1
8 5
9 1
10
9
4
11
MEAN $P_\perp$ (GeV/c)
0.7
0.5
0.3
0.1
1
2
3
4
5
6
LOG ENERGY (GeV)

FIGURE 6.1

Sources of Points in Figure 6.1(a)

1. Malholtra (1963 and 1964)
2. Lal et al. (1963)
3. Hansen and Fretter (1960)
4. Koshiba et al. (1963)
5. Lohrmann et al. (1961)
6. Dobrotin et al. (1962)
7. Abraham et al. (1967)
8. McCusker and Peak (1963)
9. ICEF (1963)
10. Malholtra et al. (1966)
11. Fowler (1964)

3) Frautschi (1963), ...6.1.3

$$N_s = 2 \times \ln(E)$$

which is obtained by assuming that fireballs are produced with numbers according to a logarithmic law and that each fireball produces about 6 pions.

All three laws agree fairly well with each other up to an energy of about 10^5 GeV, and the experimental data of figure 6.1 is insufficient to enable a choice to be made. The energies of primary cosmic rays extend to about 10^{11} GeV, so any attempt to predict air shower parameters must necessitate a choice of law.

Indirect evidence on the form of the multiplicity law at high energies has been quoted by a number of authors. Pinkau (1966), for example, has concluded from an interpretation of the variation of the height of the maximum of shower development with shower primary energy that a logarithmic law is most probable for collision energies up to 10^{10} GeV, but the magnitude of the true errors does not preclude an $E^{0.5}$ variation. A number of authors, for example Hayakawa and Ogita (1960), Bowler et al.(1962), Guseva et al.(1962) and Fowler and Perkins (1964) suggest that the mean energy of pions in the centre of mass system of the interacting particles may be independent of the energy radiated, at large primary energies:

$$\bar{E}^*_\pi \approx \text{a few GeV} \qquad \ldots 6.1.4$$

This leads, as the energy released is proportional to the Lorentz factor, γ_c, of the C.M. system to:

$$N_s = \frac{k_1 \gamma_c}{\bar{E}^{*}} = k_2 (\gamma_L + 1)^{0.5} \qquad \ldots 6.1.5$$

i.e. a form $N_s \propto E^{0.5}$. It should be noted that the points given in figure 6.1 are plotted at the mean energies of samples of jets. As pointed out by Murzin (1966), the type of errors in the energy estimates of the primary particles of jets will lead to an underestimate of multiplicity for a given primary energy. Studies, using an accelerator, on 25 GeV p −p collisions by Kamal and Rao (1967) show that the normal energy estimating methods overestimate the primary energy estimates of events in which the multiplicity fluctuates downwards. Because the mean multiplicity − energy function increases, the result of these effects will be that the true multiplicity law will be somewhat steeper than is usually taken.

A tentative conclusion for the purposes of later analysis is that the multiplicity law is of the form $N_s \propto E^{0.25}$ up to $E \approx 10^4$GeV and then lies between $N_s \propto E^{0.25}$ and $N_s \propto E^{0.5}$ thereafter.

6.1. 1-2 Transverse Momentum.

The experimental difficulties in measuring the distribution in transverse momentum of secondaries from very high energy collisions render the results even less conclusive than those of the multiplicity law. It is well established at low energies that the average transverse momentum $\langle p_\perp \rangle \sim 0.3$ GeV/c. Although there are suggestions from studies of multiple cored EAS, e.g. McCusker et al.(1968), that at an energy $\sim 10^7$GeV transverse momenta of a few GeV/c are not uncommon, more direct evidence for energies less

than 10^6GeV suggests that the average transverse momentum is constant, or varies slowly with energy, at a value near that measured at very low energies. Figure 6.1(b), which is based on the results of Kazuno (1967), shows the mean transverse momenta of secondaries measured in interactions with primary energies up to $\sim 10^6$GeV.

Various analytical forms for the distribution in transverse momentum $p_\perp$ have been given, for example:

$$g(p_\perp)\,dp_\perp = \frac{p_\perp}{p_e^2}\exp(-p_\perp/p_e)\,dp_\perp \qquad \ldots 6.1.6$$

due to Cocconi, Koester and Perkins (1961) where

$$2.p_e = \langle p_\perp \rangle$$

$$g(p_\perp)\,dp_\perp = \frac{p_\perp^2}{2.p_e^3}\exp(-p_\perp/p_e)\,dp_\perp \qquad \ldots 6.1.7$$

due to Nikolskii (1963), $3.p_e = \langle p_\perp \rangle$

$$g(p_\perp)\,dp_\perp = \frac{2.p_\perp}{p_e}\exp(-p_\perp^2/p_e)\,dp_\perp \qquad \ldots 6.1.8$$

due to Aly et al. (1964), $p_e = 2.(p_{\perp max})^2$

The distributions obtained by the examination of jets are affected by the method used to estimate the jet primary energy, and according to Lohrmann (1963) it is unlikely that, with the precision necessary, direct jet measurements will be able to provide a unique distribution.

Lock(1964) has estimated the mean transverse momenta of secondaries other than pions created in 25 GeV p-p collisions and a fit to the data produces an expression for the dependence of $\langle p_\perp \rangle$ on M, the mass of the secondary:

$$\langle p_T \rangle = 0.3 + 0.2 \times M \qquad \ldots 6.1.9$$

with $\langle p_T \rangle$ in GeV/c when M is in GeV/c^2. Although there is no supporting evidence, it is possible that at much higher primary energies, secondaries heavier than pions will be created possessing correspondingly higher transverse momenta.

6.1. 1-3 Inelasticity.

In most jet studies, N_s and $\langle p_T \rangle$ are, to a first approximation, directly measured; the inelasticity, however, is determined by comparing estimates of the primary nucleon energy, usually from the median angles of the secondaries by a method similar to those of Castagnoli et al.(1953) or Yajima and Hasegawa (1965), with an estimate of the total energy removed from the interaction by secondaries. This procedure introduces large systematic, and random, errors. Imaeda (1962) has reported a variation of the total inelasticity K_T with primary nucleon energy E_o:

$$K_T \propto E_o^{-0.5} \qquad \ldots 6.1.10$$

However, the analysis of Murzin, mentioned above, suggests that this apparent variation can be explained if the errors in energy measurements are fully taken into account. The studies of Abraham et al. (1967), Gierula and Krzywdzinski (1968), and Yameda and Koshiba(1968) suggest that K_T is independent of energy and lies in the range 0.3 to 0.6. The value of $\langle K_T \rangle = 0.5$ used by many authors to obtain information on other collision parameters is probably the best estimate of the total inelasticity. The fraction of the primary energy of an

interaction which appears as pions, $K_{\pi\pi}$, is usually taken to be ≈ 0.35. The inelasticity of π − N interactions is usually taken to be 1.0, since there are great experimental difficulties in separating a primary pion from the secondary pions created in a collision. There has been a recent suggestion, reported by de Beer et al.(1968a), that the π − N inelasticity is nearer 0.5. There is no published supporting evidence, however, and the value of 1.0 is more probable, and supported by measurements of the attenuation length of the EAS hadron component.

6.1. 1-4 Interaction lengths.

At very high energies, the cross-section for inelastic collisions is thought to approach the geometric value asymptotically. The only sources of measurements at extremely high energies are provided by observations of the attenuation of EAS hadrons in the atmosphere, and the variation of the altitude of the shower maximum with primary energy. Obviously the uncertainties in the inelasticity of interactions preclude a uniquely determined cross-section or interaction length, but analyses of experiments such as those performed by Tanahashi(1965) and Matano et al. (1964) suggest that the interaction length of nucleons in air $\lambda_N = 80 \pm 10 gm.cm^{-2}$ in the energy range $10^5 < E_N < 10^8$ GeV. The interaction lengths of other particles are less well known at these energies, but are usually taken as

$$\lambda_\pi = 120 \pm 20 gm.cm^{-2} \quad \text{and} \quad \lambda_K = 100 \pm 20 gm.cm^{-2}.$$

6.1. 1-5 Energy Distribution of Secondaries.

The energy distribution of secondaries created in extremely

high energy interactions cannot be directly obtained, but must be inferred from the angular distribution, making assumptions about the transverse momenta. Energy distributions so obtained are therefore uncertain at high and low secondary energies, but there are indications from the work of many authors, for example Malheltra(1966), Aly et al.(1964), that the distribution quoted by Cocconi, Koester and Perkins (1961), the so-called CKP distribution, is valid over a very wide range of collision primary energies:

$$F(E)\,dE = \frac{\exp(-E/T)}{T}\,dE \qquad \ldots 6.1.11$$

where T is the mean secondary energy. Some authors consider that this distribution, when combined with a CKP distribution in transverse momentum where $\langle p_\perp \rangle$ is independent of E, predicts too many secondaries with energies less than 1 GeV. The evidence for or against this is, however, inconclusive.

6.1.2 Primary Cosmic Rays.

For many years it has been accepted that the great majority of primary cosmic rays are protons. It has also been established that nuclei as heavy as uranium (Fowler et al.1967) occur in very small proportions at least at low primary energies $\sim$ 100 GeV. The charge composition is taken to be constant over a wide range of primary energies and measurements such as those of Bray et al.(1966) support this. The generally accepted composition is that quoted by Ginzburg and Syrovatskii (1964), shown in table 6.1. For energies above about 10^5 GeV, the rate of primary cosmic rays is too low ($\sim 10^{-8}$

Table 6.1

Composition of Primary Cosmic Rays.

Nucleus	Z	$\bar{A}$	% of flux	Flux, $m.^{-2} ster.^{-1} sec^{-1}$.
Proton	1	1	93	1300
Helium	2	4	6.3	88
Light	3-5	10	0.14	1.9
Medium	6-9	14	0.41	5.7
Heavy	10-20	25	0.10	1.37
Very Heavy	> 20	51	0.04	0.53

(From Ginzburg and Syrovatskii, 1964)

cm^{-2}. sec^{-1}. $sterad^{-1}$.) to enable a large sample to be obtained directly from balloon or satellite measurements. Primary cosmic rays in this energy region produce extensive air showers and it might be expected that certain properties of these showers will reflect the nature of the primaries. No firm conclusion has yet been drawn on the composition in the air shower region of primary energy, although the lines of attack on the problem have been numerous. For example, the proportion of muons in a shower is expected to increase with primary mass, and analyses by de Beer et al.(1968b and 1968c) have shown that the form of the variation is quite sensitive to the primary mass distribution. Adcock et al. (1968) have surveyed the experimental data and have shown that they are not yet precise enough to enable any conclusions at all to be drawn about the primary composition. More indirect evidence is supplied by the observation of a change in slope of the shower size spectrum at a size of about 5×10^5 particles, and from the variation of the position of this point with altitude. Glencross (1963) suggests that since the shower size at the kink does not vary significantly with altitude of measurement, the change in slope is partly or wholly caused by a change in the characteristics of nuclear interactions at primary energies greater than about 5×10^4 GeV. McCusker et al.(1968) conclude from studies of multiple-cored showers, the air shower density spectrum, and their interpretation of an observed variation in the shower size of the kink with altitude that between the energies 2×10^6 GeV and 6×10^7 GeV the primary cosmic ray beam loses first its protons and then

progressively heavier nuclei. This is interpreted as the diffusion from the galaxy of nuclei of a constant magnetic rigidity per nucleon of about 2×10^6 GV which is expected by many authors. The change of slope in the shower size spectrum at a size of about 5×10^8 particles, reported by Linsley (1963), is interpreted as an addition of extra-galactic protons to the primary flux. The size spectrum of EAS has been interpreted as a primary energy spectrum, which is divided into three regions:

a) $N(>E) = 10^{-4} \times (10^{14}/E)^{1.6}$ m.$^{-2}$ sec.$^{-1}$ ster.$^{-1}$
for $E < 2 \times 10^{15}$ eV.

b) $N(>E) = 1.5 \times 10^{-10} \times (10^{17}/E)^{2.2}$ m.$^{-2}$ sec.$^{-1}$ ster.$^{-1}$
for $2 \times 10^{15} < E < 3 \times 10^{18}$ eV.

c) $N(>E) = 3 \times 10^{-16} \times (10^{20}/E)^{1.6}$ m.$^{-2}$ sec.$^{-1}$ ster.$^{-1}$
for $E > 3 \times 10^{18}$ eV.

The question of the interpretation of the primary cosmic ray energy spectrum is still very much open, so that any information on the charge or mass composition of very high energy cosmic rays will be of great value.

6.2. Predictions of Previous Models on EAS Muons.

6.2.1 General.

In order to use the observations on EAS muons to obtain information about the processes taking place at the birth of an air shower, calculations must be made on the development of EAS. Three mathematical approaches have been employed by a variety of authors to predict

the lateral distribution of EAS muons; in some degree, the method used dictates the region of applicability. The purpose of this section is to review the approaches and to compare the predictions of various models with the experimental data.

6.2.2 Previous Models.

A solution to the diffusion equations describing the lateral and longitudinal development of the meson cascade in an EAS core has been obtained by the method of successive generations by de Beer et al. (1966), and by Oda(1957), Cowsik(1966) and Ueda and Ogita(1957) for the longitudinal development only. This method possesses the advantage that a short computation time is possible, but a disadvantage that without sufficient care in the selection of the method of integration, a cumulative error may be introduced. The Monte Carlo method has been applied by Bradt and Rappaport (1967) and McCusker et al.(1968) to the lateral development of muons and hadrons in small EAS, and by Lal (1967) to the density of extremely high energy muons in small showers. Although this method, as applied by these workers, delivers a relatively exact solution, the computation time is so long that the application is limited to use on high energy muons in small showers, at least for short-term studies. No predictions have yet been made for showers of primary energies exceeding about 10^7 GeV. The third method simulates the shower using interaction points of hadrons fixed in the atmosphere as used for example by Hillas(1966) and Holyoak(1967). Calculations based on this model can provide

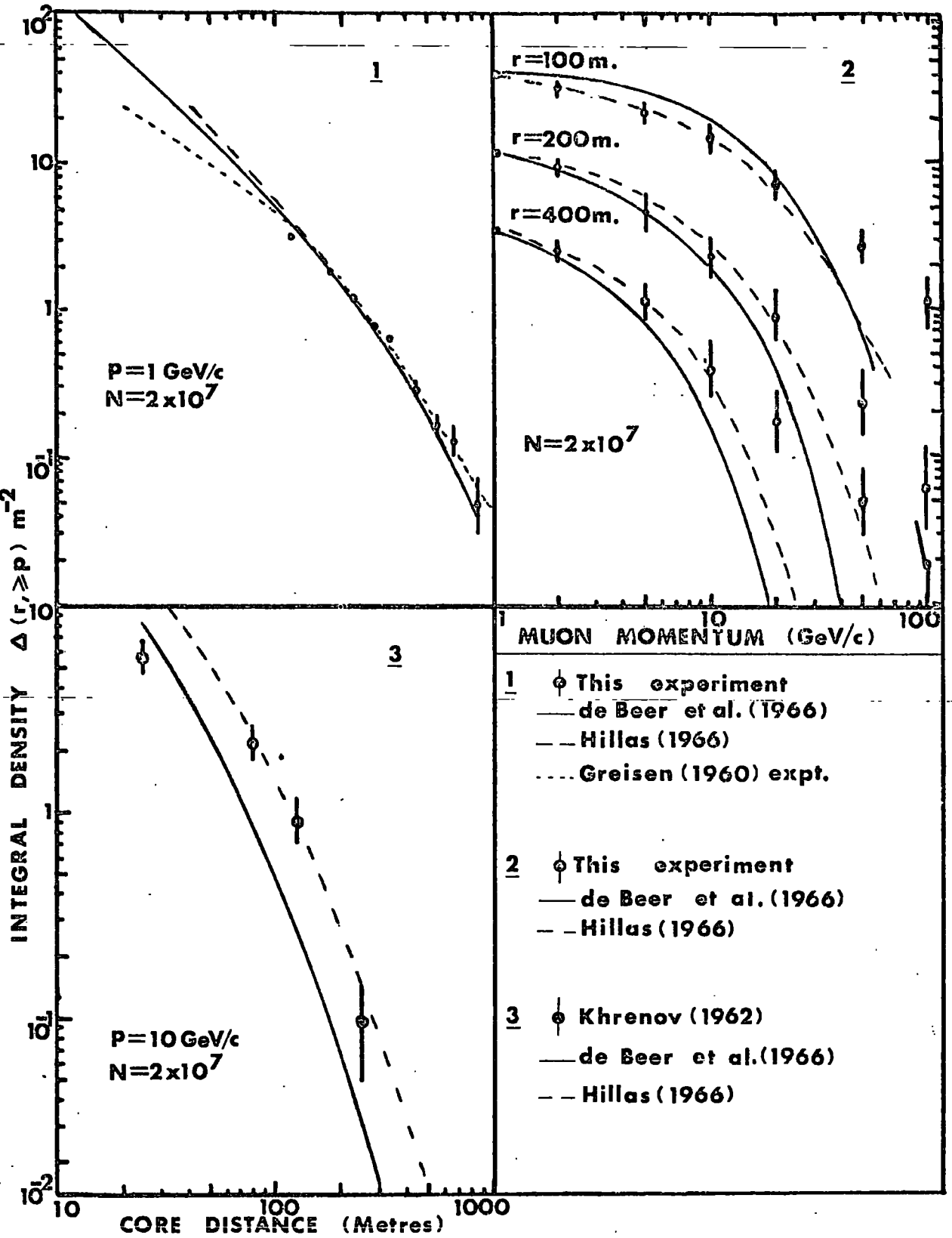
1
2
3
r=100m.
r=200m.
r=400m.
P=1 GeV/c
N=2x10^7
N=2x10^7
P=10 GeV/c
N=2x10^7
INTEGRAL DENSITY Δ(r,≥p) m^-2
MUON MOMENTUM (GeV/c)
CORE DISTANCE (Metres)
1 This experiment
de Beer et al. (1966)
Hillas (1966)
Greisen (1960) expt.
2 This experiment
de Beer et al. (1966)
Hillas (1966)
3 Khrenov (1962)
de Beer et al. (1966)
Hillas (1966)

FIGURE 6.2

useful general information about EAS, in applications where the sum of the effects of a number of fixed point interactions approximates well to the integral over the whole shower development. The method allows of extremely small computation time and consequently is useful as a preliminary calculation to determine the sensitivity of a predicted quantity to a given parameter.

6.2.3 Comparison of Predictions with Experimental Data.

Only two of the models mentioned above have been developed to provide detailed predictions of the muon lateral and momentum distributions in those regions of shower primary energy, core distance and muon momentum comparable with those covered by the experimental results presented here. The models are those of Hillas(1966) and de Beer et al. (1966 and 1968a). The calculations of de Beer et. al. provide predictions for comparison with most previous measurements of muon lateral distributions.

Figure 6.2 shows a comparison between some of these predictions, the corresponding predictions of Hillas(1966), and experimental results. It can be seen that the predictions of neither model fit all the data. The lateral distribution of muons of momenta not less than 1 GeV/c is fitted well by the predictions of both models, except for core distances less than 100 metres and greater than about 700 metres. The discrepancy for small core distances is attributed by de Beer et al. to the distribution in transverse momentum used by them, the CKP distribution, predicting too many secondaries with small transverse momenta. The effects of coulomb

scattering and geomagnetic deflection have not been included in this model, and neither have the effects of a possible variation in the shape of the lateral distribution with primary energy. All these effects could contribute to the discrepancy, the latter because the observed lateral distribution is obtained from measurements in showers originating from a wide range of primary energies.

The lateral distributions for higher muon threshold momenta are not well fitted by the predictions of either model. In particular, there is a marked discrepancy between the predicted and experimental density of high momentum muons at large core distances. The model of Hillas predated the first results from the Haverah Park spectrograph (J.C. Earnshaw et al. 1967) and so no explanation is offered. However, de Beer et al. (1968a) interpret the discrepancy as due to either experimental bias or to the existence of secondaries from high energy interactions possessing very large mean transverse momenta, or as a combination of both. It has also been suggested Davis and Davis(private communication) that the discrepancy may be interpreted as evidence for the existence of the expected weak interaction intermediary, the vector boson.

Although the utmost care has been taken to exclude them, small biases may still remain undetected in the experimental data, but the magnitude of the discrepancies, together with the failure of the models satisfactorily to explain the muon lateral distributions of other workers, using models containing reasonable values of the

interaction parameters, make it improbable that experimental bias can be the sole cause. To examine this further, a new model has been developed to attempt to provide an explanation for the apparent excess of high momentum, large distance muons, using reasonable values for the collision parameters.

6.3 Predictions of a New Model.

6.3.1 General.

The construction of a mathematical model that is supposed to represent a physical process must take into account two conflicting factors: on one hand it must be sufficiently realistic that a study of its properties enables useful information to be obtained on the physical problem; on the other, it must be simple enough that it is amenable to mathematically stringent methods.

Previous models have been examined to check their applicability in the regions of high muon momenta and large core distances. Consideration of the cause of the discrepancy between predictions and observation suggest that the muons constituting the apparent excess must originate from secondaries created in the first few interactions of the primary cosmic ray. This is only the case if the parents of these muons originate from interactions in which the values for parameters such as multiplicity and transverse momentum are those expected from an extrapolation of the results of low energy studies. The treatment of this part of the shower by previous model calculations was no more rigorous than that for any other

region. It was therefore decided to treat the early stages of the cascade in a mathematically rigorous manner. To ensure that any parameters used in this region to obtain an agreement between the predicted and observed density of high momentum muons do not distort the energy balance of the rest of the cascade, a simpler method has been adopted to calculate the rest of the shower development.

The object of these calculations has been to predict the differential density of muons of momenta less than 100 GeV/c at core distances between 100 metres and 600 metres in showers of primary energy 2×10^8 GeV. The results have been published (Orford &Turver,1968).

6.3. 2 Description of the Model.

The lateral and longitudinal development of the meson cascade has been treated by the method of successive collisions, similar to that used by Bhabha and Heitler (1937) to investigate electromagnetic cascades. Although it is one of the most laborious of the numerical methods, the accuracy conferred on the predictions by the relative lack of approximations needed makes it ideal for this type of study. Unfortunately, the number and complexity of the arithmetical operations increases sharply with the number of collisions considered. The calculation of the cascade development by this method has therefore been terminated at an altitude of 10 kilometers, which is near the lowest effective height of production of muons of momenta about 100 GeV/c observed at a core distance greater than 100 metres, if the muon parents possess normal transverse momenta.

Table 6.2

Parameters of the Basic Model

	Symbol	Value assumed
Primary Energy	E_p	2×10^8 GeV
Atomic Number	A	20
Zenith Angle	θ	0°, 20° (see text)
Multiplicity (charged secondaries)	N_s	$15 \times (KE_o/3\times10^3)^x$
		$x = 0.25$ for $E_o \leq 3\times10^3$
		$x = 0.5$ for $E_o > 3\times10^3$
Fragmentation Fraction	F	0.22
Average Transverse Momentum	$\langle p_t \rangle$	0.5 GeV/c
Inelasticity: nucleon	K_{N-N}	0.5
pion	$K_{\pi-N}$	1.0
Interaction Length: nucleon	λ_N	80 gm. cm^{-2}.
pion	λ_π	120 gm. cm^{-2}.
kaon	λ_K	100 gm. cm^{-2}.
Secondary energy spectrum	$f_s(E)$	$\frac{\exp(-E/T)}{T} + \frac{\exp(-E/G)}{G}$

Preliminary calculations indicated that an insignificantly small error is introduced into the theoretical muon densities by this assumption. The details of the arithmetical calculations are given in the appendix for the region of the atmosphere above an altitude of 10 kilometers, region A.

The lower region, B, has been treated by a method similar to that used by Hillas (1966) and is also in the appendix. A schematic diagram of the development model is shown in figure 6.3. On the basis of previous experimental and theoretical results, the most probable values for collision parameters have been chosen. Calculations have been performed for a test momentum spectrum, varying each parameter, so that the sensitivity of the result to each could be determined. The parameters used as a basis for this are given in table 6.2. All parameters given in this table have already been discussed, with the exception of F, the fragmentation fraction. This is the fraction of the nucleons in the primary cosmic ray, if it is heavier than a proton, which interact coherently in the first collision of the nucleus with an air nucleus, and are responsible for multiple pion production. The effect of fluctuations in the values of any parameter have not been included.

6.3. 3. Results and Comparisons with Experimental Data.

When considering the longitudinal development of a meson cascade initiated by a primary nucleus of atomic number A, it is a good approximation to consider the nucleus as A independent nucleons of energy E/A. It has been found important, however, for

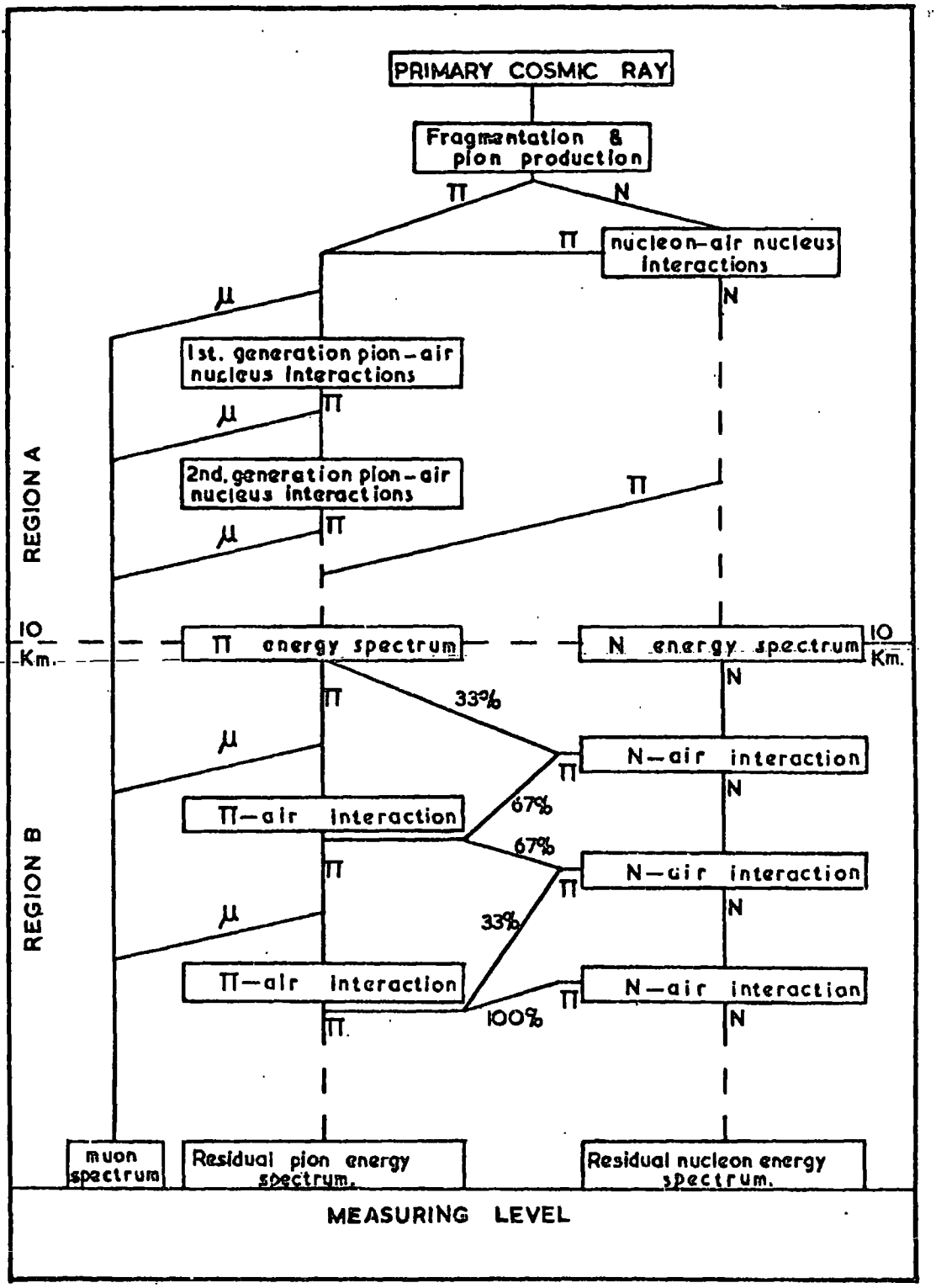
PRIMARY COSMIC RAY
Fragmentation & pion production
π
N
π
nucleon–air nucleus interactions
N
μ
1st. generation pion–air nucleus interactions
μ
π
2nd. generation pion–air nucleus interactions
π
μ
π
REGION A
10 Km.
π energy spectrum
N energy spectrum
10 Km.
π
33%
N
μ
N–air interaction
π
N
π–air interaction
67%
67%
N–air interaction
π
N
μ
33%
π–air interaction
N–air interaction
π
100%
N
π
REGION B
muon spectrum
Residual pion energy spectrum.
Residual nucleon energy spectrum.
MEASURING LEVEL

FIGURE 6.3

an accurate treatment of the three-dimensional cascade development to take some account of the secondaries produced in the first interaction which fragments the nucleus. Little is known about multiple meson production by very energetic nuclei, but the results of Abraham et al. (1967) suggest that about 30% of the nucleons in the lighter nucleus involved in the interaction interact coherently to create mesons. This fraction must, because of the paucity of experimental evidence, be an estimate, but the sensitivity of the model calculations to its value has been found to be small for values greater than 10%.

The sensitivity of the predictions to F, $\langle p_\perp \rangle$ and shower zenith angle θ are shown in figure 6.4, displayed as ratios of the density of muons for a given value of a parameter to the density of muons for the basic value of the parameter from table 6.2. The sensitivity with transverse momentum is for variations in the mean transverse momenta of secondaries from interactions of primary energy greater than 1000 GeV only, since the secondaries from lower energy interactions possess a constant mean transverse momentum. The sensitivity of the muon densities to the shower primary energy E_p has been found to be:

$$\Delta_\mu(p,\ r \geq 100\text{m.}) \propto E_p^{(1-0.003.p)} \qquad \ldots 6.3.1$$

where p is the muon momentum.

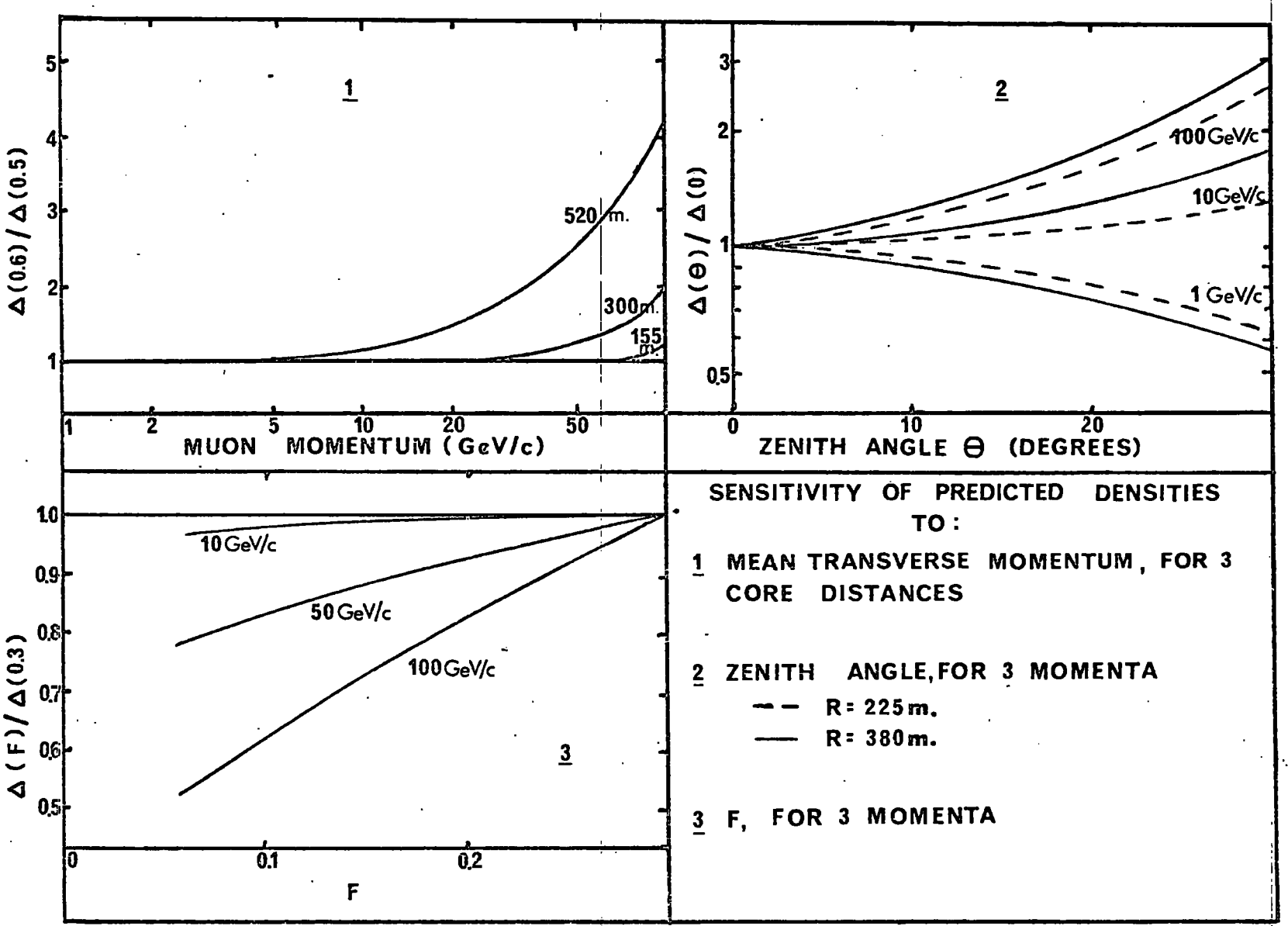
1
Δ(0.6)/Δ(0.5)
520 m.
300m.
155 m.
MUON MOMENTUM (GeV/c)
2
Δ(Θ)/Δ(0)
100GeV/c
10GeV/c
1 GeV/c
ZENITH ANGLE Θ (DEGREES)
3
Δ(F)/Δ(0.3)
10GeV/c
50GeV/c
100GeV/c
F
SENSITIVITY OF PREDICTED DENSITIES TO :
1 MEAN TRANSVERSE MOMENTUM, FOR 3 CORE DISTANCES
2 ZENITH ANGLE, FOR 3 MOMENTA
R = 225m.
R = 380m.
3 F, FOR 3 MOMENTA

FIGURE 6.4

The parameters A and N_s have been found to be the most sensitive and have been treated separately and at length. The remaining parameters, λ and K have been found to affect only marginally the predicted muon momentum spectra.

Since the effects of varying N_s and A have been found to be equally great, both have been varied simultaneously to provide a matrix of predictions.

This matrix, for the momentum spectrum at a core distance of 300 metres, is shown in figure 6.5, displayed as the ratio of the observed density of muons to that predicted. The errors on the points correspond to the statistical errors on the observed differential momentum spectrum. The parameter varied to obtain the sensitivity to N_s is γ, the energy exponent in:

$$N_s = 15 \times \frac{(KE)^{\gamma}}{(3 \times 10^3)^{\gamma}} \quad \text{when } E > 3000 \text{ GeV.} \qquad \ldots 6.3.2$$

Similar matrices have been constructed for core distances of 155 metres and 520 metres, and the conclusion from all is the same, namely that the region of agreement is confined to the ranges $0.5 \leqslant \gamma \leqslant 0.75$ and $A > 4$. The values of $\gamma > 0.5$ have been considered only for completeness, since considerations of the dynamics of an interaction exclude them, at least for the highest primary energies. It can be shown that if the energy exponent of the multiplicity law is γ and the mass of a meson is M then the mean energy of the secondary mesons in the collision C.M. system is given

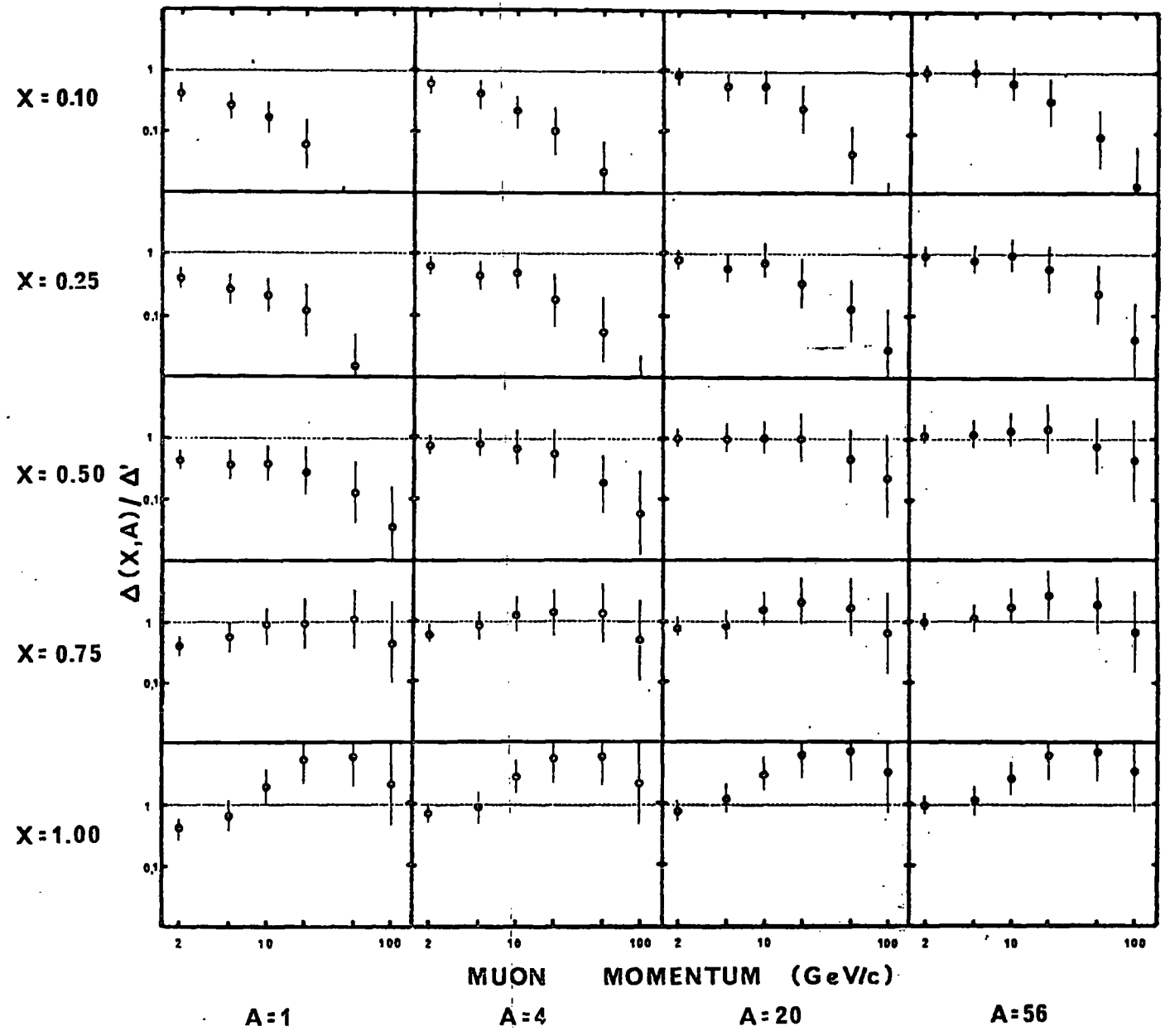
X = 0.10
X = 0.25
X = 0.50
X = 0.75
X = 1.00
Δ (X,A) / Δ'
MUON MOMENTUM (GeV/c)
A = 1
A = 4
A = 20
A = 56

FIGURE 6.5

by:

$$\overline{E^{*}_{\pi}} = \text{constant} \times K^{(1-X)} \times \sqrt{Mc^2} \times E^{0.5-X} \quad \ldots 6.3.3$$

this gives, for $X > 0.5$, $\overline{E^{*}_{\pi}} < M$ for a finite value of E, unless K is a function of E :

$$K(E) = \text{constant} \times E^{\alpha} \quad \ldots 6.3.4$$

where $\alpha > \frac{X - 0.5}{1 - X}$

The available evidence on the variation of K with E suggests that K decreases with increasing E, or is independent of E. The most probable value for X is therefore $X = 0.5$. Thus the adopted values of X and A will be assumed to be 0.5 and 20 respectively. At this stage, the effects of an increase in mean transverse momentum and the inclusion of kaons have not been added.

Since the mechanism of kaon-nucleon interactions is unknown, only the effects of kaons produced in the first interactions of the primary cosmic ray nucleons have been included. It has been assumed that 25% of the secondaries produced in such interactions are kaons, which possess a distribution in transverse momentum similar to that of pions, with a mean transverse momentum of 0.8 GeV/c, and which possess an interaction length of 100 gm. cm^{-2}. The inclusion of kaons affects the densities of the distant, high momentum muons only, as can be seen in figure 6.6. This compares the predicted densities with the observed densities for a number of core distances and for two compositions of secondaries: 100% pions in all

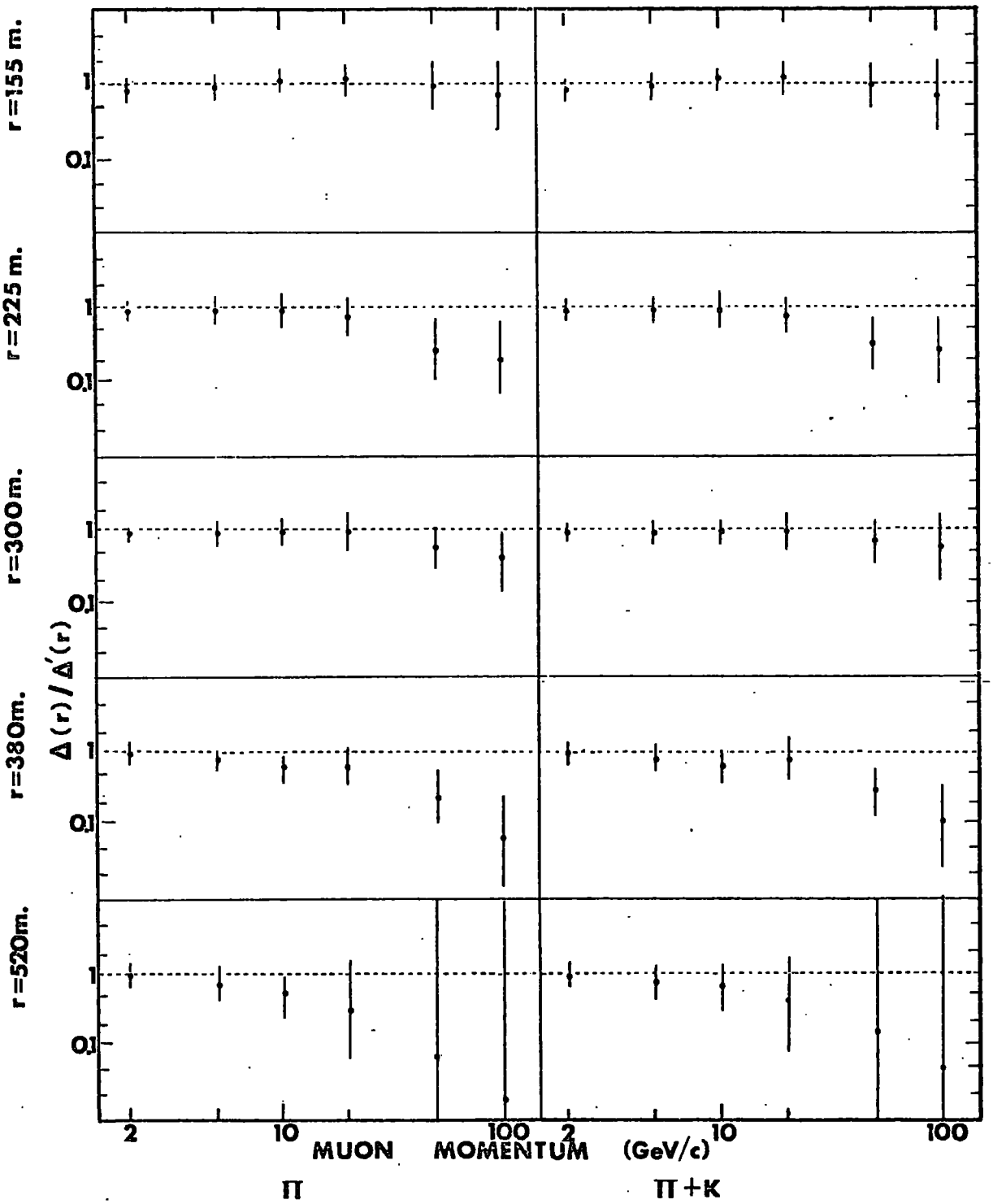
r=155 m.
r=225 m.
r=300m.
r=380m.
r=520m.
Δ(r)/Δ'(r)
1
0.1
2
10
100
MUON MOMENTUM (GeV/c)
π
π+K

FIGURE 6.6

interactions, and 25% kaons from the first interaction only, all other secondaries being pions. The inclusion of kaons does not greatly enhance the muon densities.

The predicted differential muon momentum spectra in a shower of primary energy 2×10^8 GeV, for distances corresponding to those for which spectra have been obtained by the present experiment, are shown in figure 6.7. The zenith angle of the shower is 20°.

The calculations have been extended to predict the lateral distribution of muons of momenta not less than 1 GeV/c, and the total momentum spectrum of EAS muons. Because of the uncertainties in the experimental measurements for core distances smaller than 100 metres, arising from the difference in the sizes of the showers in which these are observed, and the consequent normalisation, the latter prediction has been obtained by evaluating:

$$N_\mu(\geqslant p) = \int_{100}^{\infty} f(\geqslant p, r)\, dr \qquad \ldots 6.3.5$$

where $f(\geqslant p, r)$ is the integral momentum spectrum at a core distance r. The total momentum spectrum of EAS muons for core distances greater than 100 metres and the 1 GeV/c muon lateral distribution are shown in figure 6.8, compared with the corresponding observed distributions. In both cases the predicted distributions have been obtained for a primary proton and a primary nucleus of atomic number 20, to determine the sensitivity of the measurements to the

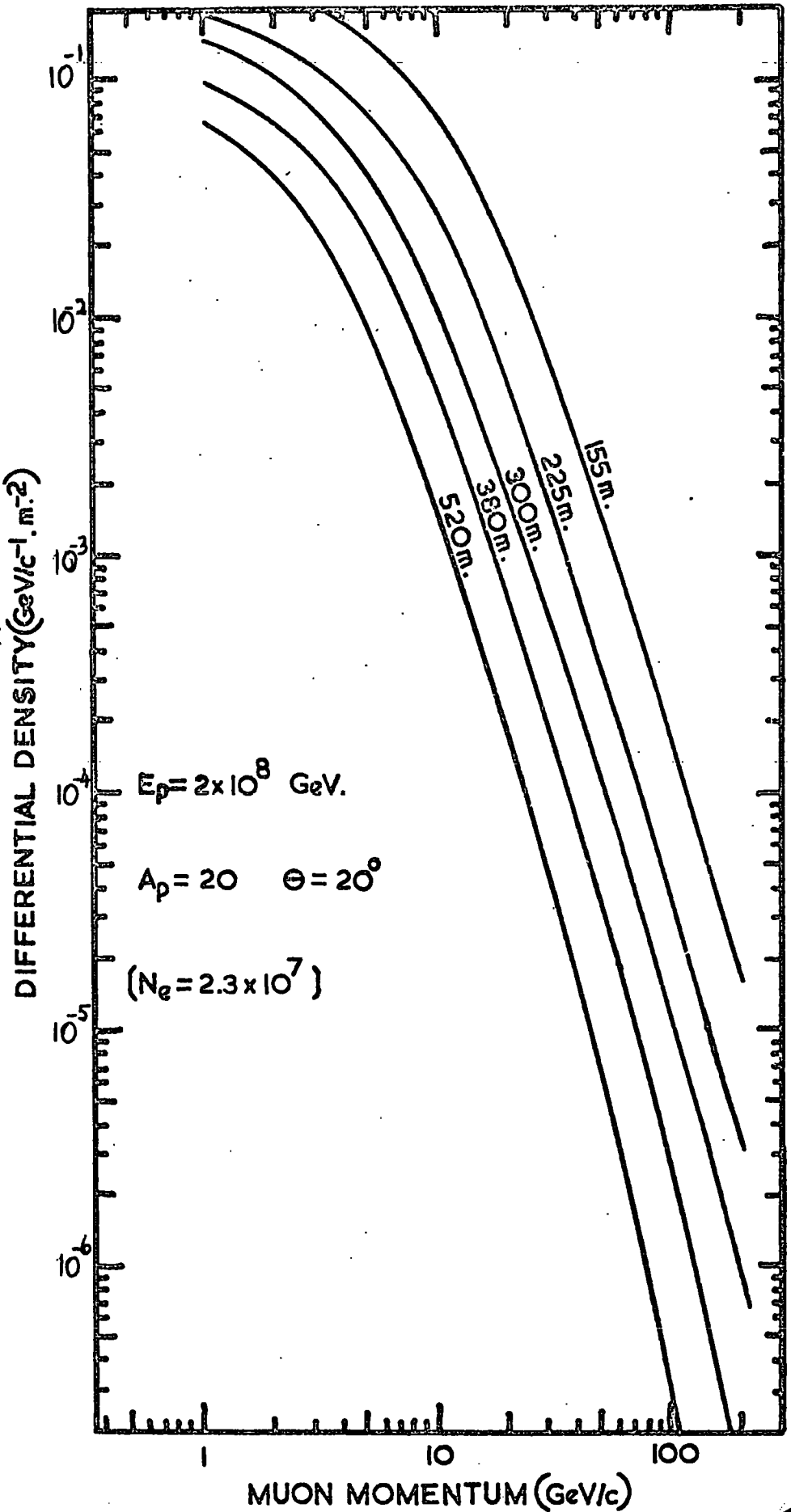
DIFFERENTIAL DENSITY (GeV/c⁻¹.m.⁻²)
10⁻¹
10⁻²
10⁻³
10⁻⁴
10⁻⁵
10⁻⁶
155m.
225m.
300m.
380m.
520m.
Ep = 2x10⁸ GeV.
Ap = 20 Θ = 20°
(Ne = 2.3x10⁷)
1
10
100
MUON MOMENTUM (GeV/c)

FIGURE 6.7

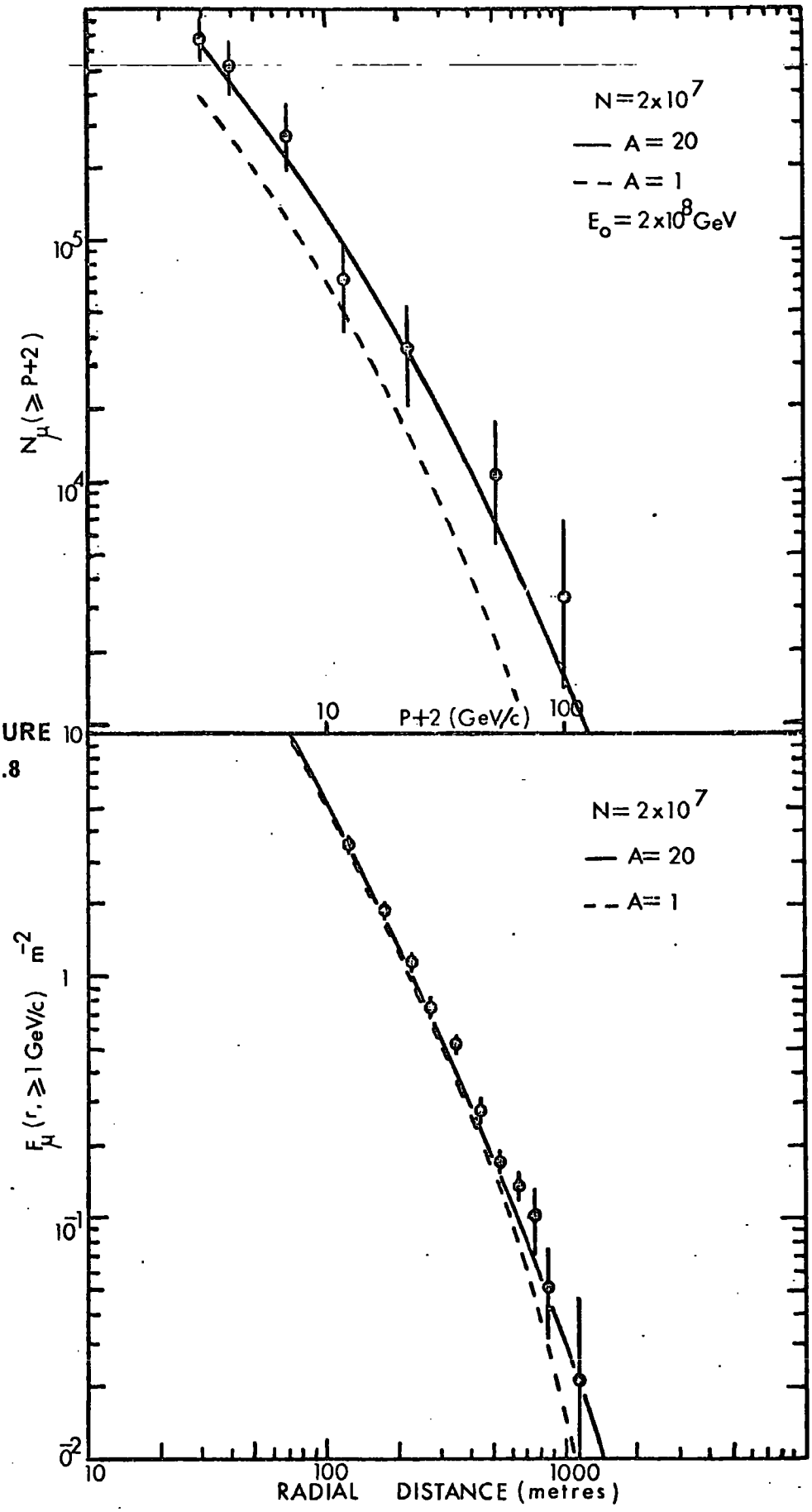
N=2x10^7
A = 20
A = 1
E_o = 2x10^8 GeV
N_μ(≥ P+2)
10^5
10^4
10
P+2 (GeV/c)
100
10
N= 2x10^7
A= 20
A= 1
F_μ(r, ≥1 GeV/c) m^-2
1
10^-1
10^-2
10
100
1000
RADIAL DISTANCE (metres)

FIGURE 6.8

primary mass. For both distributions, the difference between the predictions increases with increasing muon momentum and core distance. The prediction of the 1 GeV/c muon lateral distribution has been normalised to that for a heavy primary, to illustrate the region of separation. Because of the difficulty of measuring accurately a shower size or primary energy, a difference in absolute numbers between the predictions does not provide, unless it is very large, a means of deciding the primary composition. The separation in shape, however, for large core distances, of the predicted lateral distributions is such as to give some hope of a determination of primary composition.

To check that the assumptions made to explain the muon densities do not distort the energy balance of the shower, a calculation has been performed in order to predict the number of particles in a shower at sea level originating from a primary of atomic number 20 and primary energy 2×10^8 GeV. This has been accomplished by assuming charge symmetry for pion production and that a neutral pion decays into two photons of equal energy. The height x energy distribution of the photons has been folded with the curves of Ivanenko and Samusedev (1967), suitably modified for an air absorber, for an electron threshold energy of 80 MeV. The shower is found to contain 2.3×10^7 particles at sea level.

6.4. Conclusions.

6.4.1 The Mechanism of High Energy Interactions.

A review of the present knowledge of the parameters of extremely high energy interactions obtained from the more direct measurements indicates that very little is known about the mechanism of such interactions for collision energies greater than about 10^4 GeV. Indirect evidence from certain EAS measurements has shown that extrapolations made from the direct results up to much higher energies may be valid. For example, it is expected that the cross-section for the inelastic interaction of a nucleon in air will approach the geometrical value asymptotically with increasing energy. This cross-section is in fact consistent with the value obtained from EAS measurements such as those of Matano et al. (1964).

The interaction itself is characterised by four parameters: the multiplicity, the transverse momentum distribution, the energy spectrum and nature of the secondary particles, and the inelasticity. The transverse momentum and the secondary energy distributions quoted by Cocconi, Koester and Perkins (1961) is substantiated by the results of most experiments, and by the present experiment. However, since only these distributions have been considered in the present analysis, the existence of radically different distributions, combined with different values for other parameters, although improbable, cannot be excluded.

There is some evidence from observations of the charge ratio of muons possessing large core distance x momentum products that the kaon : pion ratio of the secondaries of extremely high energy interactions remains within the range observed at lower energies, i.e. 0.1 to 0.6 (MacKeown, 1965) with the most probable value of 0.25. The significant result is that the momentum spectra of EAS muons at various core distances are quite sensitive to the form of the multiplicity function for secondaries from the highest energy interactions. The form of this distribution which fits the present observations is:

$$N_s = 0.4 \times (K E)^{0.5} \qquad \ldots 6.4.1$$

where N_s is the multiplicity of all secondaries, K is the inelasticity and E the primary energy of the interaction. This law is valid for energies greater than 3×10^3 GeV.

6.4. 2 The Nature of Primary Cosmic Rays.

The composition of the primary cosmic ray beam is well known below about 10^3 GeV, but it is of great importance for the development of astrophysical theories that this knowledge be extended to much higher energies. The well-established change in slope in the size spectrum of EAS has been interpreted as evidence for a change in the primary composition at a primary energy close to 2×10^6 GeV. It is supposed that this change iscaused by the progressive loss from the galaxy of nuclei which at lower energies are contained by a galactic magnetic field of about 10^{-5} gauss. The consequence of this loss would be a steadily increasing average atomic number for

primary cosmic rays of energy greater than 2×10^6 GeV. The second, not so well established slope change in the size spectrum is then interpreted as evidence for the presence of extragalactic cosmic rays, possibly protons, in the primary spectrum above an energy of about 2×10^9 GeV. The present results are consistent with this theory, in that the characteristics of the muons observed in an EAS of primary energy 2×10^8 GeV are consistent with the shower originating from a primary heavy nucleus, and are inconsistent with a primary proton. There is no evidence as yet for or against the hypothesis of a pure proton beam for energies above 2×10^9 GeV.

6.5 Future Work.

In the interpretation of some EAS measurements, the problems of the nature of the cosmic ray primary and of the parameters of ultra-high energy nuclear interactions are inextricably linked. The study of EAS muons affords the best opportunity of separating and illuminating these problems, because of the non-interacting properties of muons. By a careful choice of the spacial position and momentum of muon measurements, any desired position in the development of an air shower may, in theory, be examined. The interpretation of the results presented in this thesis shows that a small proportion of muons in an air shower, those possessing large momentum x core distance products, can furnish useful information on the processes occurring at the birth of EAS. In the future, the validity of the interpretation of these results may be established by further

measurements in other momentum-distance regions. In particular, since it is expected that those muons of momenta near 100 GeV/c observed at a core distance of 300 m. which constitute the apparent excess are of the same production generation as those possessing momenta near 2 GeV/c at 1.5 km., a large area muon detector situated far from the core of a large EAS could furnish useful information on the nature of primary cosmic rays of very high energy. At the other end of the momentum scale, a measurement of the EAS muon momentum spectrum at a core distance of 100 m. for momenta $\sim$ 300 GeV/c could establish the primary cosmic ray composition in showers of size near the change of slope of the shower size spectrum.

APPENDIX

A.1 General

It is implicitly assumed that until a secondary meson decays into a muon its lateral and angular deviation from the core is negligible. This assumption is valid for all but the lowest energy mesons, for which a bias is introduced with the effect that the predicted muon momentum spectra will be underestimated at small momenta: at 300m. from the core, the density of 1GeV/c muons is underestimated by about 10%.

A shower initiated by a heavy primary is assumed to develop from the fragmentation of the primary on its first interaction after the following scheme. A fraction, F, of the nucleons of the primary interact coherently to produce secondary mesons with a multiplicity depending on the energy E radiated:

$$n_s = 15 \times (E/3 \times 10^3)^{0.5} \text{ for } E > 3000 \text{ GeV.}$$

The remaining nucleons are freed and continue individually, retaining equal shares of the primary energy.

Constants used:

1) Lifetimes of unstable particles:
$\tau(\pi^{\pm}) = 2.5 \times 10^{-8}$ sec.; $\tau(K^{\pm}) = 1.25 \times 10^{-8}$ sec.; $\tau(\mu) = 2 \times 10^{-6}$ sec

2) Particle masses:

$m_\pi = 0.14$ GeV/c^2; $m_K = 0.49$ GeV/c^2; $m_n = 0.939$ GeV/c^2;

$m_\mu = 0.107$ GeV/c^2.

3) Interaction lengths:

$\lambda_\pi = 120 gm.cm^{-2}.$; $\lambda_K = 100 gm.cm^{-2}.$; $\lambda_N = 80 gm.cm^{-2}.$

for a compound nucleus, the interaction length is calculated using a formula due to Peters (1952) :

$$\lambda_A = \frac{205}{(0.6+A^{\frac{1}{3}})^2} \qquad \ldots A.1$$

4) The atmosphere:

The atmosphere is taken to be represented, for ease of integration, by the following expressions deduced from the data given by Rossi (1952) and the Handbook of Geophysics (The Macmillan Company: 1960),

$h(x,\theta) = H1 \ln(T0/t) - H2 \exp(t/T1)$

$x(h,\theta) = T0 \exp(-h/H1) - T2 \exp(-h/H3)$

where $T0 = 1335 \sec(\theta) gm.cm^{-2}.$; $T1 = 350 \sec(\theta) gm.cm^{-2}.$;

$T2 = 300 \sec(\theta) gm.cm^{-2}.$; $H1 = 6.3 \sec(\theta) km.$;

$H2 = 0.095 \sec(\theta) km.$; $H3 = 2.7 \sec(\theta) km.$;

A.2 Calculation for region A.

Each generation of mesons is treated separately, and calculated by the method of successive collisions. The density of muons at a distance r from the core, originating from the n^{th} meson generation and meson energy E_n is obtained by numerical evaluation of the following expression:

$$\Delta(r,E_n)dr\,dE_n = \int_{x_n}\int_{x_{n-1}}\cdots\int_{x_1}\int_{E_{n-1}}\int_{E_{n-2}}\cdots\int_{E_1} P_N(E_o,E_1,0,x_1) \times \prod_{i=1}^{n} P_s(E_i,E_{i+1},x_i,x_{i+1})\,dE_1 \ldots dE_{n-1}\,dx_1\,dx_{n-1}$$

$$x\, C(E_n, r, x_n)\, dx_n\, dr\, dE_n \qquad \ldots A.2$$

where P_N, P_s are the probabilities that a nucleon and a charged meson respectively, originating at a depth x_i with an energy E_i, will survive to interact at a depth x_{i+1} and produce a secondary meson of energy E_{i+1}. The suffix i is identified with the intermediate meson generations. $C(E_n, r, x_n)$ is the probability that a secondary, produced at a depth x_n with an energy E_n will decay into a muon at such an angle from the core that, if the muon survives, it will arrive at the observation level at a distance r. It is assumed that this angle χ is given by:

$$\chi = \frac{r \times E_n}{h(x_n)} \qquad \ldots A.3$$

where $h(x_n)$ is the geometrical height from the observation level to the depth x_n. The function C is of the form:

$$C(E_n, r, x_n) dE_n\, dr = \frac{r \times \exp\left\{-r.E_n.A1/h(x_n)\right\} \times E_n^2\, dE_n\, dr}{h^2(x_n).A2.(1+A3.E_n)} \qquad \ldots A.4$$

where A1, A2, A3 are constants.

The function P_s is given by:

$$P_s \propto N(E_i, x_i).\frac{N_s(E_i)}{2}.\left\{\exp(-E_{i+1}/T_i)/T_i + \exp(-E_{i+1}/G_i)/G_i\right\} \times \exp\left\{-(x_{i+1}-x_i)/L_{eff}\right\} \qquad \ldots A.5$$

where $N_s(E_i)$, T_i and G_i are the mean charged meson multiplicity, mean forward cone energy and mean backward cone energy of the mesons in the L- system, and

$$\frac{1}{L_{eff}} = \frac{1}{\lambda(\text{interaction})} + \frac{1}{\lambda(\text{decay})} \quad \ldots A.6$$

Having produced the contribution from the n^{th} generation, the secondary meson energy spectrum as a function of height of production is modified to allow for meson decay. Assuming muons result from a two-body decay process, it can be shown that:

$$\Delta\mu = \int_{E_n}^{Q.E_n'} \frac{\Delta_s(E_n,h)\ dE_n}{(1-1/Q).E_n} \quad \ldots A.7$$

where $\Delta\mu(E_n', h)$ is the density of muons of momentum E_n', which originate from a height h, that are the decay products of mesons of energy E_n. Q is the reciprocal of the minimum fraction of energy carried away from a meson decay by a muon:

$$Q = (M_s / M_\mu)^2 \quad \ldots A.8$$

Preliminary calculations were performed to optimise the mathematical calculations, and the intervals used in the numerical evaluation of equation A.2 were quarter decades in energy and 2km. in

height. The calculation was terminated after three generations as the contribution to the density of high momentum muons at core distances greater tham 100m. from lower generations is negligible.

A.3 Calculation for Region B.

The calculation for the cascade in region B has been carried out using a method similar to that of Holyoak (1967). Interaction points of nucleons and mesons are considered fixed in the atmosphere, at intervals equal to their respective interaction lengths. The starting point of the calculation, the energy spectra of nucleons and mesons at a height of 10km., is obtained by using equation A.2, modified to consider longitudinal development only, and extending the number of generations until the required accuracy is reached. The spectra are calculated to a mathematical accuracy of 5%.

The nucleon spectrum is obtained easily from the following expression, which assumes that the number of interactions undergone by a nucleon in a given thickness of matter is distributed as a poisson function, and that the inelasticity of nucleon-nucleon collisions does not fluctuate:

$$S(E_n,x) = \frac{(x/\lambda)^A . \exp(-x/\lambda)}{A!} \qquad \ldots A.9$$

where E_n, E_o, λ are the nucleon energy, primary energy and interaction length respectively, A is given by:

$$A = \log_k (E_o/E_n) \qquad \ldots A.10$$

where k is the reciprocal of the nucleon inelasticity.

The cascade model for region B is shown diagrammatically in figure 6.3. Secondary mesons from a nucleon interaction are allocated to the meson population entering and leaving the meson interaction levels in proportions inversely proportional to the differences in depth between the nucleon interaction level and the two adjacent meson levels. Mesons are allowed to decay between meson levels, and the number which decay are assumed to originate, for the purpose of calculating the lateral distribution, from a point halfway between the levels.

As in the calculation for region A, full account is taken of the effect of meson decay, muon decay and energy loss on the muon momentum spectrum.

References.

The following abbreviations are used for the proceedings of Cosmic Ray conferences:

Proc. Moscow Conf.: Proceedings of the 6th International Conference on Cosmic Rays, Moscow, 1959 (Moscow: State Publishing House, 1960).

Proc. Kyoto Conf.: Proceedings of the 7th International Conference on Cosmic Rays, Kyoto, 1961 (Journal of the Physical Society of Japan, 1962, Supp. A-III).

Proc. Jaipur Conf.: Proceedings of the 8th International Conference on Cosmic Rays, Jaipur, India, 1963 (Bombay: Commercial Printing Press, 1964).

Proc. London Conf.: Proceedings of the 9th International Conference on Cosmic Rays, London, 1965 (London: Institute of Physics and the Physical Society, 1966).

Proc. Calgary Conf: Proceedings of the 10th International Conference on Cosmic Rays, Calgary, Canada, 1967 (Canadian Jour. Phys., 46, No.10, 1968).

ABRAHAM, F., GIERULA, J., LEVI SETTI, R., RYBICKI, K., TSAO, C.H., WOLTER, W., FRICKEN, R.L., and HUGGETT, R.W., 1967, Phys. Rev., 159, 1110-1123.

ADCOCK, C., de BEER, J.F., ODA, H., WDOWCZYK, J., and WOLFENDALE, A.W., 1968, Proc. Phys. Soc., Ser.2, 1, 82-88.

ALLAN, H.R., BEAMISH, R.F., BRYANT, D.A., KASHA, H., and WILLS, R.D., 1960, Proc. Phys. Soc., A76, 1-16.

ALLAN,H.R.,BEAMISH,R.F.,GLENCROSS,W.M.,THOMSON,D.M.,and WILLS,R.D., 1962, Proc. Phys. Soc., A79, 1170-1182.

ALLAN,H.R.,BLAKE,P.R.,NEAT,K.P.,and PIDCOCK,J.K., 1968, Proc. Calgary Conf., pt. 2, 98-101.

ALY,H.H.,DUTHIE,J.,KADDOURA,A.,PERKINS,D.H.,and FOWLER,P.H., 1960, Proc. of the Rochester Conf. on High Energy Physics (Interscience Publishers Inc., 1960).

ALY,H.H.,KAPLON,M.F.,and SHEN,M.L., 1964, Nuevo Cimento, 31, 905-918.

ASHTON,F.,and WOLFENDALE,A.W., 1963, Proc. Phys. Soc., A81, 593-603.

ASHTON,F.,and COATS,R.B., 1966, Proc. London Conf., 2, 959-961.

BABAEV,M.K.,BAIGUBEKOV,A.S.,DENIKOEV,R.Z.,EMELYANOV,Yu.A.,LUKIN,Yu.T., TAKIBAEV,Zh.S.,and KHOMENKO,G.S., 1967, Bull. Acad. Sci. USSR (Phys. Ser.), 30, 1674-1677.

BARNAVELI,T.T.,BIBILASHVILI,M.F.,GRUBELASHVILI,G.A.,JAVRISHVILI,A.K., KAZAROV,R.E.,KURIDZE,R.V.,and KHALDEEVA,I.V.,
1964, Proc. Jaipur Conf, 4, 273-276.
1965, Bull. Acad. Sci. USSR (Phys. Ser.), 28, 1782-1783.

BARRETT,P.H.,BOLLINGER,L.M.,COCCONI,G.,EISENBERG,Y.,and GREISEN,K., 1952, Rev. Mod. Phys., 24, 133-178.

BARTON,J.C.,ROGERS,I.W.,and THOMPSON,M.G., 1966, Proc. Phys. Soc., 87, 101-107.

BARTON,J.C., 1966, Proc. Phys. Soc., 88, 355-371.

BENNETT,H.W.,and NASH,W.F., 1960, Supplement to Nuevo Cimento, 15, 193-201.

BENNETT,S.,and GREISEN,K., 1961, Phys. Rev., 124, 1982-1987.

BHABHA,H.J.,and HEITLER,W., 1937, Proc. Roy. Soc., A159, 432-458.

BOROG,V.V.,KIRILLOV-UGRYUMOV,V.G.,PETRUKHIN,A.A.,ROZENTAL,I.L.,and SHESTAKOV,V.V., 1967, Bull. Acad. Sci. USSR (Phys. Ser.), 30, 1739-1743.

BOWLER,M.G.,FOWLER,P.H.,and PERKINS,D.H., 1962, Nuevo Cimento, 26, 1183-1196.

BRADT,H.V.,and RAPPAPORT,S.A., 1967, Phys. Rev., 164, 1567-1583.

BRAY,A.D.,CRAWFORD,D.F.,JAUNCEY,D.L.,McCUSKER,C.B.A.,MELLEY,D., NELSON,D.,POOLE,P.C.,RATHGEBER,M.H.,SEET,S.H.,ULRICHS,J., WAND,R.H.,and WINN,M.M., 1966, Proc. London Conf., 2, 668-671.

BUJA,Z., 1964, Nukleonika (Poland), 9, 389-392.

BULL,R.M.,COATES,D.W.,NASH,W.F.,and RASTIN,B.C., 1962a, Nuovo Cimento, 23, 28-38.

BULL,R.M.,NASH,W.F.,and RASTIN,B.C., 1962b, Nuovo Cimento, 24, 1096-1101.

BULL,R.M.,NASH,W.F.,and RASTIN,B.C., 1965, Nuovo Cimento, 40A, 348-364.

CASTAGNOLI,C.,CORTINI,G.,FRANZINETTI,C.,MANFREDINI,A.,and MORENO,D., 1953, Nuovo Cimento, 10, 1539-1558.

CHATTERJEE,B.K.,LAL,S.,MATANO,T.,MURTHY,G.T.,NARANAN,S.,SIVIPRASAD, K.,SREEKANTAN,B.V.,SRINIVASA-RAO,M.V.,and VISHWANATH,P.R., 1966, Proc. London Conf., 2, 627-631.

CHAUDHURI,N.,and SINHA,M.S., 1964, Nuovo Cimento, 32, 853-862.

CLARK,G.,EARL,J.,KRAUSHAAR,W.,LINSLEY,J.,ROSSI,B.,and SHERB,F., 1958, Supp. to Nuovo Cimento, 8, 623-652.

COCCONI,G.,KOESTER,L.G.,and PERKINS,D.H., 1961, (unpublished: Lawrence Radiation Lab. Seminar 28, part 2, UCID-1444).

COWSIK,R., 1966, Proc. London Conf., 2, 656-659.

de BEER,J.F.,CRANSHAW,T.E.,and PARHAM,A.G., 1962, Phil. Mag., 7, 499-514.

de BEER,J.F.,HOLYOAK,B.,WDOWCZYK,J.,and WOLFENDALE,A.W., 1966, Proc. Phys. Soc., 89, 567-585.

de BEER,J.F.,HOLYOAK,B.,CDA,H.,WDOWCZYK,J.,and WOLFENDALE,A.W., 1968a, Proc. Calgary Conf., pt. 2, 185-188.

de BEER,J.F.,HOLYOAK,B.,CDA,H.,WDOWCZYK,J.,and WOLFENDALE,A.W., 1968b, Proc. Calgary Conf., pt. 3, (in the press).

de BEER,J.F.,HOLYOAK,B.,CDA,H.,WDOWCZYK,J.,and WOLFENDALE,A.W., 1968c, Proc. Phys. Soc., Ser.2, 1, 72-81.

DMITRIEV,V.A.,and KHRISTIANSEN,G.B., 1963, Soviet Physics (JETP), 17, 276-281.

DOBROTIN,N.A.,GUSEVA,V.V.,KOTEL'NIKOV,K.A.,LEBEDEV,A.M.,RYABIKOV,S.V., SLAVATINSKII,S.A.,and ZELEVINSKAYA,N.G., 1962, Nuclear Physics, 35, 152-164.

DOVZHENKO,O.I.,NELEPO,B.A.,NIKOLSKII,S.I., 1957, Jer. Exp. Teer. Phiz., 32, 463-465.

EARNSHAW,J.C.,ORFORD,K.J.,ROCHESTER,G.D.,SOMOGYI,A.J.,TURVER,K.E., and WALTON,A.B., 1967, Proc. Phys. Soc., 90, 91-108.

EARNSHAW,J.C.,ORFORD,K.J.,ROCHESTER,G.D.,TURVER,K.E.,and WALTON,A.B., 1968a, Proc. Calgary Conf., pt. 2, 122-126.

EARNSHAW,J.C.,MASLIN,G.C.,TURVER,K.E., 1968b, Proc. Calgary Conf., pt. 2, 115-118.

EARNSHAW,J.C., 1968c, Ph.D. Thesis, University of Durham.

EARNSHAW,R.A.,EVANS,A.C.,HUGHES,R.R.,REID,R.J.O.,TENNENT,R.M., WATSON,A.A.,and WILSON,J.G., 1968, Proc. Calgary Conf., pt. 2, 5-8.

EYGES,L., 1948, Phys. Rev., 74, 1534-1535.

FERMI,E., 1950, Prog. Theor. Phys., 5, 570-583.

FOWLER,P.H., 1964, Proc. Jaipur Conf., 5, 182-209.

FOWLER,P.H.,PERKINS,D.H., 1964, Proc. Roy. Soc., A278, 401-415.

FOWLER,P.H.,ADAMS,R.A.,COWEN,V.G.,and KIDD,J.M., 1967, Proc. Roy. Soc., A301, 39-45.

FRAUTSCHI,S.C., 1963, Nuevo Cimento, 28, 409-422.

FURRY,W.H., 1937, Phys. Rev., 52, 569-581.

GIERULA,J.,and KRZYWDZINSKI,S., 1968, Nuevo Cimento, A55, 370-376.

GINZBURG,V.L.,and SYROVATSKII,S.I., 1964, 'The Origin of Cosmic Rays',(Oxford: Pergamon Press, 1964).

GLENCROSS,W.M., 1963, Proc. Phys. Soc., 82, 501-514.

GREISEN,K., 1960, Ann. Rev. Nucl. Sci., 10, 63-108.

GUSEVA,V.V.,DOBROTIN,N.A.,ZELEVINSKAYA,N.G.,KOTEL'NIKOV,K.A.,
LEBEDEV,A.M.,and SLAVATINSKII,S.A., 1962, Proc. Kyoto Conf.,
3, 375-383.

HANDBOOK OF GEOPHYSICS, 1960, New York: The Macmillan Company.

HANSEN,L.F.,and FRETTER,W.B., 1960, Phys. Rev., 118, 812-824.

HAYAKAWA,S.,and OGITA,N., 1960, Proc. Moscow Conf., 2, 220-223.

HAYMAN,P.J.,and WOLFENDALE,A.W., 1962, Proc. Phys. Soc., 80,
710-728.

HEISENBERG,W., 1952, Z.Phys., 133, 65-79.

HILLAS,A.M., 1966, Proc. London Conf., 2, 758-761.

HOLYOAK,B., 1967, Ph.D. Thesis, University of Durham.

ICEF, 1963, Reports on the International Co-operative Emulsion
Flight, Nuovo Cimento, Supplement 1, 1037-1090.

IMAEDA,K., 1962, Nuovo Cimento, 26, 417-439.

IVANENKO,I.P.,and SAMUSODOV,B.E., 1959, Soviet Physics (JETP), 35,
884-887.

IVANENKO,I.P.,and SAMUSODOV,B.E., 1967, Bull. Acad. Sci. USSR
(Phys. Ser.), 30, 1722-1726.

KAMAL,A.A.,and RAO,G.K., 1967, Proc. Indian Acad. Sci., A66, 15-32.

KAZUNO,M., 1967, Ph.D. Thesis, Institute of Advanced Studies,
Dublin.

KHRENOV,B.A., 1962, Soviet Physics (JETP), 14, 1001-1007.

KHRENOV,B.A., 1963, Bull. Acad. Sci. USSR (Phys. Ser.), 26, 688-
690.

KHRENOV,B.A., 1965, Soviet Jour. Nucl. Phys., 1, 384-388.

KOSHIBA,M.,TSAO,C.H.,DENEY,C.L.,FRICKEN,R.L.,HUGGETT,R.W.,
HILDEBRAND,B.,SILBERBERG,R.,and LORD,J.J., 1963,
Nuovo Cimento, Supplement 1, 1091-1117.

KRAUSHAAR,W.L.,and MARKS,L.J., 1954, Phys. Rev., 93, 326-330.

GUSEVA,V.V.,DOBROTIN,N.A.,ZELEVINSKAYA,N.G.,KOTEL'NIKOV,K.A.,
LEBEDEV,A.M.,and SLAVATINSKII,S.A., 1962, Proc. Kyoto Conf.,
3, 375-383.

HANDBOOK OF GEOPHYSICS, 1960, New York: The Macmillan Company.

HANSEN,L.F.,and FRETTER,W.B., 1960, Phys. Rev., 118, 812-824.

HAYAKAWA,S.,and OGITA,N., 1960, Proc. Moscow Conf., 2, 220-223.

HAYMAN,P.J.,and WOLFENDALE,A.W., 1962, Proc. Phys. Soc., 80,
710-728.

HEISENBERG,W., 1952, Z.Phys., 133, 65-79.

HILLAS,A.M., 1966, Proc. London Conf., 2, 758-761.

HOLYOAK,B., 1967, Ph.D. Thesis, University of Durham.

ICEF, 1963, Reports on the International Co-operative Emulsion
Flight, Nuovo Cimento, Supplement 1, 1037-1090.

IMAEDA,K., 1962, Nuovo Cimento, 26, 417-439.

IVANENKO,I.P.,and SAMUSODOV,B.E., 1959, Soviet Physics (JETP), 35,
884-887.

IVANENKO,I.P.,and SAMUSODOV,B.E., 1967, Bull. Acad. Sci. USSR
(Phys. Ser.), 30, 1722-1726.

KAMAL,A.A.,and RAO,G.K., 1967, Proc. Indian Acad. Sci., A66, 15-32.

KAZUNO,M., 1967, Ph.D. Thesis, Institute of Advanced Studies,
Dublin.

KHRENOV,B.A., 1962, Soviet Physics (JETP), 14, 1001-1007.

KHRENOV,B.A., 1963, Bull. Acad. Sci. USSR (Phys. Ser.), 26, 688-
690.

KHRENOV,B.A., 1965, Soviet Jour. Nucl. Phys., 1, 384-388.

KOSHIBA,M.,TSAO,C.H.,DENEY,C.L.,FRICKEN,R.L.,HUGGETT,R.W.,
HILDEBRAND,B.,SILBERBERG,R.,and LORD,J.J., 1963,
Nuovo Cimento, Supplement 1, 1091-1117.

KRAUSHAAR,W.L.,and MARKS,L.J., 1954, Phys. Rev., 93, 326-330.

LAL,S.,RAGHAVAN,R.,RANGASWAMY,T.N.,SUBRAMANIAN,A.,TONWAR,S.C., and VATCHA,R.H., 1964, Proc. Jaipur Conf., 5, 377-381.

LAL,S., 1967, Nuovo Cimento, 48, 466-481.

LANDAU,L.D., 1953, Izv. Akad. Nauk., Fiz. Ser., 17, 51-64.

LINSLEY,J., 1964, Proc. Jaipur Conf., 4, 77-99.

LOCK,W.O., 1964, Proc. Jaipur Conf., 5, 105-138.

LOHRMANN,E.,TEUCHER,M.W.,and SCHEIN,M., 1961, Phys. Rev., 122, 672-686.

LOHRMANN,E., 1963, Nuovo Cimento, Supplement 1, 1226-1229.

McCUSKER,C.B.A.,and PEAK,L.S., 1964, Proc. Jaipur Conf., 5, 35-39.

McCUSKER,C.B.A.,PEAK,L.S.,and RATHGEBER,M.H., 1968, preprint: University of Sydney.

MacKEOWN,P.K., 1965, Ph.D. Thesis, University of Durham.

MALHOLTRA,P.K., 1963, Nuclear Physics, 46, 559-571.

MALHOLTRA,P.K., 1964, Proc. Jaipur Conf., 5, 40-47.

MALHOLTRA,P.K.,SHUKLA,P.G.,STEPHENS,S.A.,VIJAYALAKSHIMI,B.,BOULT,J., CLAPHAM,V.M.,FOWLER,P.H.,HACKFORTH,H.L.,KEEREETAVEEP,J., and TOVEY,S.N., 1966, Proc. London Conf., 2, 840-843.

MATANO,T.,MIURA,I.,NAGANO,M.,ODA,M.,SHIBATA,S.,TANAKA,Y.,TANAHASHI, G.,and HASEGAWA,H., 1964, Proc. Jaipur Conf., 4, 129-142.

MURZIN,V.S., 1966, Proc. London Conf., 2, 872-874.

NIKOLSKII,S.I., 1963, Soviet Physics (Uspecki), 5, 849-877.

O'CONNOR,P.V.,and WOLFENDALE,A.W., 1960, Nuovo Cimento, Supplement 2, 15, 202-210.

ODA,M., 1957, Nuovo Cimento, 5, 615-627.

ORFORD,K.J.,and TURVER,K.E., 1968a, Proc. Calgary Conf.,pt. 2, 127-130.

ORFORD,K.J.,TURVER,K.E.,and WALTON,A.B., 1968b, Proc. Calgary Conf., pt. 2, 119-121.

ORFORD,K.J.,and TURVER,K.E., 1968c, Nature, 219, 706-708.

OSBORNE,J.L.,PALMER,N.S.,and WOLFENDALE,A.W., 1964a, Proc. Phys. Soc., 84, 911-913.

OSBORNE,J.L., 1964b, Nuovo Cimento, 32, 816-826.

OSBORNE,J.L.,and WOLFENDALE,A.W., 1964c, Proc. Phys. Soc., 84, 901-909.

PAL,Y.,and PETERS,B., 1964, K. Danske Vidensk. Selsk. Mat.-Fys. Medd., 33, No. 15.

PETERS,B., 1952, Prog. in Cosmic Ray Phys., 1, 191-242.

PINKAU,K., 1966, Proc. London Conf., 2, 895-897.

RANFT,J., 1964, CERN Internal Report No. 64-47.

RASTIN,B.C., 1964, Ph.D. Thesis, University of Nottingham.

ROSSI,B., 1952, 'High Energy Particles',(Prentice-Hall,1952).

SAID,S.S., 1966, Ph.D. Thesis, University of Durham.

SURI,A.N., 1966, Ph.D. Thesis, University of Leeds.

TANAHASHI,G., 1965, Jour. Phys. Soc. Japan, 20, 883-906.

TENNENT,R.M., 1967, Proc. Phys. Soc., 92, 622-631.

TURVER,K.E., 1963, Ph.D. Thesis, University of Leeds.

UEDA,A.,and OGITA,N., 1957, Prog. Theor. Phys., 18, 269-286.

VERNOV,S.N.,KHRISTIANSEN,G.B.,NECHIN,Yu.A.,STOYANOVA,D.A.,and KHRENOV,B.A., 1967, Bull. Acad. Sci. USSR (Phys. Ser.), 30, 1763-1766.

VERNOV,S.N.,and KHRISTIANSEN,G.B., 1968, Proc.Calgary Conf., Vol. A, 345-396, University of Calgary,1968.

WALTON,A.B., 1966, M.Sc. Thesis, University of Durham.

WARD,C.B., 1967, Nucl. Inst. Meth., (to be published).

WILSON,J.G.,ALLAN,H.R.,LILLICRAP,S.C.,REID,R.J.O.,and TURVER,K.E., 1964, Proc. Jaipur Conf., 4, 27-34.

YAJIMA,N.,and HASEGAWA,S., 1965, Prog. Theor. Phys., 33, 184-198.

YAMEDA,S.,and KOSHIBA,M., 1968, Proc. Calgary Conf., pt. 3, (in the press).

Acknowledgements.

I am deeply indebted to my supervisor Professor G.D. Rochester, F.R.S. for the provision of the facilities which made this study possible and for his continual support and guidance. I am also grateful to Dr. K.E. Turver for his advice and encouragement in all aspects of the work.

I should like to thank Professor J.G. Wilson and his colleagues of the Department of Physics of the University of Leeds for their co-operation and for the provision of the results of their EAS analysis.

My colleagues Professor A.J. Somogyi, Mr. J.C. Earnshaw, Mr. G.C. Maslin and Mr. A.B. Walton are thanked for their contributions to the collection and analysis of data.

Mr. W. Leslie and the technical staff of the Physics Department Workshop are thanked for their willing help and support in the construction of apparatus.

I am indebted to Miss A.M. Bevils for her patience in the laborious tasks of film scanning and track reconstruction.

For the typing of this thesis Mrs. J.W. Orford is sincerely thanked.

Finally, I am grateful to the University of Durham for the provision of a Research Studentship.